



Theses and Dissertations

2006-11-03

Characterization of Cucurbituril Complex Ions in the Gas Phase Using Electrospray Ionization Fourier Transform Ion Cyclotron Resonance Mass Spectrometry

Haizhen Zhang
Brigham Young University - Provo

Follow this and additional works at: <https://scholarsarchive.byu.edu/etd>

 Part of the [Biochemistry Commons](#), and the [Chemistry Commons](#)

BYU ScholarsArchive Citation

Zhang, Haizhen, "Characterization of Cucurbituril Complex Ions in the Gas Phase Using Electrospray Ionization Fourier Transform Ion Cyclotron Resonance Mass Spectrometry" (2006). *Theses and Dissertations*. 814.

<https://scholarsarchive.byu.edu/etd/814>

This Dissertation is brought to you for free and open access by BYU ScholarsArchive. It has been accepted for inclusion in Theses and Dissertations by an authorized administrator of BYU ScholarsArchive. For more information, please contact scholarsarchive@byu.edu, ellen_amatangelo@byu.edu.

Characterization of Cucurbituril Complex Ions in the Gas Phase Using
Electrospray Ionization Fourier Transform Ion Cyclotron Resonance
Mass Spectrometry

by

Haizhen Zhang

A dissertation submitted to the faculty of
Brigham Young University
in partial fulfillment of the requirements for the degree of

Doctor of Philosophy

Department of Chemistry and Biochemistry

Brigham Young University

December 2006

Copyright © 2006, Haizhen Zhang

All Rights Reserved

BRIGHAM YOUNG UNIVERSITY

GRADUATE COMMITTEE APPROVAL

of a dissertation submitted by

Haizhen Zhang

This dissertation has been read by each member of the following graduate committee
and by majority vote has been found to be satisfactory.

Date _____ David V. Dearden, Chair

Date _____ Adam T. Woolley

Date _____ Matthew C. Asplund

Date _____ Roger G. Harrison

Date _____ Matthew R. Linford

BRIGHAM YOUNG UNIVERSITY

As chair of the candidate's graduate committee, I have read the dissertation of Haizhen Zhang in its final form and have found that (1) its format, citations and bibliographical style are consistent and acceptable and fulfill university and department style requirements; (2) its illustrative materials including figures, tables, and charts are in place; and (3) the final manuscript is satisfactory to the graduate committee and is ready for submission to the university library.

Date

David V. Dearden
Chair, Graduate Committee

Accepted for the Department

Date

David V. Dearden
Graduate Coordinator

Accepted for the College

Date

Thomas W. Sederberg
Associate Dean, College of Physical and Mathematical
Sciences

ABSTRACT

Characterization of Cucurbituril Complex Ions in the Gas Phase Using
Electrospray Ionization Fourier Transform Ion Cyclotron Resonance
Mass Spectrometry

Haizhen Zhang

Department of Chemistry and Biochemistry

Doctor of Philosophy

Host-guest interactions have been well studied in the new century to obtain fundamental insights into supramolecular chemistry. Most of the pioneering works have been done using techniques such as NMR, X-ray crystallography, IR spectroscopy and so on. However, none of these techniques is universal for the investigation of all types of supramolecules, and usually they have one or more limiting factors such as relatively large sample consumption, matrix effects from solvents, etc.

Electrospray mass spectrometry has been widely used to investigate host-guest interactions in the gas phase. A particular advantage of gas phase host-guest research is that the experimental results can be directly compared to computational results

because complicating interferences from solvents are not present. Thus electrospray mass spectrometry coupled with high-level computational methods becomes a powerful tool to elucidate binding behavior in host-guest complexes.

With rigid, symmetric structures available in a range of sizes, cucurbiturils have been ideal prototypical host molecules in host-guest chemistry since they were characterized in 1980s. Recent research in my group has shown cucurbiturils can form various complexes with positive ions in the gas phase, such as molecular containers trapping small neutral guest molecules inside or wheel-and-axle architectures with linear molecules threaded through.

Fourier transform ion cyclotron resonance mass spectrometry (FT-ICR-MS) is an ideal technique for investigation of host-guest supramolecular complexes due to its ultra-high mass resolving power, ultra-high mass accuracy, and high sensitivity. Moreover it has the capability of trapping ions for ion chemistry, and versatile tandem mass spectrometry capabilities.

This dissertation focuses on the characterization of cucurbituril complexes in the gas phase using electrospray ionization FT-ICR mass spectrometry. Chapter 1 describes FTICR mass spectrometry techniques including principles, performance, instrumentation and applications. Electrospray ionization methods are also discussed in this chapter. Chapter 2 introduces structures, properties, synthesis and host-guest chemistry of the cucurbituril family. Chapters 3 investigate cucurbituril complexation behavior with amino acids and peptides. Chapter 4 investigates the alkali metal ions “lids removal” from cucurbit[5]uril molecular box. Chapter 5

characterizes the cucurbit[6]uril pseudorotaxanes in the gas phase. Chapter 6 characterizes the complexes formed by cucurbit[6]uril and α,ω -alkyldiammonium cations in the gas phase, using energy-resolved SORI-CID method. High-level computational methods were also performed to explain the experimental results.

ACKNOWLEDGEMENTS

I would like first of all to express my sincere appreciation to my science instructor, Dr. David V. Dearden. It would have been impossible for me to accomplish the work without his guidance, support, encouragement, and patience.

I would like to have special thanks to my Ph. D. committee and qualification examination members, Dr. Matthew R. Linford, Dr. Adam T. Woolley, Dr. Roger G. Harrison, and Dr. Matthew C. Asplund, for their advice and time through my Ph. D. studies. I would like to thank the Department of Chemistry & Biochemistry, Brigham Young University, for the financial support for my graduate studies.

I gratefully thank R. Jon Willies for his help in computational calculations. I would like to thank the group member, Nannan Fang, for her help and friendship.

I would like to thank my parents and my brothers, who have provided great help and encouragement during my studies in USA.

Finally I would like to dedicate this work to my wife, Liyan Feng, and my son, Jason B. Zhang. They have been the greatest source for all of my passion and imagination on the research work.

Table of Contents

Abstract	V
Acknowledgements	VIII
Chapter 1	
Fourier Transform Ion Cyclotron Resonance Mass Spectrometry	1
Introduction	1
Principles	2
Ion motion in ICR trapping cell.....	2
Ion excitation and detection.....	6
FT-ICR-MS Instrumentation	10
Ionization source.....	10
ICR trapping cell.....	11
Magnet.....	13
High-vacuum system.....	14
FT-ICR-MS Performance	14
Resolving power.....	14
Mass accuracy.....	15
Mass range.....	16
Dynamic range.....	18
Selected FT-ICR-MS Applications	19
Electrospray Ionization.....	19

Tandem mass spectrometry using FT-ICR-MS.....	20
Host-Guest interactions in the gas phase	22
Proteomics	22
Petroleomics.....	23
References	24
Chapter 2	
Cucurbiturils: New Developments in Host-Guest Chemistry	29
Introduction	29
Synthesis, Structure, and Properties	31
Synthesis	31
Structures and Properties	32
Host-Guest Chemistry of the Cucurbituril Family	36
CB6 with Alkylammonium.....	36
Binding with Metal Ions to Form “Molecular Boxes”	37
Host-Guest Chemistry of CBn with Amino Acids, Peptides and Small Proteins	38
Applications of the Cucurbituril Family	40
Catalysis.....	40
Drug Delivery	41
DNA Transfer Carriers.....	41
Waste Water Purification.....	42
Summary and Perspectives	42

References	44
Chapter 3	
Supramolecular Modification of Ion Chemistry: Modulation of Peptide Charge State and Dissociation Behavior through Complexation with α -Cyclodextrin or Cucurbit[<i>n</i>]uril (<i>n</i> = 5, 6)	
	48
Introduction	48
Experimental Section	51
Materials	51
Sample Preparation	52
ESI Mass Spectrometry	52
SORI-CID Experiments	52
Reactivity Experiments	53
Ion Mobility Experiments	53
Electronic Structure Calculations	55
Results	56
Lysine complexation with CB5, CB6 and α -CD	56
Pentalysine complexation	65
Discussion	68
Threaded vs. non-threaded structures in the gas phase	68
Influence of complexation on zwitterion stability	70
Influence of complexation on collision-induced dissociation	75
Conclusions.	80

References	83
Chapter 4	
Controlling Lid Removal from a Molecular Box: Ion Molecule Reactions of Supramolecular Mixed-Metal Cucurbituril Complexes Via Electrospray Ionization	
Fourier Transform Ion Cyclotron Resonance Mass Spectrometry	87
Introduction	87
Experimental	91
Instrument	91
Materials	91
SORI-CID experiments.....	91
Reactivity experiments	92
Computational methods	92
Results	93
Formation of molecular box by electrospray.....	93
Collisional removal.....	95
Computational results	98
Chemical removal of metals by ionophores	99
Discussion	102
Collisional removal vs. chemical removal.....	102
Influence of included guests on lid removal	103
Lid repulsion effects	105
Conclusions	107

Acknowledgements	108
References	109
Chapter 5	
Cucurbit[6]uril Pseudorotaxanes: Distinctive Gas-Phase Dissociation and Reactivity	112
Introduction	112
Experimental	113
Results and Discussion	114
Electrospray of DAB with CBn	115
SORI-CID experiment	115
Reactivity experiment	118
Conclusions	120
References	121
Chapter 6	
Binding Affinities of Alkyldiammonium Ions of Various Chain Lengths for Cucurbit[6]uril in the Gas Phase Using Electrospray Ionization FT-ICR Mass Spectrometry	123
Introduction	123
Experimental	125
Instrument	125
Materials	125
SORI-CID experiments.....	126
Computational methods	126

Results and Discussion	127
Binding affinity in solution compared with the gas phase.....	127
Characteristic dissociation channels during SORI-CID	129
Conclusions	131
References	132
Chapter 7	
Summary and Perspective	134

Table of Figures

Figure 1.1	2
Figure 1.2	4
Figure 1.3	5
Figure 1.4	6
Figure 1.5	7
Figure 1.6	13
Figure 1.7	17
Figure 1.8	18
Figure 1.9	20
Figure 2.1	32
Figure 2.2	34
Figure 2.3	34
Figure 2.4	35
Figure 2.5	36
Figure 2.6	37
Figure 2.7	39
Figure 2.8	40
Figure 2.9	40
Figure 2.10	41
Figure 2.11	42
Figure 3.1	51

Figure 3.2	57
Figure 3.3	58
Figure 3.4	63
Figure 3.5	64
Figure 3.6	66
Figure 3.7	67
Figure 3.8	73
Figure 3.9	75
Figure 4.1	88
Figure 4.2	94
Figure 4.3	95
Figure 4.4	96
Figure 4.5	97
Figure 4.6	97
Figure 4.7	98
Figure 4.8	101
Figure 4.9	105
Figure 4.10	106
Figure 5.1	113
Figure 5.2	115
Figure 5.3	116
Figure 6.1	122

Figure 6.2.....	127
Figure 6.3.....	129

Table of Tables

Table 1.1.....	9
Table 1.2.....	23
Table 2.1.....	38
Table 3.1.....	52
Table 3.2.....	72
Table 4.1.....	99
Table 4.2.....	102
Table 4.3.....	106

Chapter 1

Fourier Transform Ion Cyclotron Resonance Mass Spectrometry

Introduction

The evolution of modern Fourier transform ion cyclotron resonance mass spectrometry (FT-ICR-MS) can be traced from the first ion cyclotron mass selector built by E. O. Lawrence in 1930.^{1,2} It was not until 1974, when Marshall and Comisarow first applied FT methods to previous ICR work,³ that FT-ICR-MS became an attractive analysis technique due to its advantages of speed, high resolution and effective data processing. Since then, at least 325 FT-ICR-MS instruments have been installed worldwide as of 2000,⁴ and three books, four journal special issues, and more than 65 review articles were published as of 1998.⁵

The advantages of FT-ICR-MS can be summarized as ultra high resolving power and mass accuracy, ultra high sensitivity, the capability of trapping ions for ion chemistry and photo chemistry, versatile tandem mass spectrometry techniques (CID, BIRD, ECD, SID etc.) available to determine molecular structure, and adaptability to various external ionization sources (EI, CI, FAB, ESI, MALDI etc.). Coupling FT-ICR with more recently developed ionization sources such as ESI and MALDI has dramatically intensified its application in biological supramolecular analysis.

This chapter introduces important topics dealing with FT-ICR-MS, including

principles, instrumentation, performance, and applications. Also, the electrospray ionization source is discussed in this chapter.

Principles

Ion motion in the ICR trapping cell. Figure 1.1 shows a schematic of a cubic ICR trapping cell, which is composed of trap plates, transmitter plates and receiver plates. The trapping cell is placed in a magnetic field that is perpendicular to the trapping plates. Ions are produced from the external ionization source and injected into the trapping cell. When ions are in the ICR trapping cell, three different types of ion motion occur: cyclotron motion, trapping oscillation, and magnetron motion.

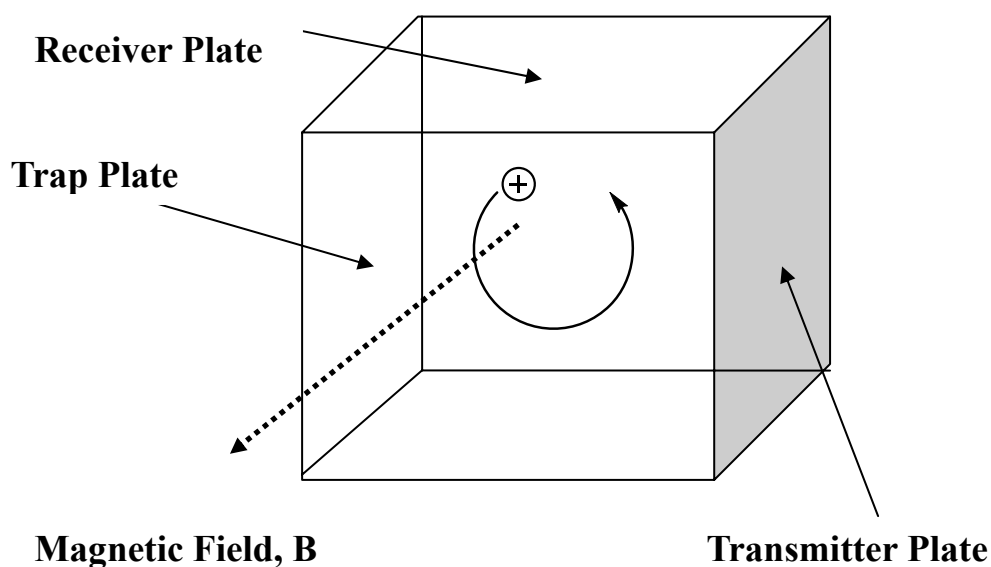


Figure 1.1: Schematic of a cubic ICR trapping cell, which is composed of trap plates (front and back), transmitter plates (left and right), and receiver plates (top and bottom). The trapping cell is placed in a magnetic field orthogonal to the trap plates.

Cyclotron Motion. When an ion with a mass m , charge q and velocity \mathbf{v} , is injected into a constant magnetic field \mathbf{B} , it is subject to the Lorentz force given by equation (1-1).

$$\text{Lorentz force } \mathbf{F} = q\mathbf{v} \times \mathbf{B} \quad (1-1)$$

The direction of the Lorentz force is perpendicular to the plane determined by the vectors \mathbf{v} and \mathbf{B} . It thus bends the path of the ion into a circle with a radius r (Figure 1.2). If the ion velocity v and circle radius r remain constant, it follows that the Lorentz force equals the centrifugal force on the ion.

$$qvB = mv^2 / r \quad (1-2)$$

Angular velocity, ω , is defined as

$$\omega = v / r \quad (1-3)$$

From equation (1-2) and (1-3), it is derived:

$$\omega_c = qB / m \quad (1-4)$$

ω_c is defined as the ion cyclotron frequency. It can be concluded from equation (1-4) that the ion's mass-to-charge ratio is inversely proportional to its cyclotron frequency, and a group of ions with a certain mass-to-charge ratio has the same cyclotron frequency independent of their velocity. Thus, accurate mass-to-charge ratio measurements can be achieved by measuring the cyclotron frequency without worrying about the translational energy distribution of the ions. Typically, ICR frequencies range from a few kHz to a few MHz, which can be easily measured using commercially available electronics.

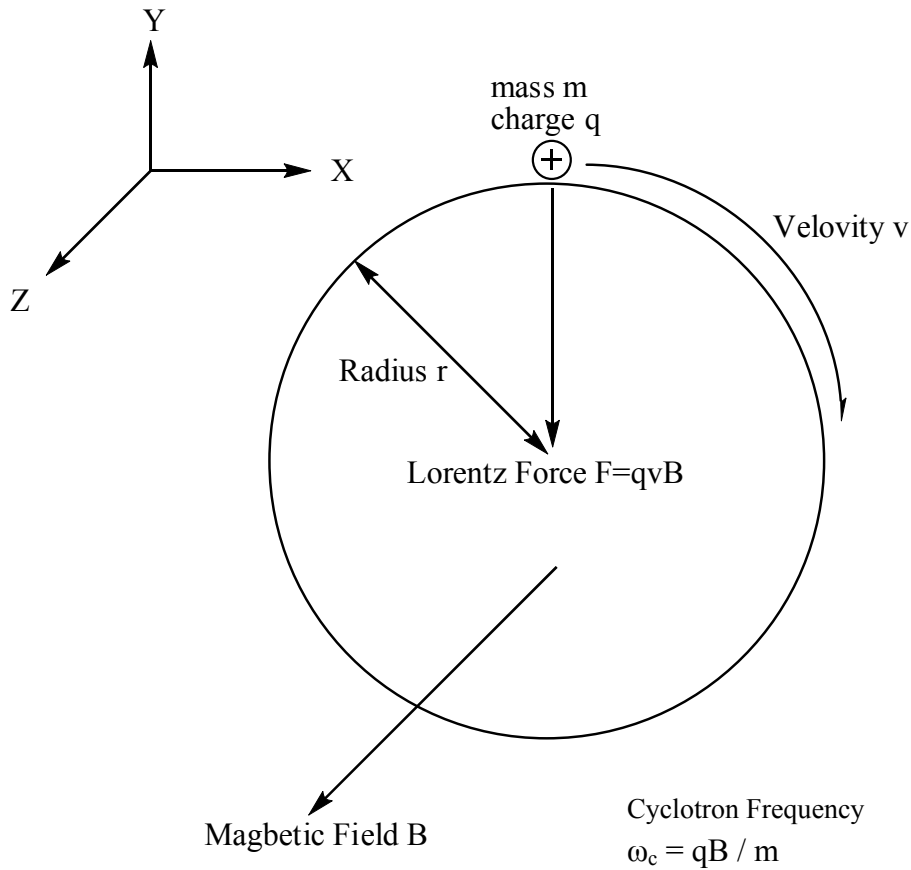


Figure 1.2: Ion cyclotron motion

Trapping Oscillation. After ions are produced in the external ionization source, they are injected into the trapping cell along the direction of the magnetic field (z direction). If no force along the z direction is applied to the ions, they will fly out of the trap cell quickly. In order to capture the ions in the trap cell, a voltage is applied on the front and back plates. Thus, ions move in harmonic oscillation along the z direction between the two trapping plates (Figure 1.3). The trapping oscillation frequency f_t , can be described using equation (1-5).

$$f_t = (2q\alpha V / mb^2)^{1/2} \quad (1-5)$$

In the equation, b is the cubic cell length, V is the trapping potential, and α is the cell

geometry factor (0.814 for the cubic cell). Typically the trapping oscillation frequency has a value of tens of kHz.

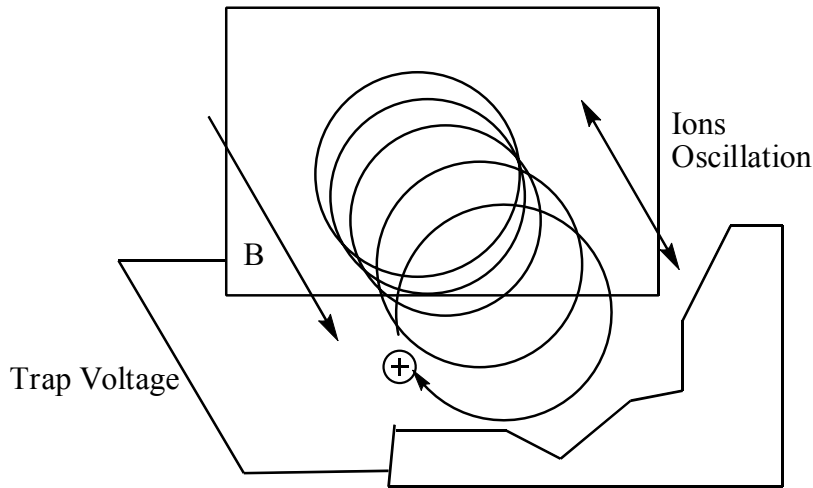


Figure 1.3: Trapping oscillation of the ion between two trap plates along the z (magnetic field) direction.

Magnetron Motion. Another fundamental ion motion in the ICR trapping cell is called magnetron motion, which results from the combination of magnetic field and radial electric field. Ideally the trap electric field has the same direction as that of the magnetic field. However the finite dimension of the trap cell results in a radial component of the trap electric field. This radial electric field produces an electrostatic force on the ion in a direction opposite to the Lorentz force, which causes a modification to the theoretical cyclotron frequency in equation (1-4). The modified cyclotron frequency ω_c' actually is a little bit lower than the unmodified ω_c , as shown in equation (1-6). ω_t is the frequency of the trap voltage in the equation.

$$\omega_c' = \omega_c/2 + [(\omega_c/2)^2 - (\omega_t/2)^2]^{1/2} \quad (1-6)$$

Figure 1.4 shows both cyclotron motion and magnetron motion in the x-y plane. The magnetron frequency is much lower than that of cyclotron motion and usually is not detected. Actually the design of the trap cell tends to eliminate magnetron motion by minimizing the radial electric field from the trap potential because this “perturbed” electric field has adverse effects such as shifting the cyclotron frequency, reducing the ion trap time, decreasing the mass resolution, hurting the mass accuracy and so on.⁶

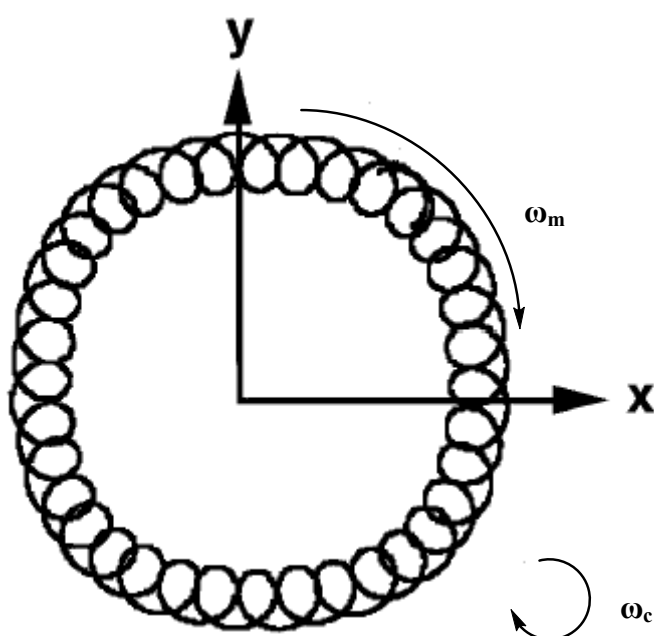


Figure 1.4: Cyclotron motion and magnetron motion in the x-y plane in the cubic trapping cell.⁶

Ion excitation and detection. Although the cyclotron frequency provides information about the ion mass-to-charge ratio, it is necessary to find a way to measure this frequency. The ion cyclotron frequency can be determined by measuring the image current produced on the receiver plates by the orbiting ions (Figure 1.5).

However, ions injected in the ICR cell have very small initial orbit radii, so they do not approach the receiver plates closely enough to produce a detectable image current. In addition, ions are randomly distributed along the cyclotron orbit. The net motion of these incoherent ions does not generate any significantly detectable signal.

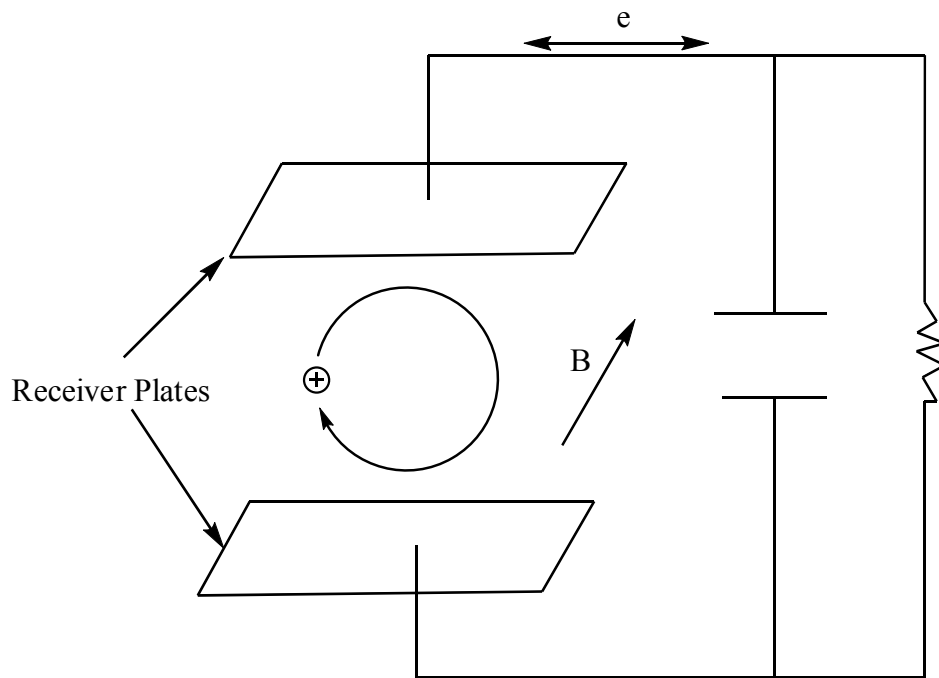


Figure 1.5: Cyclotron motion of ions can produce image current on the receiver plates that has the same frequency as the cyclotron frequency.

Thus in order to achieve a significant image current signal, a radio frequency (RF) pulse is applied to the transmitter plates (right and left plates in Figure 1.1) to accelerate ions into larger orbits. Ions that are resonant with the excitation frequency efficiently absorb RF energy. As a result, ions of the same mass-to-charge ratio are excited into a coherent packet with a larger orbit, which can produce detectable image signal on the receiver plates. The final radius of the ion packet is derived as equation



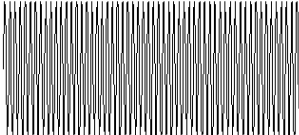
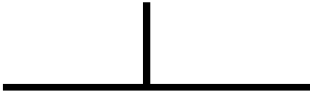
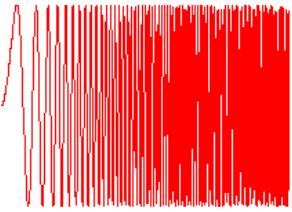

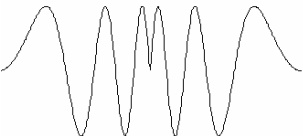



(1-7):

$$r = E_{\text{ex}} t / 2B \quad (1-7)$$

In this equation E_{ex} is the electric field induced by the excitation voltage, t is the excitation time and B is the magnetic field intensity. From the equation it is evident that the cyclotron orbit radius is independent of mass-to-charge ratio. Thus all the ions in the trap cell can be excited into the same orbit radius with a constant excitation field.

Several types of excitation pulses have been developed. Table 1.1 shows the time domain waveform, the frequency domain spectrum obtained by performing a Fourier transform on the time domain waveform, and the corresponding features for several excitation pulses. Among them, impulse excitation⁷ is one of the first methods used in FT ICR excitation, chirp excitation³ is one of the most widely used waveforms, and stored waveform inverse Fourier transform (SWIFT) excitation⁸⁻¹⁰ was introduced in 1985 by Marshall's group. SWIFT is believed to yield excitation with the greatest power uniformity as a function of frequency and the greatest frequency resolution. In addition ion excitation in the ICR cell has other applications. It is also used to eject the ions from the trap, and to add kinetic energy to the ions for collisional activation.

Table 1.1: Excitation pulses used in FT ICR mass spectrometry.¹¹

	Time Domain Waveform	Frequency Spectrum	Domain	Features
Impulse Excitation				One of the first methods used Excites a broad range of m/z Simple to generate
Single Frequency Excitation				Excites only one m/z Simple to generate
Chirp Excitation				Excites a range of m/z Simple to generate
Phase Inversion Excitation				Phase is inverted at some point during pulse Used for selective ion isolation
SWIFT Excitation				Great uniformity in excitation Highest excitation resolution Can achieve very complex excitation profiles with one pulse

FT-ICR-MS Instrumentation

FT-ICR-MS instruments are composed of four essential parts: ionization source, ICR trapping cell, magnet, and high-vacuum system. Each of them has been significantly developed since the birth of the technique.

Ionization source. FT-ICR-MS ionization can be classified into two different types. One is internal ionization, which happens within the magnetic field, in or adjacent to the ICR trap cell. The other is external ionization, which is performed outside the magnetic field.

In the early days, internal ionization dominated FT-ICR-MS instruments because it avoids the problem of injecting ions through the magnetic field fringe. Ions are produced within or very close to the trapping cell, decreasing ion loss significantly. Further, internal ionization minimizes the time distribution of the ions because they travel only a short distance before arriving at the trapping cell. Classical internal ionization sources include electron impact (EI),^{12,13} chemical ionization (CI),¹⁴ laser desorption (LD),^{15,16} and ²⁵²Cf ionization.¹⁷

However, internal ionization causes overlap of the regions where ion reaction and ionization take place. Methods such as electrospray ionization (ESI)¹⁸⁻²⁰ or matrix assisted laser desorption ionization (MALDI)^{21,22} can not be performed close to the trapping cell due to vacuum concerns. With the development of ion guide and ion cooling techniques, today most ionization sources for FT-ICR-MS are external except electron ionization and chemical ionization. For high pressure ionization sources such as ESI, external ionization allows introduction of the ions through multiple stages of

differential pumping to facilitate high vacuum in the ICR trapping cell.

ICR trapping cell. The most important and unique component of FT-ICR-MS is the ICR ion trap cell, which functions for ion storage, ion reaction, and ion detection. When ions are injected into the trapping cell, they are confined on the x-y plane by the magnetic field, with the z-direction being that of the magnetic field. The ions are constrained to orbit the magnetic field lines, and hence cannot escape along the x-y plane. To trap the ions along the z direction, an electric field along the z-axis is produced by applying potentials on the two trap plates. The transmitter and receiver electrode plates are placed in the x and y directions for ion excitation and image current detection, respectively.

Theoretically, three electric potentials are ideal for ion trapping and excitation.⁵ The first is a three-dimensional axial quadrupolar (Penning trap) potential. The Penning trap potential is ideal for ion trapping because ion cyclotron motion is independent of either other ion motions (trap oscillation or magnetron) or the position within the ion trap. The second is a two-dimensional quadrupolar potential, and the third is a one dimension dipolar potential. Both of these are ideal for linear excitation of ions in the trapping cell.

However it is extremely difficult to achieve all three types of electric potential simultaneously from a set of conductive plates. In addition, each ideal isopotential surface extends to infinity, which is not consistent with the finite size of real ion trap cells. Different configurations of ion trap have been developed to optimize the ions' trapping, excitation and detection. Figure 1.6 shows the configurations of different

ICR ion traps. The cubic cell design²³ (Figure 1.6, a) was the first to be utilized in FT-ICR-MS instruments, with three pairs of plates functioning as trap, transmitter and receiver plates, respectively. Elongated cells (rectangular cells) were also used to achieve better dynamic range because larger cell sizes may relieve space charge effects. The dual trap design²⁴ (Figure 1.6, b) consists of two adjacent traps separated by a plate with a small hole in the center to allow ion passage, while maintaining a 100-fold pressure difference between the two trap cells. The first trap cell works as a pumping stage to achieve high vacuum in the second trap cell. The closed-end cylindrical geometry^{25,26} (Figure 1.6, c) is another popular design in FT-ICR-MS instruments due to its nice fit in the bore of a superconducting solenoid magnet. Two novel designs have been developed recently based on the cylindrical ion trap. The “Infinity” trap²⁷ (Figure 1.6, d) was built in 1991 by segmenting the end caps of a closed cylindrical trap to simulate the potential of an infinitely extended cylindrical trap. Another trap design, which is widely used today, is the open cylindrical trap,^{28,29} in which the closed end caps are replaced by cylinders (Figure 1.6, e). The open cylindrical trap has the advantages that ions can access the trap more easily, and capacitive coupling between the central and end cap cylinder can effectively optimize the excitation and detection potentials in the central trap. More recently the matrix-shimmed trap³⁰ (Figure 1.6, f) has been designed, in which each side of a cubic trap is cut into multiple segments and optimized voltages are applied on each segment electrode to achieve near-perfect potentials in the ICR trap center.

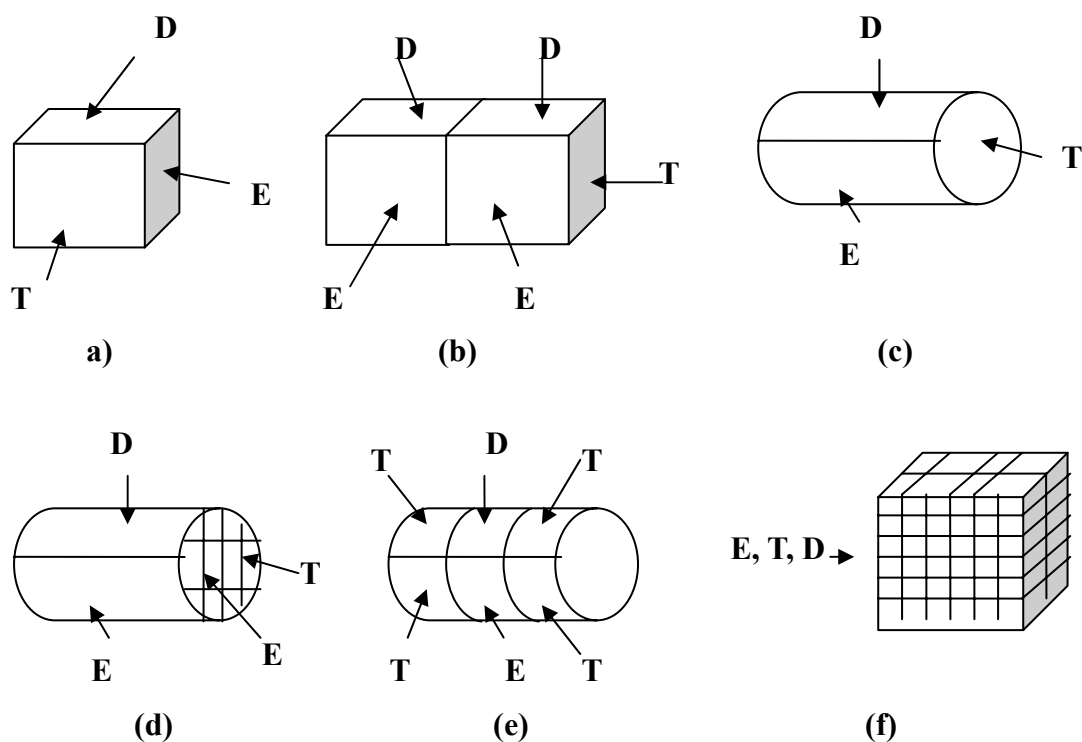


Figure 1.6: ICR ion trap configurations. E – Excitation, D – Detection, T – Trapping. (a) Cubic trap, (b) Dual trap cell, (c) Cylinder trap, (d) Infinity trap (e) Open cylinder trap (f) Matrix-shimmed trap.⁵

Magnet. The magnet is probably the highest-cost part in today’s FT-ICR-MS instrument. High magnetic field is desirable because several performance factors such as resolving power, signal-to-noise ratio, and upper mass limit improve with increasing magnetic field strength.³¹ Thus increasing the magnetic field has been an important way to increase the capability of FT-ICR instruments. Magnetic field strength has increased from 1.4 T in the mid 1960s to 11.5 T³² and even 25 T in 2000.³³ Superconducting magnets have been preferred for FT-ICR-MS due to their high strength and stable field. Modern superconducting solenoids can produce an elongated homogenous magnetic field region with an inner diameter of 150-220 mm,

which can hold a larger trap cell inside, decreasing the space charge effect within the ion trap, and improving the dynamic range of the instrument.

High-vacuum system. Ultra-high vacuum, $10^{-8} - 10^{-9}$ Torr, is required during ion excitation and detection in the ICR trap cell to achieve high resolving power and mass accuracy. High vacuum is preferable because collisions between the ion packet and air molecules can result in a loss of coherent motion, decreasing the performance of the instrument. Usually three or four differential pumping stages are performed between an external ionization source and the trapping cell. High-capacity pumps ($10^4 - 10^5$ liters/sec) such as cryogenic pumps or turbomolecular pumps are utilized to achieve ultra-high vacuum in FT-ICR-MS instruments.

FT-ICR-MS Performance

The performance of FT-ICR-MS can be evaluated in terms of resolving power, mass accuracy, mass range and dynamic range.

Resolving power. Resolving power or resolution is the ability of the mass analyzer to distinguish two adjacent mass peaks. Mathematically it can be defined as in equation (1-8)³⁴:

$$R_p = 1 / R = m / \delta m = qB\tau / 2m \quad (1-8)$$

In which R_p is the resolving power, R is the resolution, m is the ion mass, q is the ion charge, B is the magnetic field strength, and τ is the signal decay constant. The equation indicates that higher resolving power can be achieved by applying higher

magnetic field or longer signal acquisition time. The equation also shows resolving power is inversely proportional to the ion mass.

One of the most prominent advantages of FT-ICR-MS is its ultra-high resolving power, which is usually many orders of magnitude better than that achieved by any other mass analyzer. Today FT-ICR-MS still retains the world record for highest resolving power: 200,000,000, for singly-charged ^{40}Ar and ^3He ,³⁵ and 8,000,000, for electrosprayed multiply-charged bovine ubiquitin at a mass of 8.6 kDa.³⁶

Mass accuracy. High mass accuracy is essential for unknown molecule determination. Mathematically, mass accuracy is the relative difference between actual mass and measured mass of the ion, and can be defined as in equation (1-9) in the unit of parts per million:

$$\text{Mass Accuracy (ppm)} = \left| m_{\text{actual}} - m_{\text{measured}} \right| / m_{\text{aver}} \times 10^6 \quad (1-9)$$

The lower the value is, the higher the mass accuracy. The highest mass accuracy reported using FT-ICR-MS is 0.5 ppm over 90-300 Da in 1998.³⁷

Mass accuracy to some extent relates to the mass resolution of the instrument. High mass resolution can not guarantee high mass accuracy, but low mass resolution can hurt mass accuracy.

High mass accuracy can be achieved by accurate determination of the cyclotron frequency. However, perturbation of the cyclotron frequency can be caused by radial electric fields and space charge effects. Other perturbation factors such as magnetic field inhomogeneity are not significant with superconducting magnets. Considering the error in radial electric field and space charge effects, the mass-frequency

relationship in FT-ICR-MS can be calibrated as equation (1-10):³⁸

$$m = qB / 2\pi f - 2qG_t V_{\text{eff}} / 4\pi f^2 = a / f + b / f^2 \quad (1-10)$$

In this equation G_t is the trap geometry factor, V_{eff} is the effective trapping potential, and a and b are constants. Internal calibration also can be utilized to achieve high mass accuracy by introducing a calibrant reference compound such as perfluorotributylamine.

Mass range. The mass range of FT-ICR is decided by the lower and upper mass limits. Based on the cyclotron equation (1-4), the lower the mass, the higher the frequency it produces. Thus the lower mass limit is mostly decided by limitations of the detection electronics because of the Nyquist criterion (the sampling rate must be at least twice as fast as the measured frequency). With the higher capabilities of modern electronics, the lower mass limit usually is not a significant problem.

The upper mass limit of FT-ICR-MS is determined by factors such as the trap dimension and the radial electric field of the trapping potential.

Trap dimension limit. An ion has to be trapped within the trap cell to be excited and detected, so the cyclotron radius of the ion can not be larger than the trap cell dimensions. The upper mass limit is given by equation (1-11):

$$m_{\text{upper}} = q^2 B^2 r_t / 2kT \quad (1-11)$$

In this equation q is the charge, B is the magnetic field strength, r_t is the trap cell diameter, and kT gives the thermal translational energy. Based on equation (1-11), if the magnetic field strength and temperature are constant, the upper mass limit can be increased by enlarging the trap cell diameter. However, the diameter of the trap cell is

usually decided by the size of the superconducting solenoid. Figure 1.7 shows the relationship between ion cyclotron radius and mass-to-charge ratio at different magnetic field strengths. It is evident that heavy ions can be confined within a smaller radius under higher magnetic field.

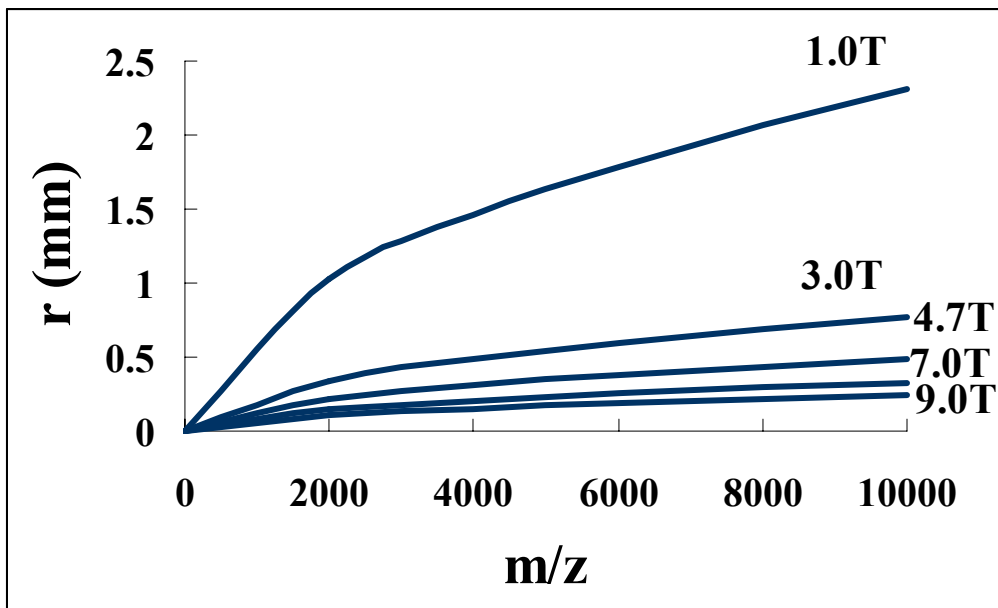


Figure 1.7: Relation between ion ICR radius and mass-to-charge ratio at different magnetic field strengths.⁵

Radial electric field of trap potential limit. I have already described how a nonideal trap potential results in a radial electric field, which produces an outward electric force on the ions. When this outward force is stronger than the inward Lorentz force, ions will be ejected from the trap cell. Thus, the critical mass related to trapping potential can be summarized in equation (1-12):

$$m_c = qB^2r^2 / 8V_{\text{eff}}\alpha \quad (1-12)$$

In this equation q is the ion charge, B is the magnetic field strength, r is the cell

diameter, V_{eff} is the effective trap potential, and α is the cell geometry constant. Figure 1.8 gives the relationship between upper mass limit and trap potential at different magnetic field strengths. Higher magnetic field strengths result in higher upper mass limits.

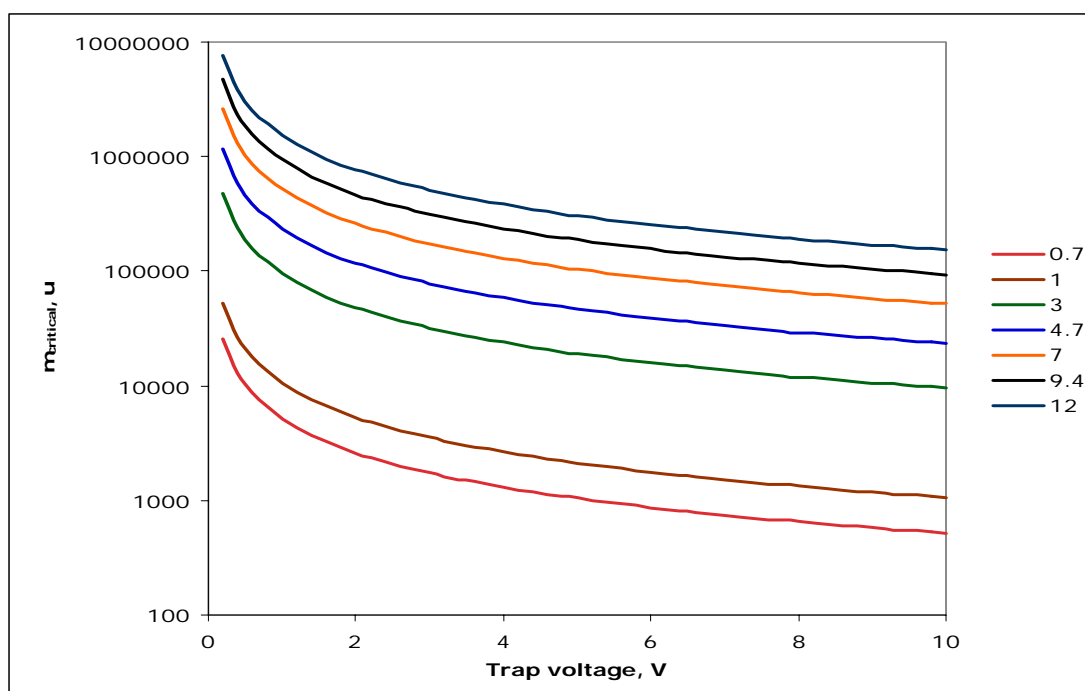


Figure 1.8: Upper mass limit of a singly-charged ion in an ICR trap at several magnetic field strengths.⁵

Additionally, space charge effects would decrease the upper mass limit. Electro spray ionization methods to some extent increase the upper mass limit for FT-ICR detection because this ionization can produce multiply-charged ions.

Dynamic range. Dynamic range can be defined as the difference between the maximum and minimum number of ions that can be detected without signal distortion. Compared to other types of mass spectrometry (i.e., magnetic sector), FT-ICR-MS has

a relative lower dynamic range of about $10^3 - 10^4$. Space charge effects are the most significant factor that limits the dynamic range when abundant ions are trapped in the analysis cell. In order to increase the dynamic range, methods such as suspended trapping have been utilized to selectively remove more abundant components.³⁹

Selected FT-ICR-MS Applications

Electrospray Ionization. In 1984, Yamashita and Fenn et al. introduced electrospray ionization methods into mass spectrometry. The detailed mechanism of electrospray has not been elucidated. One generally accepted description of the electrospray process,^{40,41} known as “ion evaporation,” is presented as shown in Figure 1.9. For generation of positive ions, analyte solution is pumped through a capillary on which a high voltage is applied. The liquid sprays from the capillary tip, and is drawn out into a so-called “Taylor cone” with positive charges accumulating at the surface. When the surface tension is exceeded by the applied electrostatic force, droplets containing an excess of positive charge detach from the tip. These charged droplets are drawn toward the orifice because of electrostatic potential and pressure gradients. “The droplets gradually shrink due to solvent evaporation and collision with surrounding molecules, and eventually reach the Rayleigh limit—the point at which the magnitude of the charge is sufficient to overcome the surface tension holding the droplet together.”⁴¹ Then the droplets experience fission (“Coulombic explosion”), and are divided into smaller droplets. This process occurs repeatedly. Droplets

become more numerous and smaller, and finally become single gaseous ions.

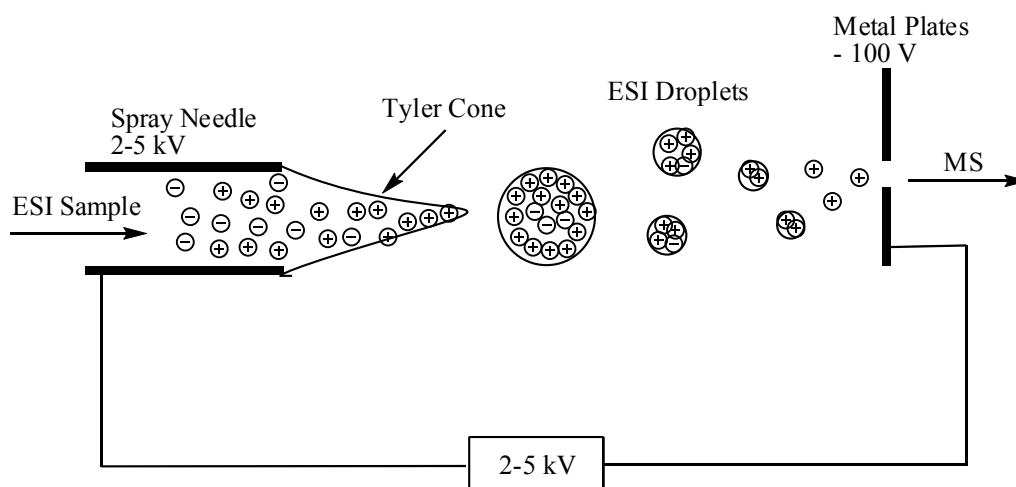


Figure 1.9: Schematic of electro spray ionization with an “ion evaporation” process.⁴¹

Electrospray ionization can not only easily bring thermally labile molecules into the gas phase, but also produces multiply-charged ions, which extends the mass range of the measurement. Electrospray also provides an interface between separation techniques such as liquid chromatography (LC) and mass spectrometry to achieve effective analysis of complex mixtures. Coupling FT-ICR-MS with electrospray ionization has brought extensive applications in characterizing biological supramolecules, host-guest complexes, petroleum mixtures, medicines and so on.

Tandem mass spectrometry using FT-ICR-MS. FT-ICR-MS has powerful analysis capability not only due to its ultrahigh mass accuracy and ultrahigh resolving power but also due to its versatile tandem mass spectrometry capabilities (MS^n). Specifically, during MS^n ions are trapped in the cell and activated / dissociated in

different ways into secondary ions. Secondary ions are analyzed to determine the structure of complex molecules. Table 1.2 shows a few activation / dissociation techniques for FT-ICR-MSⁿ. During SORI-CID,⁴² an off-resonant RF pulse is applied to the ions to mildly activate the ions in the trap cell, followed by leaking neutral molecules (typically air) into the trap cell to collide with parent ions. Collisions produce secondary ions, which give structural information about the parent ions. SID⁴³ is performed by generating ions outside the trap and then accelerating them to strike the end cap of the trap cell to produce ion fragments. Typically SID is efficient only for a narrow range of initial ion kinetic energies. UVPD¹⁵ and IRMPD⁴⁴ can heat ions to dissociation using lasers. No collision gas is required for either of these techniques. BIRD⁴⁵ has proven to be a quantitative slow-heat dissociation technique, which has been used for biological noncovalent complexes. Most recently ECD⁴⁶ was developed for protein dissociation by capture of low-energy electrons (< 1eV). ECD is able to cause different characteristic peptide fragmentation from CID, which thus provides complimentary structural information about proteins.

Table 1.2: Activation / Dissociation techniques for tandem FT-ICR mass spectrometry

SORI-CID ⁴²	Sustained Off-Resonance Irradiation- Collision Induced Dissociation
SID ⁴³	Surface Induced Dissociation
UVPD ¹⁵	Ultraviolet Photodissociation
IRMPD ⁴⁴	Infrared Multiphoton Photodissociation
BIRD ⁴⁵	Blackbody Infrared Radiative Dissociation
ECD ⁴⁶	Electron Capture Dissociation

Host-guest interactions in the gas phase. Host-guest interactions have been well studied to obtain fundamental insights into supramolecular chemistry.^{47,48} Electrospray mass spectrometry has been widely used to investigate host-guest interactions in the gas phase.⁴⁹⁻⁵³ A particular advantage of gas phase host-guest research is that the experimental results can be directly compared to computational results because complicating interferences from solvents are not present. FT-ICR-MS can trap the ion in the cell for a long time, and is ideal to investigate ion reaction and dissociation behaviors. Our group has focused on characterization of macrocyclic molecules in the gas phase using electrospray FT-ICR-MS. Progress has been published in a number of papers.⁵⁴⁻⁶³

Proteomics. Analysis of the proteins present in organisms, tissues or cells has been a challenge due to the large number of proteins and the complexity of the

samples. FT-ICR-MS coupled with separation techniques such as liquid chromatography (LC) or capillary electrophoresis (CE) has become an effective analytical tool for protein analysis due to its ultrahigh mass accuracy and resolving power. Some of the work in proteomics has been reviewed in a recent paper.⁶⁴

Usually two strategies are utilized for protein analysis. One is the “bottom up” approach, which is performed by cleaving the protein molecules into peptide fragments. Mass analysis of the peptide fragments can then yield protein identification. Peptide fragments can be produced by either enzymatic digestion or tandem mass spectrometry such as CID or ECD. The other approach is “top down”, which introduces the intact protein into the instrument (facilitating direct determination of the molecular weight) followed by fragmentation in the instrument to determine the sequence. “Top down” approaches are limited by the mass range of FT-ICR-MS.

Petroleomics. Marshall and Rodgers have utilized FT-ICR-MS to analyze petroleum crude oil without any sample preparation.⁶⁵ Crude oil contains more than 20,000 elemental compositions. The ultrahigh-resolution of FT-ICR-MS is required to resolve the compositions. However, high resolution itself is not enough to fulfill the requirements of petroleum analysis. High-magnetic field (9.4 T) and a front end mass filter are used to extend the mass range and dynamic range of the instrument, respectively. Mathematical plots are further utilized to analyze the complex components in the crude oil samples.

References

- (1) Lawrence, E. O.; Edlefsen, N. E. *Science* **1930**, 72, 376.
- (2) Lawrence, E. O.; Livingston, M. S. *Phys. Rev.* **1932**, 40, 19.
- (3) Comisarow, M. B.; Marshall, A. G. *Chem. Phys. Lett.* **1974**, 25, 282.
- (4) Marshall, A. G. *Int. J. Mass Spectrom.* **2000**, 200, 331-356.
- (5) Marshall, A. G.; Hendrickson, C. L.; Jackson, G. S. *Mass Spectrom. Rev.* **1998**, 17, 1-35.
- (6) Wood, T. D.; Marshall, A. G.; Schweikhard, L. *Rapid Commun. Mass Spectrom.* **1994**, 8, 14-21.
- (7) McIver R. T., B. G., Hunter R. L. *Int. J. Mass Spectrom* **1989**, 89, 489-491.
- (8) Marshall, A. G.; Wang, T. C.; Ricca, T. L. *J. Am. Chem. Soc.* **1985**, 107, 7893-7897.
- (9) Goodman, S., Hanna, R.: U.S. Patent, **1986**, No. 4945234.
- (10) Guan, S.; Marshall, A. G. *Anal. Chem.* **1993**, 65, 1288-1294.
- (11) Dearden, D. V. FT-ICR-MS Tutorial Presentation.
- (12) Irion, M. P.; Bowers, W. D.; Hunter, R. L.; Rowland, F. S.; McIver, R. T., Jr. *Chem. Phys. Lett.* **1982**, 93, 375-379.
- (13) Carlin, G. J.; Freiser, B. S. *Anal. Chem.* **1983**, 55, 955.
- (14) Ghaderi, S.; Kulkarni, P. S.; Ledford, E. B.; Wilkins, C. L.; Gross, M. L. *Anal. Chem.* **1981**, 53, 428.
- (15) Bowers, W. D.; Delbert, S. S.; Hunter, R. L.; McIver, R. T. *J. Am. Chem. Soc.* **1984**, 106, 7288.

- (16) McCrery, D. A.; Gross, M. L. *Anal. Chim. Acta.* **1985**, *178*, 91.
- (17) Tabet, J. C.; Rapin, J.; Porteti, M.; Gaumann, T. *Chimia* **1986**, *40*, 169.
- (18) Henry, K. D.; Williams, E. R.; Wang, B. H.; McLafferty, F. W.; Shabanowitz, J.; Hunt, D. F. *Proc. Natl. Acad. Sci., U.S.A.* **1989**, *86*, 9075.
- (19) Winger, B. E.; Light-Wahl, K. J.; Ogorzalek Loo, R. R.; Udseth, H. R.; Smith, R. D. *J. Am. Soc. Mass Spectrom.* **1993**, *4*, 536-545.
- (20) Beu, S. C.; Senko, M. W.; Quinn, J. P.; McLafferty, F. W. *J. Amer. Soc. Mass Spectrom.* **1993**, *4*, 190-192.
- (21) Hettich, R. L.; Buchanan, M. V. *Int. J. Mass Spectrom. Ion Proc.* **1991**, *111*, 365-380.
- (22) Koster, C.; Castoro, J. A.; Wilkins, C. L. *J. Am. Chem. Soc.* **1992**, *114*, 7572-7574.
- (23) Comisarow, M. B. *Int. J. Mass Spectrom. Ion Phys.* **1981**, *37*, 251.
- (24) Littlejohn, D. P.; Ghaderi, S.: USA Patent, **1986**, No. 4581533.
- (25) Comisarow, M. B.; Marshall, A. G.: USA Patent, 1976.
- (26) Lee, S. H.; Wanczek, K. P.; Hartmann, H. *Adv. Mass Spectrom.* **1980**, *8B*, 1645.
- (27) Caravatti, P.; Allemann, M. *Org. Mass Spectrom.* **1991**, *26*, 514-518.
- (28) Dabrielse, G.; Haarsma, L.; Rolston, S. L. *Int. J. Mass Spectrom. Ion Process* **1989**, *88*, 319.
- (29) Beu, S. C.; Laude, D. A. *Int. J. Mass Spectrom. Ion Proc.* **1992**, *112*, 215-230.

- (30) Jackson, G. S.; White, F. M.; Guan, S.; Marshall, A. G. *J. Am. Soc. Mass Spectrom.* **1999**, *10*, 759.
- (31) Marshall, A. G.; Guan, S. *Rapid Commun. Mass Spectrom.* **1996**, *10*, 1819.
- (32) Gorshkov, M. V.; Pasa Tolic, L.; Udseth, H. R.; Anderson, G. A.; Huang, B. M.; Bruce, J. E.; Prior, D. C.; Hofstadler, S. A.; Tang, L.; Chen, L.-Z.; Willett, J. A.; Rockwood, A. L.; Sherman, M. S.; Smith, R. D. *J. Am. Soc. Mass Spectrom.* **1998**, *9*, 692-700.
- (33) Shi, S. D.; Drader, J. J.; L., H. C.; Marshall, A. G. *J. Am. Soc. Mass Spectrom.* **1999**, *10*, 265.
- (34) Marshall, A. G.; Comisarow, M. B.; Parisod, G. *J. Chem. Phys.* **1979**, *71*, 4434-4444.
- (35) Marshall, A. G.; Schweikhard, L. *Int. J. Mass Spectrom. Ion Proc.* **1992**, *118/119*, 37-70.
- (36) Shi, S. D.; Hendrickson, C. L.; Marshall, A. G. *Proc. Natl. Acad. Sci., U.S.A.* **1998**, *95*, 11532.
- (37) Rodgers, R. P.; Andersen, K. V.; White, F. M.; Hendrickson, C. L.; Marshall, A. G. *Anal. Chem.* **1998**, *70*, 4743.
- (38) Ledford, E. B.; Rempel, D. L.; Gross, M. L. *Anal. Chem.* **1984**, *56*, 2744-2748.
- (39) Bruce, J. E.; Anderson, G. A.; Smith, R. D. *Anal. Chem.* **1996**, *68*, 534-541.
- (40) Fenn, J. B. *J. Am. Soc. Mass Spectrom.* **1993**, *4*, 524-535.
- (41) Cech, N. B.; Enke, C. G. *Mass Spectrum. Rev.* **2001**, *20*, 362-387.

- (42)Gauthier, J. W.; Trautman, T. R.; Jacobson, D. B. *Anal. Chim. Acta* **1991**, *246*, 211-225.
- (43)Castoro, J. A.; Nuwaysir, L. M.; Ijames, C. F.; Wilkins, C. L. *Anal. Chem.* **1992**, *64*, 2238-2243.
- (44)Little, D. P.; Chorush, R. A.; Speir, J. P.; Senko, M. W.; Kelleher, N. L.; McLafferty, F. W. *J. Am. Chem. Soc.* **1994**, *116*, 4893-4897.
- (45)Dunbar, R. C.; McMahon, T. B. *Science* **1998**, *279*, 194-197.
- (46)Xu, L. X.; Huang, Y. L.; Giese, R. W. *Journal of Mass Spectrometry* **1998**, *33*, 615-620.
- (47)Cram, D. J.; Cram, J. M. *Science* **1974**, *183*, 803-809.
- (48)Schneider, H. J. *Angew. Chem. Int. Ed. Engl.* **1991**, *30*, 1417-1436.
- (49)Vincenti, M. *J. Mass Spectrom.* **1995**, *30*, 925-939.
- (50)Brodbelt, J. S.; Dearden, D. V. In *Physical Methods in Supramolecular Chemistry*; Davies, J. E. D., Ripmeester, J. A., Eds.; Pergamon: Oxford, 1996; Vol. 8, pp 567-591.
- (51)Dearden, D. V. In *Physical Supramolecular Chemistry*; Echegoyen, L., Kaifer, A. E., Eds.; Kluwer: Dordrecht, the Netherlands, 1996, pp 229-247.
- (52)Dearden, D. V.; Zhang, H.; Chu, I.-H.; Wong, P.; Chen, Q. *Pure Appl. Chem.* **1993**, *65*, 423-428.
- (53)Vincenti, M.; Pelizzetti, E.; Dalcanale, E.; Soncini, P. *Pure Appl. Chem.* **1993**, *65*, 1507-1512.
- (54)Dearden, D. V.; Chu, I.-H. *J. Incl. Phenom. Mol. Recognit. Chem.* **1997**, *29*,

269-282.

(55) Kellersberger, K.; Dearden, D. V. In *46th ASMS Conference on Mass Spectrometry and Allied Topics*; ASMS: Orlando, FL, 1998, p 844.

(56) Kellersberger, K. A.; Dejsupa, C.; Liang, Y.; Pope, R. M.; Dearden, D. V. *Int. J. Mass Spectrom.* **1999**, *193*, 181-195.

(57) Kellersberger, K.; Dearden, D. V. In *47th ASMS Conference on Mass Spectrometry and Allied Topics*; American Society for Mass Spectrometry: Dallas, TX, 1999.

(58) Liang, Y.; Dearden, D. V. In *46th ASMS Conference on Mass Spectrometry and Allied Topics*; ASMS: Orlando, FL, 1998, p 845.

(59) Liang, Y.; Bradshaw, J. S.; Izatt, R. M.; Pope, R. M.; Dearden, D. V. *Int. J. Mass Spectrom.* **1999**, *185/186/187*, 977-988.

(60) Shen, N.; Pope, R. M.; Dearden, D. V. *Int. J. Mass Spectrom.* **2000**, *195-196*, 639-652.

(62) Dearden, D. V.; Liang, Y.; Nicoll, J. B.; Kellersberger, K. A. *J. Mass Spectrom.* **2001**, *36*, 989-997.

(63) Zhang, H.; Paulsen, E. S.; Walker, K. A.; Krakowiak, K. E.; Dearden, D. V. *J. Am. Chem. Soc.* **2003**, *125*, 9284-9285.

(64) Bogdanov, B.; Smith, R. D. *Mass Spectrom. Rev.* **2005**, *24*, 168-200.

(65) Marshall, A. G.; Rodgers, R. P. *Acc. Chem. Res.* **2004**, *37*, 53-59.

Chapter 2

Cucurbiturils: New Developments in Host-Guest Chemistry

Introduction

Cucurbiturils are cyclic polymers of glycoluril. The name derives from the Latin for “pumpkin” due to the pumpkin shape of these molecules. Although the first cucurbituril molecule was synthesized in 1905, it is not until 1981 that the chemical nature and structure were fully characterized by Mock and coworkers.¹

Host-guest interactions have been well studied to obtain fundamental insights into supramolecular chemistry.^{2,3} Receptors such as cyclodextrins, crown ethers and calixarenes have been well developed in this field. Recently, interest has turned to the cucurbituril family due to its rigid structure, wide size-range and high binding selectivity.

Cucurbit[6]uril (CB6), the most common of the cucurbituril family, was originally synthesized by reaction of glycoluril and formaldehyde under acidic conditions. Mock and co-workers were first to determine that CB6 is a macrocyclic hexamer composed of six glycoluril rings.¹ CB6 has a hydrophobic cavity with a diameter of 5.8 Å, accessible via two carbonyl-lined portals of 3.9 Å diameter.

CB6 is a rigid host with many potential applications, but compared to other macrocyclic molecules such as cyclodextrins, cucurbiturils have problems that limited application development in the beginning. These problems include poor aqueous

solubility, limited available size range, and relatively high cost.

However, recently most of the major problems have been either partially or completely resolved. First, CB6 has been found to be soluble not only in strongly acidic solutions, but also in aqueous solutions of alkali metal ions due to coordination of the metal ions to the electronegative portals. Second, new cucurbituril homologues, CB5-CB10, were synthesized and isolated by Kim and co-workers in 2000,⁴ which dramatically expanded the available size range of the cucurbituril family as a macrocyclic host molecule. Further, syntheses of cucurbituril derivatives such as decamethylcucurbit[5]uril⁵ and diphenylcucurbit[6]uril⁶ made more flexible cucurbituril hosts. Finally cucurbiturils have been produced in larger scale and CB5-CB8 are now commercially available. As a result, the cucurbituril family has been the focus of a large number of publications^{5,7-30} in the last ten years.

As macrocyclic hosts with electronegative portals, cucurbiturils are ideal for binding with positive ions. Mock and co-workers first characterized the structures of non-covalently bound complexes of CB6 and alkyldiammonium ions in solution.³¹ Alkyldiammonium ions thread through the hollow CB6 cavity to form pseudorotaxane complexes. Also Dearden et al. had proved that alkyldiammonium ions form pseudorotaxanes with CB6 in the gas phase using electrospray FT mass spectrometry.³²

With the synthesis of different cucurbituril homologues and derivatives, more types of guests can be bound or captured by cucurbiturils. Dearden et al. observed the encapsulation of small guest molecules such as N₂, O₂, methanol or acetonitrile in

decamethylcucurbit[5]uril (mc5) with two ammonium ions attached on the portals as “molecular box lids” using electrospray FT mass spectrometry.³³ Interestingly ethanol molecules can not be captured inside the mc5 cavity, which indicates the high size selectivity of this host molecule. Recently amino acids, peptides, small proteins, DNA,^{20,34} and small drug molecules²⁶ have been observed to form complexes with cucurbiturils or their derivatives. The hollow cavity of CB8 is even large enough to hold another host molecule such as cyclen, which can bind with an additional guest (Cu^{2+} , Zn^{2+}), to form nested “Russian doll” complexes.²⁸ Today application of the cucurbituril family has expanded into numerous areas such as drug delivery, gas purification, reaction catalysis, gene carriers, molecular machines, and so on.

This chapter will begin by describing cucurbituril synthesis, structure and chemical and physical properties. Next, emphasis will be given to the host–guest chemistry of the cucurbituril family. Finally, applications of cucurbituril host molecules will be briefly discussed.

Synthesis, Structure, and Properties

Synthesis. In 1905, CB6 was synthesized by the reaction of glycoluril and formaldehyde in concentrated sulfuric acid at a fairly high temperature ($>110\text{ }^{\circ}\text{C}$). No other homologues were found at that time. Ninety-five years later, Kim’s and Day’s groups found CB5-CB8 and CB5@CB10 can be produced at a lower synthesis temperature ($75\text{-}90\text{ }^{\circ}\text{C}$) (Figure 2.1).^{4,35} However the mechanism of the synthesis

reaction is still not clear.

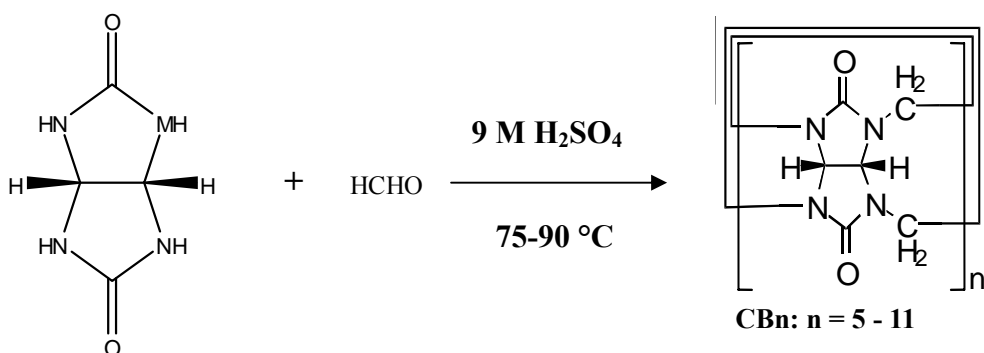


Figure 2.1: Synthesis of CBn, n = 5 – 11.

Structures and Properties. Crystal structures of cucurbituril homologues have been fully characterized by Kim's and Day's groups (Figure 2.2).^{4,35,36} Electronegative carbonyl groups line the cucurbituril portals, which makes these molecules selective to bind with positive ions. The hydrophobic hollow cavity can capture either positive or neutral guests inside.

Figure 2.3 shows the dimensional parameters of cucurbituril homologues. From CB5 to CB8, the hollow cavity diameters increase from 4.4 to 8.8 Å and portal sizes increase from 2.4 to 6.9 Å. It makes sense that larger cucurbituril homologues are able to bind larger guest molecules inside. Figure 2.4 lists the typical guest molecules that can be included inside CBn homologues.³⁷

In terms of cavity size, CB6, CB7 and CB8 are analogous to α -, β -, and γ -cyclodextrins (CDs), respectively. Although the cavity sizes of CBn and CDs are comparable, there are distinct binding differences because of the structural differences. CBn have a symmetric geometry with two identical openings that are lined with electronegative carbonyl groups. However, CDs have a less symmetric geometry with

one opening to the interior lined with primary hydroxyl groups; the other opening is lined with secondary hydroxyls.^{38,39} The carbonyls of CBn act as electronegative sites favorable for binding positive ions; they are also good hydrogen bond receptors. The hydroxyl groups that line the CDs' portals can also bind cations, but function both as hydrogen bond donors and as acceptors. Further, the CDs' molecular scaffold is much more flexible than that of the CBn species, particularly on the side that consists of secondary hydroxyl groups.

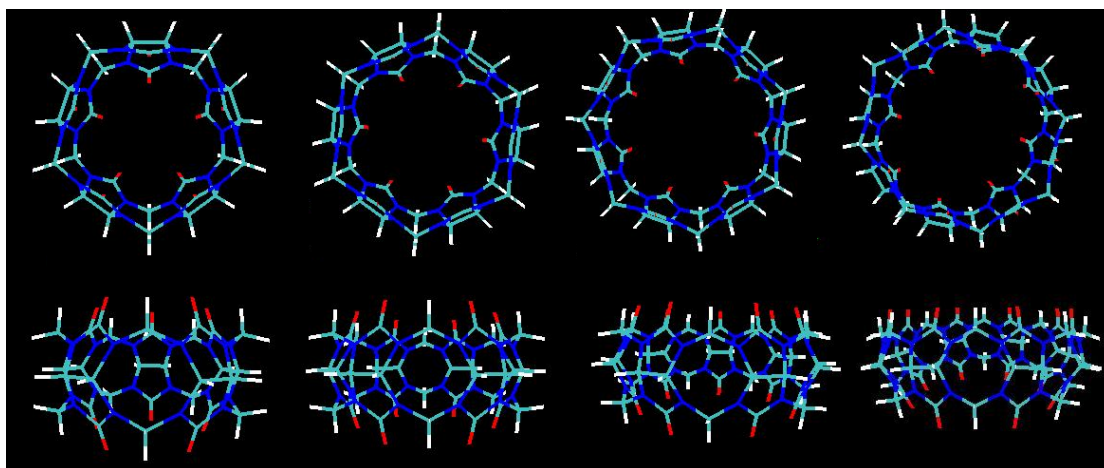
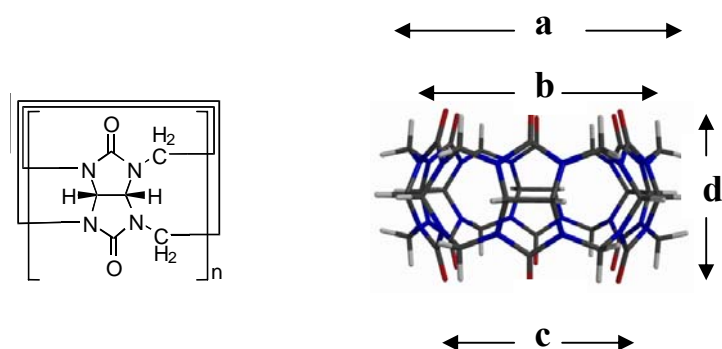


Figure 2.2⁴: X-ray crystal structures of CBn (n = 5 – 8). White: H; Blue: N; Red: O.



	CB5	CB6	CB7	CB8
Outer diameter a (Å)	13.1	14.4	16.0	17.5
Inner cavity size b (Å)	4.4	5.8	7.3	8.8
Portal size c (Å)	2.4	3.9	5.4	6.9
Height d (Å)	9.1	9.1	9.1	9.1
Cavity Volume (Å³)	82	164	279	479

Figure 2.3⁴: Dimensional parameters of CBn (n = 5 – 8).

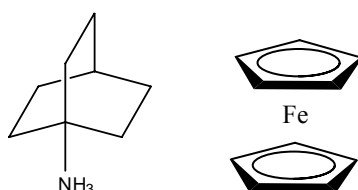
CB5: N₂, O₂, Xe, Ar, MeOH, EtOH

CB6: α,ω-alkyldiammonium ions (H₃N⁺(CH₂)_nNH₃⁺, n=3-10)

[Lysine + 2H]²⁺, [Arginine + 2H]²⁺,

THF, Benzene

CB7:



CB8: [2Lysine + 3H]³⁺, [2Arginine + 3H]³⁺,

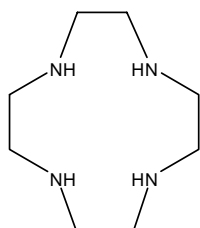


Figure 2.4³⁷: Typical Guest molecules included inside CB_n (n = 5-8).

One of the problems that limits the application development of cucurbiturils is their poor solubility in water. CB₆ and CB₈ are essentially not soluble, whereas CB₇ and CB₅ have modest solubility in water ($2-3 \times 10^{-2}$ M).³⁷ Generally the solubility of cucurbiturils is lower than that of cyclodextrins in water. However the carbonyl groups lining the portals of CB_n cause them to act as weak bases. As a result the solubility of CB_n dramatically increases in concentrated acidic solutions or aqueous solutions with alkali metal ions.

CB_n homologues have a relatively high thermal stability. No decomposition is

observed up to 420 °C for CB5, CB6 or CB8. CB7 decomposes at a lower temperature of 370 °C³⁶

Host-Guest Chemistry of the Cucurbituril Family

CB6 with Alkylammonium. In the pioneering work of Mock and coworkers, the host guest chemistry between CB6 and alkylammonium was investigated using NMR or UV spectral perturbations.³¹ Alkyldiammonium ions were deduced to be threaded through the CB6 hollow cavity due to hydrophobic interactions and charge-dipole attractions.

Recently Dearden's group has electrosprayed CBn (n = 5-8) with diaminobutane (DAB) from acidic solution and various complexes were observed in the gas phase (Figure 2.5).³² CB5 forms a lidded molecular box, whereas CB6, CB7, and CB8 form pseudorotaxanes. Host-guest chemistry between CB6 and alkyldiammonium ions will be discussed in Chapter 5.

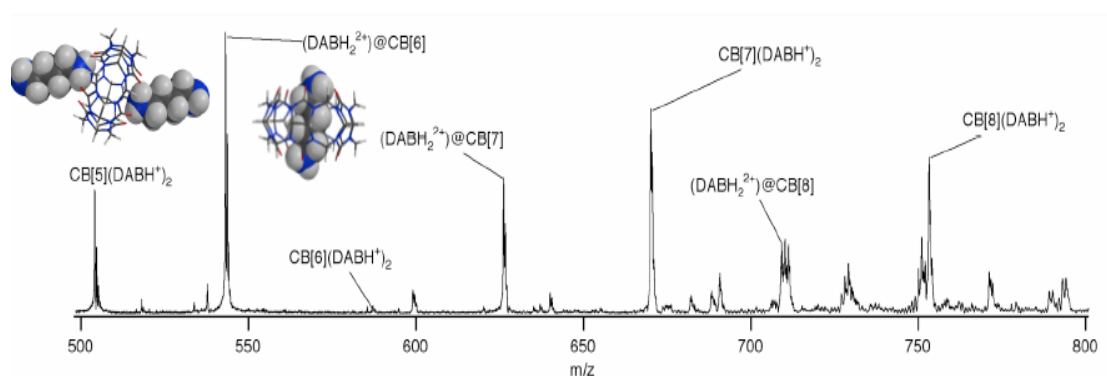


Figure 2.5: Electrospray ionization mass spectrum of a mixture of CBn, n = 5—8, with 1,4-butanediamine from aqueous formic acid.

Binding with Metal Ions to Form “Molecular Boxes.” Dearden et al. observed the encapsulation of small guest molecules such as N₂, O₂, methanol or acetonitrile in decamethylcurcubit[5]uril (mc5) with two ammonium ions attached on the portals as “molecular box lids” using electrospray FT mass spectrometry (Figure 2.6a).³³ Interestingly, ethanol molecules can not be captured inside the mc5 cavity, which indicates the high size selectivity of this host molecule (Figure 2.6b). CB5 can form “molecular boxes” just like mc5 does, except CB5 is more flexible compared to mc5 and can trap some larger molecules, such as ethanol, that can not be trapped inside mc5. The “lids” of the “molecular box” can be alkali metal ions (Li⁺, Na⁺, K⁺, Cs⁺), NH₄⁺, or other higher charged metal ions. Usually prisoner molecules will escape from the cavity when the “box lids” are removed.

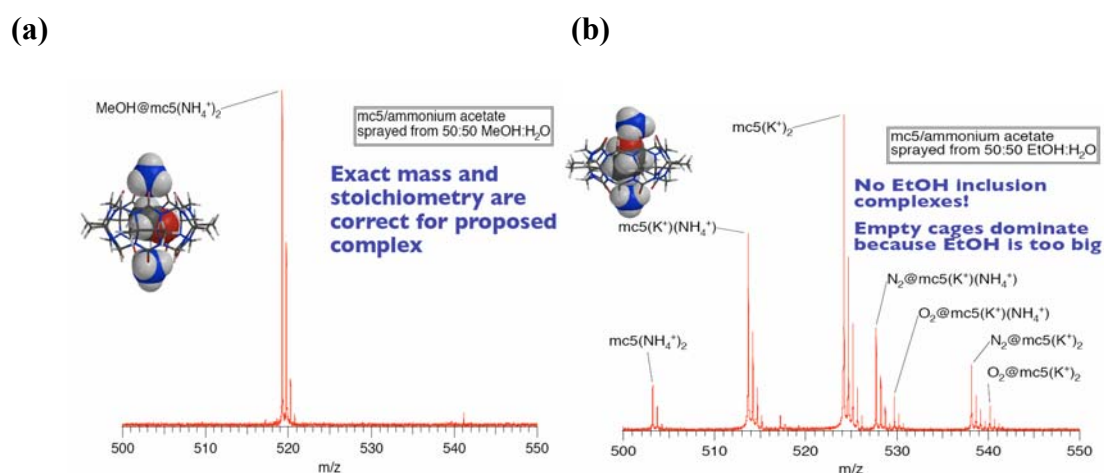


Figure 2.6³³: (a) Electrospray mass spectrum of mc5 molecular box with methanol included inside and two ammonium ions attached on the portals as “lids”. (b) No EtOH inclusion complex is observed in the electrospray mass spectrum of mc5 due to its size selectivity.

CB6 has been reported to bind alkali-metal, alkaline-earth, transition metal, and lanthanide cations in solution.⁸ Buschmann et al. have determined binding constants for CB6 with several metal ions by calorimetric titration (Table 2.1).⁸

Table 2.1: $\log K$ values for the complexation of metal ions with CB6 in HCOOH/H₂O (1:1) at 25 °C and with 18-crown-6 in water⁸

	Li⁺	Na⁺	K⁺	Rb⁺	Ca²⁺	Sr²⁺	Ba²⁺
CB6	2.48	3.23	2.79	2.68	2.80	3.18	2.83
18-crown-6	--	0.80	2.03	1.56	<0.5	2.72	3.87

Logically, CB6 has a larger size so should capture larger guests than CB5. However, when CB6 is electrosprayed with CsCl from solvent mixtures consisting of methanol, ethanol, water and formic acid, only empty molecular boxes, [CB6+2Cs]²⁺, are observed without any guest molecules captured. Apparently Cs⁺ is not big enough to seal the portal of CB6 and hold the guest molecule inside.

Host-Guest Chemistry of CBn with Amino Acids, Peptides and Small Proteins. Buschmann et al. have characterized cucurbituril complexes with amino acids in solution using calorimetric titration methods.²⁵ Our group first electrosprayed CBn with amino acids into the gas phase from acidic solutions and characterized the complexes using FT mass spectrometry. The basic amino acids (Lys, Arg, His) are observed to form doubly-protonated 1:1 complexes with CB6. Other non-basic amino

acids form either doubly-charged, 2:1 complexes or singly-charged 1:1 complexes. Lys and Arg have been further observed to form pseudorotaxane complexes (Figure 2.7 a-b) with CB6 based on ion mobility experimental results. In contrast, α -cyclodextrin (α -CD), with a similar size hollow cavity, shows different binding behavior from that of CB6. Ion mobility cross section values as well as computational methods indicate α -CD forms an externally bound complex with lysine (Figure 2.7 c), and the hydroxyl groups along the α -CD portals stabilize the zwitterion form of lysine. These results are presented in detail in Chapter 3. Larger homologues such as CB8 can include two lysine molecules inside the hollow cavity with higher charge states on the complex.

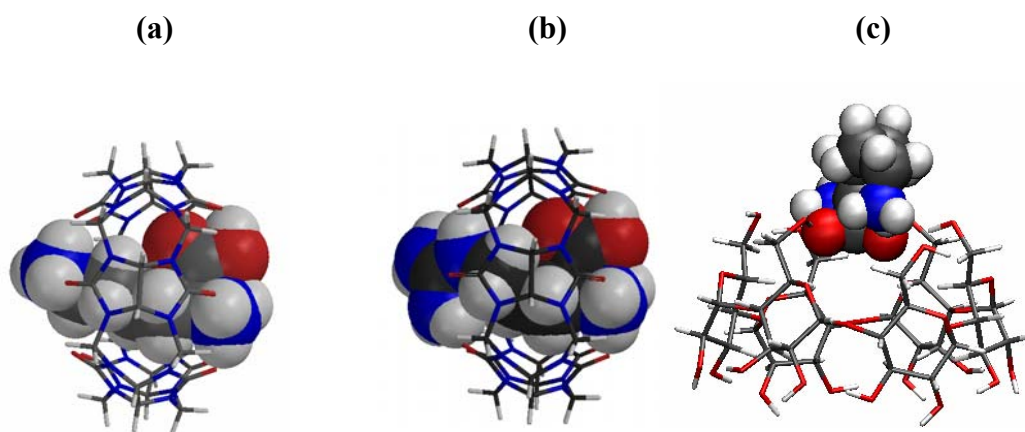


Figure 2.7: Computationally modeled structures of pseudorotaxane complexes formed by CB6 with (a) Lys and (b) Arg. (c) Externally bound complex of α -CD with Lys.

Complexation of host substrates and peptides has been recently investigated using mass spectrometry. Julian and Beauchamp recently demonstrated that addition of

18-crown-6 to a peptide solution resulted in increases in the observed charge state, enhanced the electrospray signal, and suppressed H/D exchange.^{40,41} Our group has observed similar effects from the CB6 complexation with peptides or small proteins using electrospray FT mass spectrometry.

Applications of the Cucurbituril Family

Catalysis. Some of the larger cucurbituril homologues, such as CB8, are able to include more than one guest molecule inside the hollow cavity. Sometimes the reaction between these two guests can be enhanced within the limited space of the host cavity. In other words, the cucurbituril cavity works as a reaction chamber, which catalyzes the reaction between the guests inside. The best example is the strong charge transfer reaction between *N,N'*-dimethyl-4,4'-bipyridinium (MV^{2+}), and 2,6-dihydroxynaphthalene (HN) within the cavity of CB8 (Figure 2.8).³⁰ The charge transfer reaction between MV^{2+} and HN is very slow without CB8. The highly enhanced charge transfer reaction probably results from close contact within the CB8 cavity.

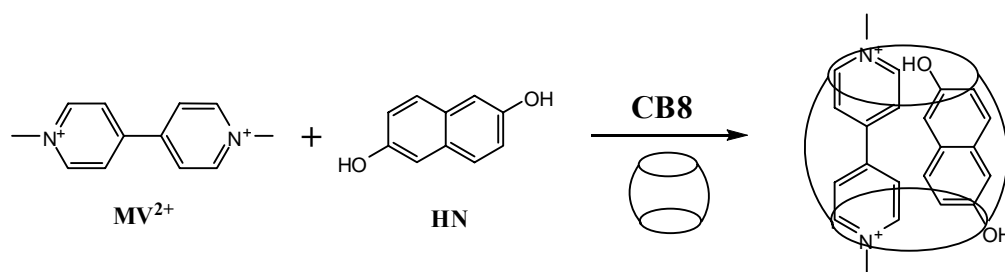


Figure 2.8:³⁰ The charge transfer reaction between MV^{2+} and HN is enhanced within the limited cavity of CB8.

Mock et al. investigated the catalyzed [3+2] dipolar cycloaddition between azide

and alkyne within the CB6 cavity (Figure 2.9),⁴² which is another important example of catalysis by cucurbiturils.

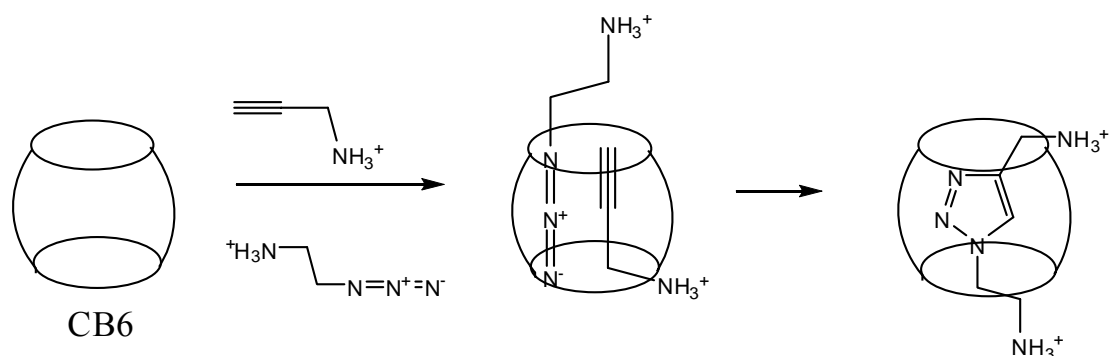


Figure 2.9:⁴³ Catalysis of a [3+2] dipolar cycloaddition inside CB6.

Drug Delivery. Among the CBn homologues, CB7 has a similar cavity size and aqueous solubility to that of β -cyclodextrin. It has been reported that CB7 complexes with oxaliplatin, an anticancer drug, by encapsulating a cyclohexyl ring inside the cavity (Figure 2.10),²⁶ which suggests an important potential application for cucurbiturils in drug delivery.

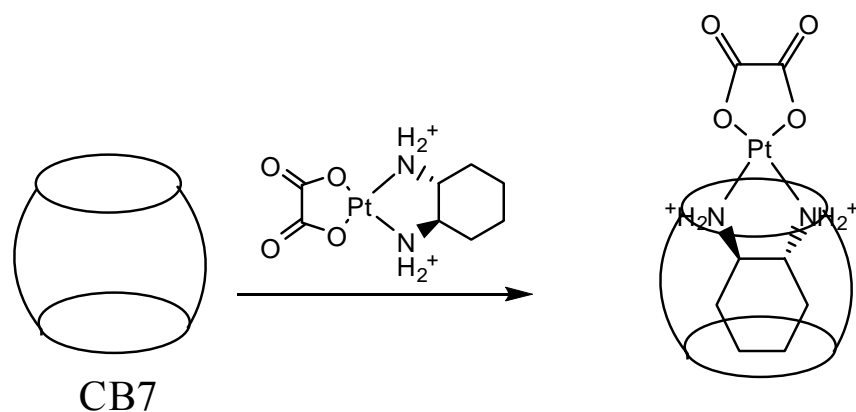


Figure 2.10:²⁶ CB7 encapsulates a cyclohexyl ring of oxaliplatin inside its cavity.

DNA Transfer Carriers. Nakamura et al. have complexed DNA with CB6

through a third intercalator molecule (AT) which contains acridine and tetramine groups. The acridine group binds with DNA and the tetramine group threads through the CB6 cavity to form a termolecular complex of DNA·AT·CB6 (Figure 2.11).²⁰ Partial DNA protection from cleavage has been observed for the DNA·AT·CB6 complex. Kim and co-workers demonstrated in their recent research that diaminobutane dendrimers bind to CB6, working as a gene delivery carrier.³⁴

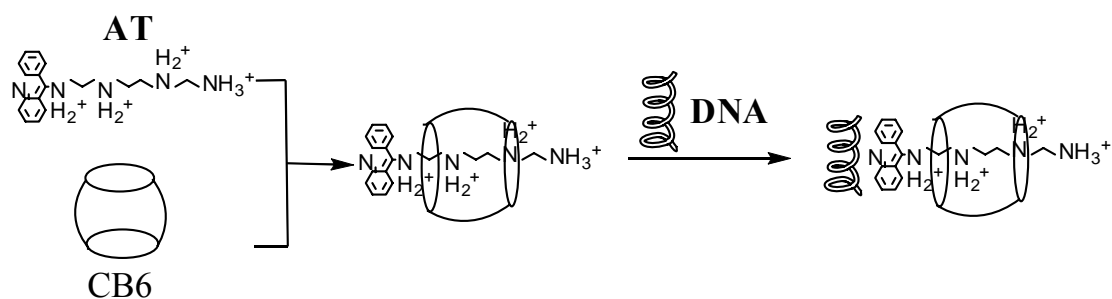


Figure 2.11:²⁰ Complexation of DNA and CB6 by intercalation molecule AT.

Waste Water Purification. In 1905, Behrend et al. investigated CB6 complexation with indicator dyes such as congo red and methylene blue. Since then, Buschmann et al. have reported that CB6 has the capability to remove heavy metals, chromates and dichromate, aromatic compounds, and all kinds of dyes from textile waste streams.⁸ Major problems to be resolved include CB6 attachment to the solid phase in fixed-bed filters, costs, and so on.

Summary and Perspectives

Molecular nanotechnology built from supramolecular assemblies has been one of the most promising areas of the new century. Synthesis and design of supramolecular

nanodevices have become urgent jobs for supramolecular scientists. 100 years ago, cucurbiturils were born in the lab of Behrend and coworkers. But not until 76 years later was this molecule fully characterized by Mock et al., and the potential of being an important host molecule was demonstrated.

This paper discussed important issues relating to the cucurbituril family of molecules, including synthesis, structure, properties, host-guest chemistry, and applications. Successful research in the last 20 years has expanded the range of homologues, solved most of the limiting problems, and made cucurbiturils more flexible hosts with great potential not only in fundamental but also in applied areas. Many cucurbituril applications such as chemical reaction catalysis, drug delivery, waste stream purification, gene carrier applications, and so on have just started, and large amounts of realistic problems will likely be addressed in the future.

Our group has investigated the host guest chemistry of cucurbiturils in the gas phase using electrospray FT mass spectrometry. Being free of interference from the solvent, the gas phase binding behavior of cucurbiturils is directly comparable to theoretical results, which gives further insight into fundamental aspects of their binding properties.

As supramolecule receptors, cucurbiturils have been extensively developed in the last 20 years and have rivaled other receptors such as cyclodextrins. I believe a brighter future for cucurbiturils is coming in the new century.

References

- (1) Freeman, W. A.; Mock, W. L.; Shih, N.-Y. *J. Am. Chem. Soc.* **1981**, *103*, 7367-7368.
- (2) Cram, D. J.; Cram, J. M. *Science* **1974**, *183*, 803-809.
- (3) Schneider, H. J. *Angew. Chem. Int. Ed. Engl.* **1991**, *30*, 1417-1436.
- (4) Kim, J.; Jung, I.-S.; Kim, S.-Y.; Lee, E.; Kang, J.-K.; Sakamoto, S.; Yamaguchi, K.; Kim, K. *J. Am. Chem. Soc.* **2000**, *122*, 540-541.
- (5) Flinn, A.; Hough, G. C.; Stoddart, J. F.; Williams, D. J. *Angew. Chem. Int. Ed. Engl.* **1992**, *31*, 1475-1477.
- (6) Isobe, H. S., S.; Nakamura, E. *Org. Lett.* **2002**, *4*, 1287-1289.
- (7) Mock, W. L.; Shih, N.-Y. *J. Org. Chem.* **1983**, *48*, 3618-3619.
- (8) Buschmann, H.-J.; Cleve, E.; Jansen, K.; Wego, A.; Schollmeyer, E. *J. Inclusion Phenom. Macrocyclic Chem.* **2001**, *40*, 117-120.
- (9) Mock, W. L. In *Comprehensive Supramolecular Chemistry*; Vogtle, F., Ed.; Elsevier: New York, 1996; Vol. 2, pp 477-493.
- (10) Lee, J. W.; Samal, S.; Selvapalam, N.; Kim, H.-J.; Kim, K. *Acc. Chem. Res.* **2003**, *36*, 621-630.
- (11) Zhao, J.; Kim, H.-J.; Oh, J.; Kim, S.-Y.; Lee, J. W.; Sakamoto, S.; Yamaguchi, K.; Kim, K. *Angew. Chem. Int. Ed.* **2001**, *40*, 4233-4235.
- (12) Mock, W. L.; Shih, N.-Y. *J. Org. Chem.* **1983**, *48*, 3619-3620.
- (13) Jeon, Y.-M.; Kim, J.; Whang, D.; Kim, K. *J. Am. Chem. Soc.* **1996**, *118*,

9790-9791.

(14) Fedin, V. P.; Gramlich, V.; Wörle, M.; Weber, T. *Inorg. Chem.* **2001**, *40*, 1074-1077.

(15) Dearden, D. V.; Anderson, J. D.; Ward, S. N.; Kellersberger, K. A. *In 49th ASMS Conference on Mass Spectrometry and Allied Topics*; American Society for Mass Spectrometry: Chicago, IL, 2001.

(16) Wagner, B. D.; Fitzpatrick, S. J.; Gill, M. A.; MacRae, A. I.; Stojanovic, N. *Can. J. Chem.* **2001**, *79*, 1101-1104.

(17) El Haouaj, M.; Luhmer, M.; Ko, Y. H.; Kim, K.; Bartik, K. *J. Chem. Soc. Perkin Trans. 2* **2001**, 804-807.

(18) Buschmann, H.-J.; Wego, A.; Schollmeyer, E.; Döpp, D. *Supramolecular Chem.* **2000**, *11*, 225-231.

(19) Buschmann, H.-J.; Jansen, K.; Schollmeyer, E. *Thermochim. Acta* **2000**, *346*, 33-36.

(20) Isobe, H.; Tomita, N.; Lee, J. W.; Kim, H.-J.; Kim, K.; Nakamura, E. *Angew. Chem. Int. Ed. Engl.* **2000**, *39*, 4257-4259.

(21) Buschmann, H.-J.; Jansen, K.; Schollmeyer, E. *J. Inclusion Phenom. Macrocyclic Chem.* **2000**, *37*, 231-236.

(22) Buschmann, H.-J.; Cleve, E.; Mutihac, L.; Schollmeyer, E. *Microchem. J.* **2000**, *64*, 99-103.

(23) Kim, K. *Chem. Soc. Rev.* **2002**, *31*, 96-107.

(24) Choi, S.; Lee, J. W.; Ko, Y. H.; Kim, K. *Macromolecules* **2002**, *35*,

3526-3531.

(25) Buschmann, H.-J.; Jansen, K.; Schollmeyer, E. *Thermochim. Acta* **1998**, *317*, 95-98.

(26) Kim, K.; Jeon, Y. J.; Kim, S. Y.; Ko, Y. H. *PCT Int. Appl.* **2003**, *WO*, 0324978 A0324971 20030327.

(27) Zhang, X. X.; Krakowiak, K. E.; Xue, G.; Bradshaw, J. S.; Izatt, R. M. *Ind. Eng. Chem. Res.* **2000**, *39*, 3516-3520.

(28) Kim, S.-Y.; Jung, I.-S.; Lee, E.; Kim, J.; Sakamoto, S.; Yamaguchi, K.; Kim, K. *Angew. Chem. Int. Ed. Engl.* **2001**, *40*, 2119-2121.

(29) Jeon, W. S.; Kim, H.-J.; Lee, C.; Kim, K. *Chem. Commun.* **2002**, 1828-1829.

(30) Kim, H.-J.; Heo, J.; Jeon, W. S.; Lee, E.; Kim, J.; Sakamoto, S.; Yamaguchi, K.; Kim, K. *Angew. Chem. Int. Ed.* **2001**, *40*, 1526-1529.

(31) Mock, W. L.; Shih, N.-Y. *J. Org. Chem.* **1986**, *51*, 4440-4446.

(32) Zhang, H.; Paulsen, E. S.; Walker, K. A.; Krakowiak, K. E.; Dearden, D. V. *J. Am. Chem. Soc.* **2003**, *125*, 9284-9285.

(33) Kellersberger, K. A.; Anderson, J. D.; Ward, S. M.; Krakowiak, K. E.; Dearden, D. V. *J. Am. Chem. Soc.* **2001**, *123*, 11316-11317.

(34) Lim, Y. B.; Kim, T.; Lee, W. J.; Kim, H. J.; Kim, K.; Park, J. s.; *Bioconjugate Chem.* **2002**, *13*, 1181-1185.

(35) Day, A. I.; Arnold, A. P.; Blanch, Rodney J. World Intellectual Property Organization, 2000.

(36) Day, A.; Amoid, A. P.; Blanch R. J.; Snushall B. *J. Org. Chem.* **2001**, *66*,

8094-8100.

(37) Lee, J. W.; Samal, S.; Selvapalam, N.; Kim, H.-J.; Kim, K. *Acc. Chem. Res.* **2003**, *36*, 621-630.

(38) Bender, M. L.; Komiyama, M. *Cyclodextrin Chemistry*; Springer-Verlag: Berlin, 1978.

(39) Szejtli, J.; Osa, T., *Eds. Cyclodextrins*; Elsevier: Oxford, 1996; Vol. 3.

(40) Julian, R. R.; Beauchamp, J. L. *Int. J. Mass Spectrom.* **2001**, *210/211*, 613-623.

(41) Julian, R. R.; Akin, M.; May, J. A.; Stoltz, B. M.; Beauchamp, J. L. *Int. J. Mass Spectrom.* **2002**, *220*, 87-96.

(42) Mock, W. L.; Irra, T. A.; Wepsiec, J. P.; Adhya, M. *J. Org. Chem.* **1989**, *54*, 5302-5308.

(43) Kolb, H. C.; Fin, M. G.; Sharpless, K. B. *Angew. Chem. Int. Ed.* **2001**, *113*, 2056-2075.

Chapter 3

Supramolecular Modification of Ion Chemistry: Modulation of Peptide Charge State and Dissociation Behavior through Complexation with α -Cyclodextrin or Cucurbit[*n*]uril (*n*= 5, 6)

Introduction

Studies of host-guest interactions often give fundamental insights into supramolecular chemistry.^{1,2} For example, cyclodextrins (CDs)^{3,4} and cucurbiturils (CBs)⁵⁻⁷ are both important host molecules that have been extensively studied and characterized. Cyclodextrins are cyclic sugars with a torus-like shape. The most common CDs are α , β , and γ -CD which are composed of 6, 7, and 8 glucose units, respectively. The interior cavity of CDs is relatively hydrophobic, so CD hosts can form inclusion complexes with appropriately-sized molecular guests.

Cucurbiturils are pumpkin-shaped cyclic polymers of glycoluril with hollow interior cavities. Carbonyl oxygen atoms line the portals and form binding sites for positive ions, while the interior cavities are again relatively hydrophobic and can host neutral molecules that fit within. Cucurbiturils with cavities of varying sizes have been synthesized, ranging from CB5, composed of five glycoluril units, up to CB10, built from ten glycolurils. The most well known cucurbituril is CB6, which was originally synthesized over 100 years ago and was extensively characterized during

the latter half of the 20th century. Figure 3.1 shows the three-dimensional structures of α -CD (a) and CB6 (b).

Although the sizes and shapes of these two hosts are similar, there are distinct binding differences because of the structural differences. CB6 has a symmetric geometry with two identical openings that are lined with electronegative carbonyl groups. However, α -CD has a less symmetric geometry with one opening to the interior lined with primary hydroxyl groups; the other opening is lined with secondary hydroxyls. The carbonyls of CB6 act as electronegative sites favorable for binding positive ions; they are also good hydrogen bond receptors. The hydroxyl groups that line the α -CD portals can also bind cations, but function both as hydrogen bond donors and as acceptors. Further, the α -CD scaffold is much more flexible than that of CB6, particularly on the side that consists of secondary hydroxyl groups.

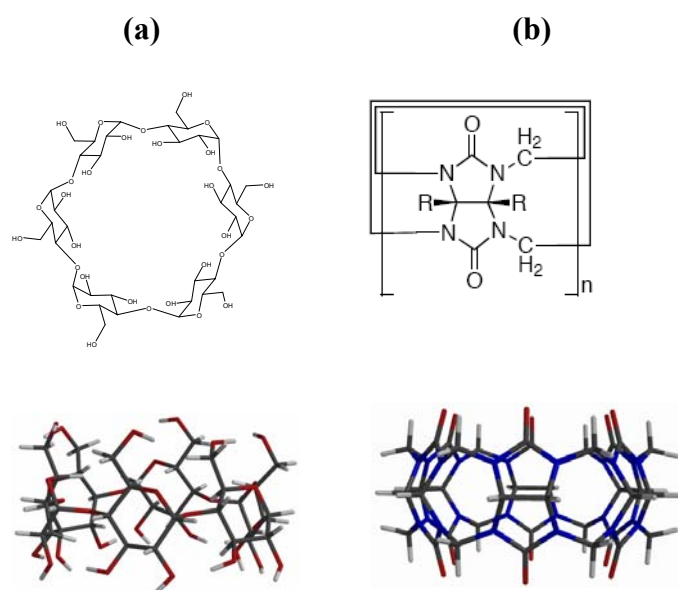


Figure 3.1: Chemical and three dimensional structures of (a) α -CD and (b) CB6.

Electrospray mass spectrometry has been widely used to investigate host-guest interactions in the gas phase.⁸⁻¹² A particular advantage of true gas phase host-guest research is that the experimental results can be directly compared to computational results because complicating interferences from solvents are not present. Thus electrospray mass spectrometry coupled with high-level computational methods becomes a powerful tool to elucidate binding behavior in host-guest complexes.

Prior studies of the effects of supramolecular complexation on ion chemistry include the pioneering work of Julian and Beauchamp,¹³ who examined interactions of polylysines and small proteins with the crown ether 18-crown-6. They found that complexation with 18-crown-6 resulted in a shift of the observed charge states toward higher charge, and an improvement in the mass spectrometric signal-to-noise ratio over what is observed when the crown is not present. This chapter will show that such effects are sensitive to the type of complexing agent used: CB6 produces results similar to those previously observed for 18-crown-6, whereas α -CD does not.

In this paper I examine the effects of supramolecular complexation on the behavior of amino acid and small peptide ions in the gas phase. Specifically, I use both high level calculations and mass spectrometric experiments to compare the effects of a set of complexing agents that differ in size and structure: CB5, CB6 and α -CD. I will show that these agents can be used to modify both the distribution of observed charge states and the dissociation behavior of the analytes.

Most of the amino acids favor a non-zwitterionic structure in the gas phase.^{14,15} This contrasts with their chemistry in solution at neutral pH, where the

zwitterion form is the most stable. Lebrilla et al. demonstrated that β -CD can form inclusion complexes with amino acids,^{16,17} and that the interaction between the amino acid and the narrow (secondary) rim of β -CD stabilizes zwitterion formation.¹⁸ The CD therefore presents a solvent-like environment to an included amino acid. Compared to β -CD, α -CD has a smaller cavity and portal size. On the basis of size alone, I would expect complexes between amino acids and α -CD to be different from those with β -CD. In this chapter I substantiate this expectation by showing that lysine binds externally with α -CD. However, even in this external complex, α -CD retains the ability to stabilize the Lys zwitterion, which I demonstrate through a combination of experimental and computational results.

Dearden et al. characterized the rotaxane structure of CB6-diammonium complexes in the gas phase.¹⁹ In those rotaxane complexes, linear alkyldiammonium ions were threaded through CB6. Hydrogen bonds between the ammonium groups and the carbonyl laden portals of CB6 hold the complex together. With amino groups at both ends of an alkyl chain, Lys is structurally similar to the alkyldiammonium species previously studied, and so might also be expected to form a rotaxane with CB6. Herein I present evidence that it does.

Experimental Section

Materials. Cucurbit[6]uril, α -cyclodextrin, L-lysine, pentalysine, ubiquitin, cytochrome c and insulin were purchased from Sigma Chemical Co. (St. Louis MO)

and used without further purification.

Sample Preparation. 1.8 mg/ml CB6 stock solution was prepared by dissolving solid sample in 88% formic acid (Fisher Scientific, Fair Lawn, NJ); all other stock solutions were prepared by dissolving samples in HPLC grade water (Mallinckrodt Baker Inc., Phillipsburg, NJ). Electrospray solutions were prepared by mixing CB6 or α -CD with peptide solutions, or diluting directly from the stock solutions. Final electrospray solutions contained equimolar analytes (10^{-4} M) with 50:50 water/methanol solvent. All the solutions also contained 4.4% formic acid following final dilution.

ESI Mass Spectrometry. Mass spectrometric measurements were carried out using a Bruker model APEX 47e FT-ICR mass spectrometer controlled by a MIDAS data system²⁰ and equipped with a microelectrospray source modified from an Analytica design, with a heated metal capillary drying tube based on the design of Eyley.²¹ The source was typically operated at a flow rate of $10 \mu\text{L hr}^{-1}$. To avoid possible influences of tuning on the observed analyte charge states, I collected mass spectra for charge state comparison within a short period without changing any tuning parameters. All the mass spectra reported are the average of 10 scans for each experiment.

SORI-CID Experiments. Stored waveform inverse Fourier transform (SWIFT)²² techniques were used to isolate target peaks. Sustained off-resonance irradiation collision-induced dissociation (SORI-CID)²³ experiments were performed by irradiating 1 kHz below the resonant frequency of the ion of interest. Collision gas

(air) was introduced using a Freiser-type pulsed leak valve.²⁴ SORI events involved pulsing the background pressure in the trapping cell up to 10^{-5} mbar and applying the off-resonance irradiation for 5 seconds, followed by a 10 second delay to allow the trapping cell to return to baseline pressure (about 10^{-8} mbar) prior to detection. The amplitude of the SORI RF pulse was varied through a range of values from less than the threshold for dissociation to several times the threshold value. Ten scans were averaged for each SORI amplitude.

Reactivity Experiments. Neutral n-propylamine was introduced into the trapping cell using a controlled variable leak valve to a constant pressure ($\sim 10^{-7}$ mbar). The reaction time (between SWIFT isolation of the ionic reactant and detection of reactants and products) was varied programmatically. Data analysis was performed with a modified version of the MIDAS Analysis software that was capable of extracting peak amplitudes from a set of spectra that differ in one or more experimental parameters (in this case, reaction time).

Ion Mobility Experiments. Ion mobility experiments were performed on a home built instrument consisting of a nano-electrospray ionization (nano-ESI) source, an ion funnel, a drift cell, and a quadrupole mass filter. The details and typical operating parameters of the instrument have previously been published,²⁵ so only a brief description will be given here. In the ion mobility experiments,^{26,27} ions are generated in the source from approximately 5 μ L of sample solution contained in a metal-coated borosilicate capillary (Proxeon, Odense, Denmark), enter the ion funnel through a 0.01in. ID capillary, are transmitted to the mobility cell, stored and then pulse injected

at low energy into the mobility cell, which is filled with around 4 mbar of He gas. The ions are rapidly thermalized by collisions with the He gas as they travel through the cell under the influence of a weak dc electric field, E . The ions drift through the cell with a constant drift velocity, v_D , proportional to the electric field:

$$v_D = KE \quad (3-1)$$

where the proportionality constant, K , is the ion mobility. By measuring the arrival time at the detector for several values of the field E , an accurate value of K is determined. Through the use of kinetic theory,²⁸ the collision cross section σ can be obtained from the experimental value of K . Ions exiting the drift cell are collected as a function of time, yielding an arrival time distribution (ATD). Compact ions with small cross sections drift faster and have shorter arrival times than more extended ions with larger cross sections. Thus, different conformers can be separated in the drift cell and appear as separate peaks in the ATD. The cross section for each conformer can be obtained as described above and their relative abundances obtained from the ATDs.

Atomic level conformational information for the complexes was obtained by comparing the experimental collision cross sections to calculated values from molecular models. A simulated annealing protocol using the AMBER 7 package of molecular dynamics (MD) software²⁹ was used to generate 150-200 low energy candidate structures for each of several possible initial structures of the complex. In this protocol an initial structure was subjected to 30 ps of molecular dynamics at 600 K followed by 10 ps of dynamics during which the temperatures was lowered to 0 K. The resulting structure was then energy minimized, saved, and used as the starting

structure for the next cycle. The collision cross sections of these candidate structures were then calculated using an angle averaged projection model.³⁰ The average cross sections of the lowest energy family of structures, which for the systems considered in this work showed only minor structural deviations, were then compared to experiment.

Electronic Structure Calculations. The overall strategy is to use fast, relatively less accurate methods (molecular mechanics conformational searching) to screen for low-energy complex structures, which are then examined with more accurate, more costly techniques (primarily B3LYP/6-31G* and related methods). In general, our calculations used the following protocols. Structures were sketched using the Maestro/Macromodel modeling package (Macromodel version 7.1; Schrödinger, Inc.; Portland, OR). Conformational searches were performed using the MMFF94s³¹ force field with no nonbonded cutoffs and with conjugate gradient minimization, and using the MCMM search method with automatic setup and 50,000 starting structures. Torsional rotations within the cucurbituril ring, or within the α -cyclodextrin ring, were disabled. It should be noted that the molecular mechanics calculations always leave the protons associated with the atoms where they were originally sketched; these calculations do not include proton transfer as a possibility.

The lowest-energy structures found in the conformational searches were used as the starting point for B3LYP/6-31G* DFT geometry optimizations. These calculations were performed using NWChem (version 4.7; Pacific Northwest National Laboratory; Richland, WA)³² and used NWChem default convergence criteria. No

atoms were constrained in the geometry optimizations. For example, if proton transfer is energetically feasible, the geometry optimization algorithm of NWChem will carry out the transfer.

Results

Lysine complexation with CB5, CB6, and α -CD

a) Electrospray of lysine, lysine+CB5, lysine+CB6 and lysine+ α -CD solutions

Lysine, lysine+CB5, lysine+CB6 and lysine+ α -CD solutions were each electrosprayed into the FTICR mass spectrometer (Figure 3.2). Sprayed alone, lysine yields a +1 ion. The lysine+CB5 ESI spectrum is the most complex, partially because the CB5 samples contained potassium salt impurities. Observed singly-charged ions include $[\text{CB5} + \text{H}_3\text{O}]^+$ (m/z 849), $[\text{CB5} + \text{K}]^+$ (m/z 869), and $[\text{CB5} + \text{Lys} + \text{H}]^+$ (m/z 977). Experimental observation of $[\text{CB5} + \text{H}_3\text{O}]^+$ is significant, as H_3O^+ has been proposed as a template ion in the formation of CB5.³³ Doubly-charged ions include $[\text{CB5} + 2\text{Lys} + 2\text{H}]^{2+}$ ($m/z = 562$) and $\text{EtOH} @ [\text{CB5} + 2\text{Lys} + 2\text{H}]^{2+}$ ($m/z = 585$). We observed 1:1 complexes of lysine with CB6 and with α -CD, but the CB6 complex was doubly protonated and doubly charged, yielding a strong signal, whereas the α -CD complex was singly protonated and singly charged and gave a relatively weak signal. All of these spectra were sufficiently well resolved that significant populations of doubly-charged dimers (with the same nominal m/z as singly-charged monomeric complexes) would easily be observed via their isotopic peaks. However, no evidence of such species was apparent in the FTICR mass spectra.

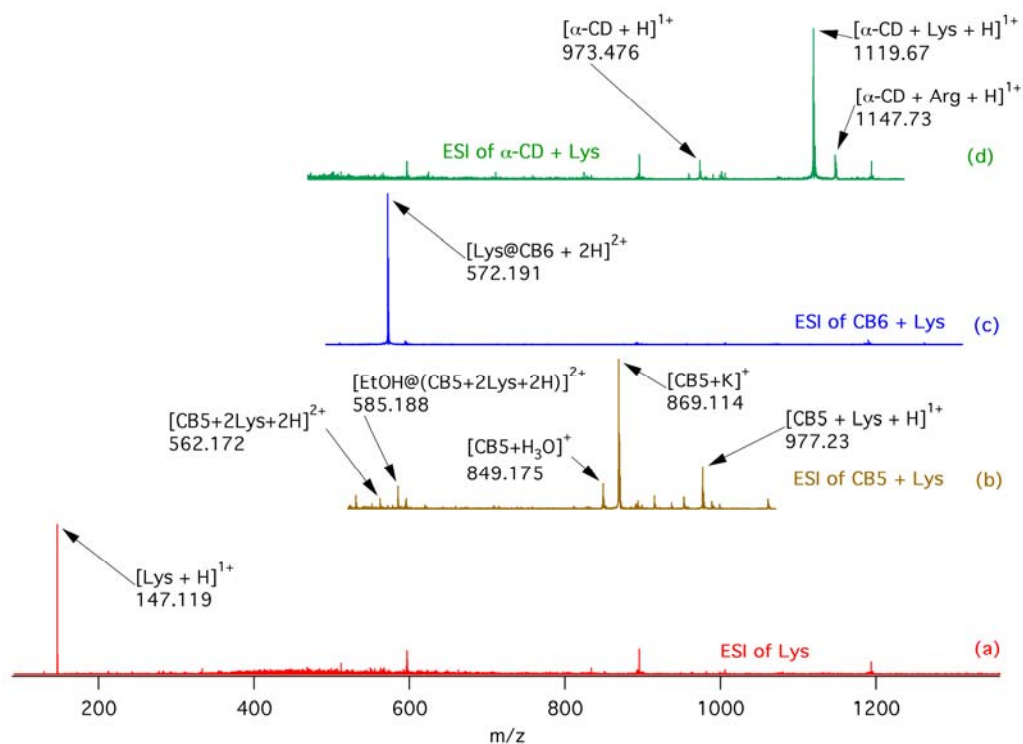


Figure 3.2: Mass spectra of a) isolated lysine, b) lysine+CB5, c) lysine+CB6 and d) lysine+ α -CD.

b) Computational results

The lowest energy conformations found in our computational study have singly charged lysine bound externally on CB5, doubly charged lysine threaded through the cavity of CB6, and singly charged lysine bound externally on the secondary rim of α -CD (Figure 3.3). For CB5, lysine externally binds to the cucurbituril, the protonated lysine side chain hydrogen bonding to the electronegative portal of CB5; steric constraints prevent the side chain from threading into the cavity. In the CB6 complex, which was modeled with a +2 charge to be consistent with the ESI-FTICR results, lysine protonated at both N-terminal and side chain amino sites is threaded through the cucurbituril. This complex is held together by hydrogen bonds between the

ammonium groups and the electronegative oxygen atoms that line the portals of CB6. In contrast, the lowest energy structure found for the α -CD complex is singly-charged with the protonated lysine having a salt bridge structure. In the singly-charged α -CD complex, both protonated amino groups and the deprotonated carboxylate group are associated with the primary rim of α -CD, where all form hydrogen bonds with the primary hydroxyl groups of the cyclodextrin.

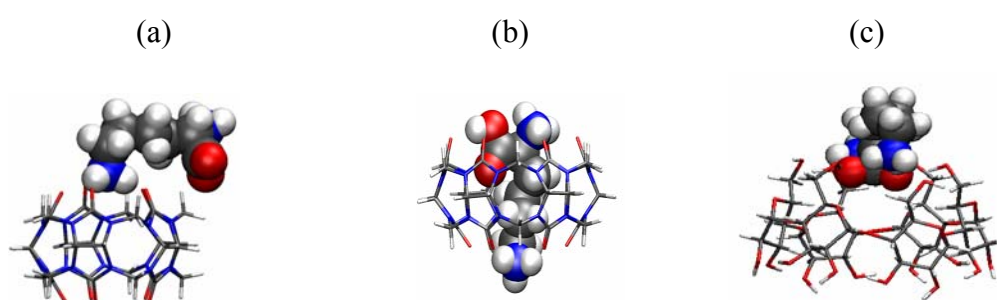


Figure 3.3: Lowest energy computed structures of lysine-CB5, lysine-CB6 and lysine- α -CD complexes. (a) Side chain protonated lysine externally binds to CB5. (b) The side chain of lysine threads through the CB6 cavity to form a rotaxane complex with both amine groups protonated. (c) Protonated lysine (in salt bridge form) externally attaches to the primary hydroxyl, narrower rim of α -CD.³⁴

Relative energies and lysine ion binding energies for the lowest-energy external and threaded structures found for the lysine complexes of CB5, CB6, and α -CD are given in Table 3.1. For CB5, in accordance with experimental observation, we examined singly-protonated complexes. Of these, the externally bound lysine structure lies more than 230 kJ mol^{-1} lower in energy than the lowest-energy threaded structure found in our conformational search. The computed binding energy of

protonated lysine in CB5 is 327 kJ mol^{-1} at the B3LYP/6-31G* level of theory. Placement of protonated lysine within the CB5 cavity both introduces steric strain into the system and constrains placement of the lysine to a less than optimal position for hydrogen bonding with the CB5 carbonyl oxygen groups.

To be consistent with experimental observations, the CB6-lysine complex was modeled as a doubly-protonated system. For CB6, the threaded structure is far lower in energy (by more than 660 kJ mol^{-1}) than the externally-bound structure; in fact, the latter lies higher in energy than separated and relaxed $\text{CB6} + (\text{Lys}+2\text{H})^{2+}$. For the threaded structure, the computed binding energy of doubly-protonated lysine is 600 kJ mol^{-1} .

The α -CD complex of lysine was observed and modeled as a singly-protonated system. As with CB5, the externally-bound lysine complex lies at far lower energy than the lowest-energy threaded structure located in our searches (by almost 650 kJ mol^{-1}). The computed lysine binding energy in the most favorable complex is less than was found for either of the cucurbiturils, at 226 kJ mol^{-1} .

Table 3.1: Computational results for external and threaded lysine complexes of CB5, CB6, and α -CD

Complex	B3LYP/6-31G*	Relative	
	Energy, Hartrees	Energy, kJ mol ⁻¹	D[(Lys+nH) ⁿ⁺ -Host], kJ mol ⁻¹
[CB5+Lys+H] ¹⁺			
(external)	-3506.42517	0	-327
[Lys@CB5+H] ¹⁺			
(threaded)	-3506.33645	233	-150
[CB6+Lys+2H] ²⁺			
(external)	-4108.33722	661	61
[Lys@CB6+2H] ²⁺			
(threaded)	-4108.58910	0	-600
[α -CD+Lys+H] ¹⁺			
(external)	-4162.16963	0	-226
[Lys@ α -CD+H] ¹⁺			
(threaded)	-4161.92308	647	101

c) Ion mobility experiments

Ion mobility experiments were conducted to provide confirmation for the structures of the lysine complexes of CB5, CB6 and α -CD. The arrival time distribution for [CB5+Lys+H]⁺ is shown in Figure 3.4 a. The distribution peaks at

about 690 μsec , which corresponds to a cross section of 184 \AA^2 . Structures with lysine externally bound to the CB5 portal have computed collision cross sections of about 180 \AA^2 , whereas structures with the lysine threaded through the CB5 cavity have smaller cross sections (around 170 \AA^2). The externally bound structure is therefore most consistent with the measured ion mobility data.

The arrival time distribution for $[\text{CB6}+\text{Lys}+2\text{H}]^{2+}$ is given in Figure 3.4 b. It consists of a single peak with an arrival time of about 410 μs , corresponding to a collision cross section of 189 \AA^2 . This is similar to the computed 193 \AA^2 cross section for a structure with doubly-protonated Lys threaded through CB6. In contrast to this threaded structure, the computed cross sections for externally bound complexes are much larger ($218\text{-}225 \text{ \AA}^2$), depending on details of the lysine conformation). The threaded structure is consistent with the ion mobility measurements, whereas the externally bound structures are not.

The ion mobility results for the electrosprayed mixture of Lys and α -CD are more complex. For the mass spectrometric peak at m/z 1119, the arrival time distribution consists of two peaks, one at about 625 μs and the other at about 770 μs (Figure 3.4 c). The relative amplitudes of the two peaks are dependent on injection energies, with the peak at 625 μs most prominent at low injection energies and only the peak at 770 μs remaining at 100 eV injection energies. The peak at 770 μs corresponds to a collision cross section of 220 \AA^2 . For comparison, the mass spectrometric peak at m/z 973, assigned as $[\alpha\text{-CD}+\text{H}]^{1+}$, yields a single peak arrival time distribution, with the peak at about 700 μs , corresponding to a collision cross section of 200 \AA^2 . Computed

collision cross sections for singly-charged α -CD complexes of salt bridged Lys, with Lys bound to the primary and secondary rims of α -CD, are 217 \AA^2 and 224 \AA^2 , respectively, bracketing the experimental result. The m/z 1119, 625 \mu s arrival time peak is consistent with a doubly-charged dimer ion ($[2\alpha\text{-CD}+2\text{Lys}+2\text{H}]^{2+}$, 312 \AA^2), which dissociates at higher injection energies. Interestingly, the high resolution FTICR data provide no evidence for the doubly-charged dimer ion, but this is not particularly surprising because the ion mobility instrument and the FTICR used different ion sources.

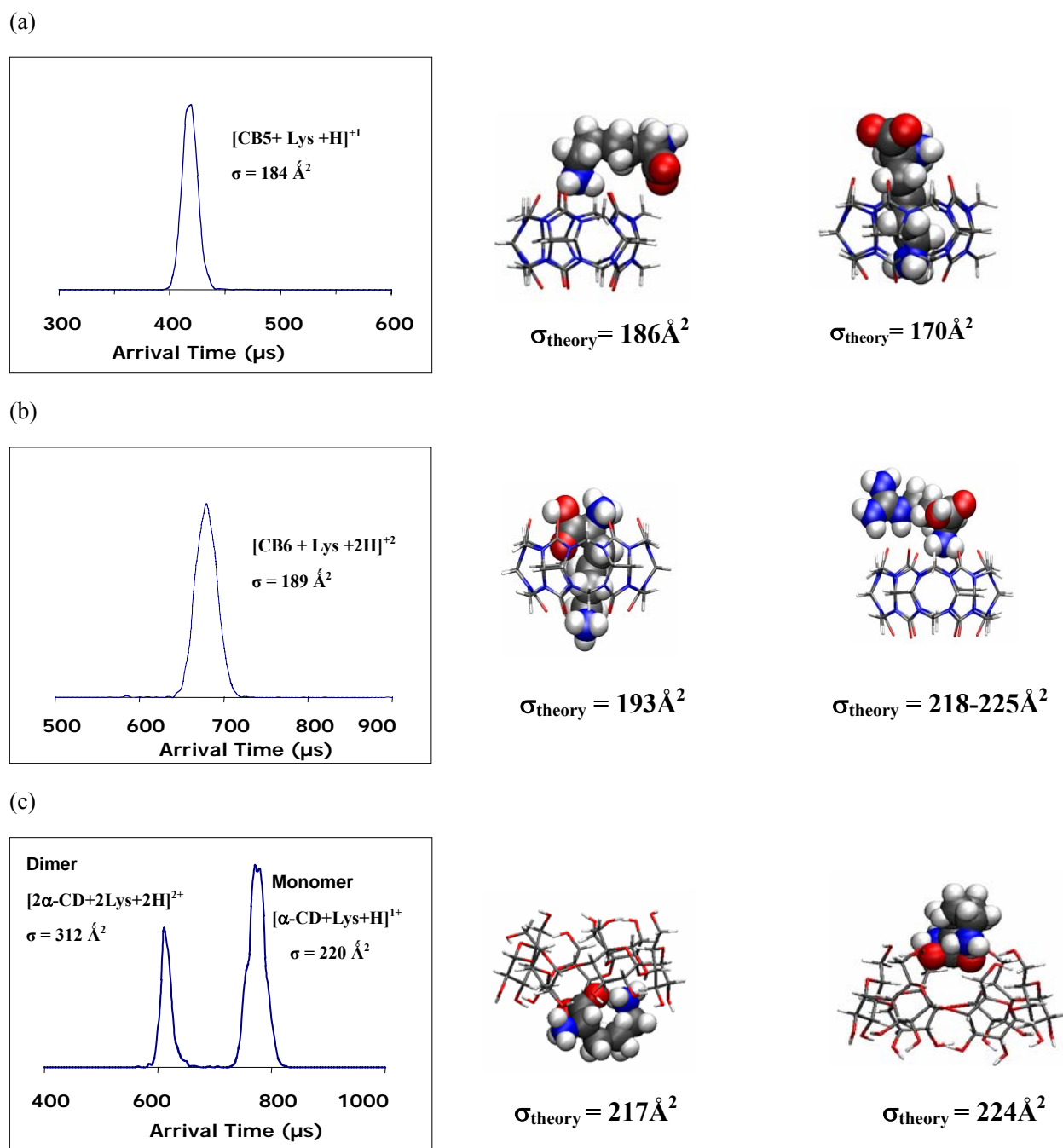


Figure 3.4: Ion mobility cross section along with calculated cross section values for lysine complexes. (a) CB5+lysine, (b) CB6+lysine, and (c) α -CD+lysine

d) SORI-CID of uncomplexed lysine, lysine-CB6 complex, and lysine- α -CD zwitterion complex.

Figure 3.5 shows SORI-CID mass spectra for singly-charged lysine, the

singly-charged lysine-CB5 complex, the doubly-charged lysine-CB6 complex, and the singly-charged lysine- α -CD salt bridge complex.

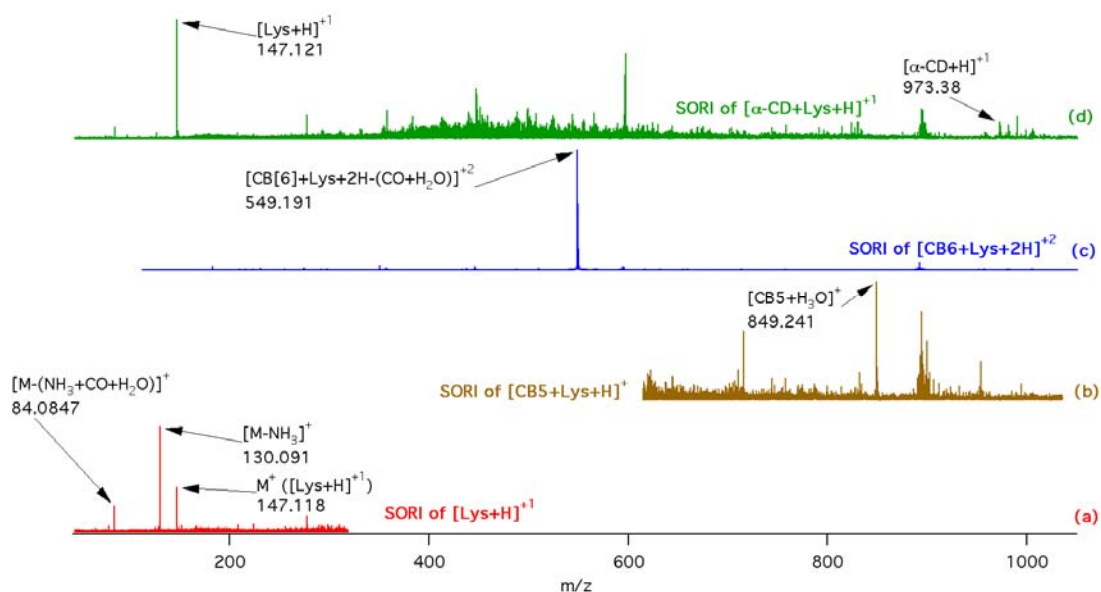


Figure 3.5: SORI-CID mass spectra for (a) singly-charged lysine, (b) singly-charged lysine-CB5 complex, (c) doubly-charged lysine-CB6 complex, and (d) singly-charged lysine- α -CD zwitterion complex.

The singly-charged lysine ion dissociates by losing neutral ammonia, water, and carbon monoxide (Figure 3.5 a). The singly-charged lysine-CB5 complex yields only one observed ionic fragment, an ion corresponding to $[CB5+H_3O]^+$ (Figure 3.5 b). Dissociation of the doubly-charged lysine-CB6 complex is similar to that of protonated lysine, loss of neutral water and carbon monoxide (Figure 3.5 c). However, in this case the product is a doubly-charged ion. In contrast, the lysine- α -CD salt bridge complex dissociates without breaking covalent bonds, via loss of either neutral lysine or loss of neutral α -CD (Figure 3.5 d).

Pentalysine complexation.

Pentalysine includes the same functional groups as lysine, but has three times as many basic sites (six). With more basic sites, under acidic spray conditions it is possible to achieve higher charge states than can be observed for lysine alone. Further, with this larger peptide additional binding motifs are possible. To probe the greater complexity afforded by pentalysine, we examined its complexes with CB5, CB6, or α -CD.

a) ESI mass spectra of pentalysine and its complexes

ESI-FTICR/MS spectra of pentalysine and its complexes with CB5, CB6, and α -CD are given in Figure 3.6. Sprayed alone, the dominant charge state for pentalysine is +2, with the +3 charge state being only a few percent as intense (Figure 3.6 a). Addition of cucurbituril yields complexes with enhanced abundance of higher charge states. For both CB5 and CB6, the $[\text{CB}_n+(\text{Lys})_5+3\text{H}]^{3+}$ peak is more intense than that corresponding to $[\text{CB}_n+(\text{Lys})_5+2\text{H}]^{2+}$. The CB5 spectrum is significantly contaminated with K^+ adducts, and the peak for uncomplexed $[(\text{Lys})_5+2\text{H}]^{2+}$ is more than 50% as strong as the base peak, $[\text{CB}_5+(\text{Lys})_5+3\text{H}]^{3+}$ (Figure 3.6 b). Addition of CB6 results in simpler spectra, the only prominent peaks being the triply- and doubly-protonated complexes of pentalysine with CB6 (Figure 3.6 c). As with lysine, the α -CD complexes of pentalysine are fundamentally different from the cucurbituril complexes. In addition to uncomplexed, singly protonated pentalysine and α -CD, a prominent signal corresponding to $[\alpha\text{-CD}+(\text{Lys})_5+2\text{H}]^{2+}$ is observed, whereas the triply-protonated $[\alpha\text{-CD}+(\text{Lys})_5+3\text{H}]^{3+}$ is barely discernable; the doubly- and

triply-protonated complex intensities have approximately the same relative intensities as were observed for doubly- and triply-protonated pentalysine alone. An additional interesting peak is observed at m/z 1302.6, corresponding to attachment of two α -CD molecules to doubly-protonated pentalysine (Figure 3.6 d); for the cucurbiturils, we observed a maximum of one cucurbituril attached to a single pentalysine.

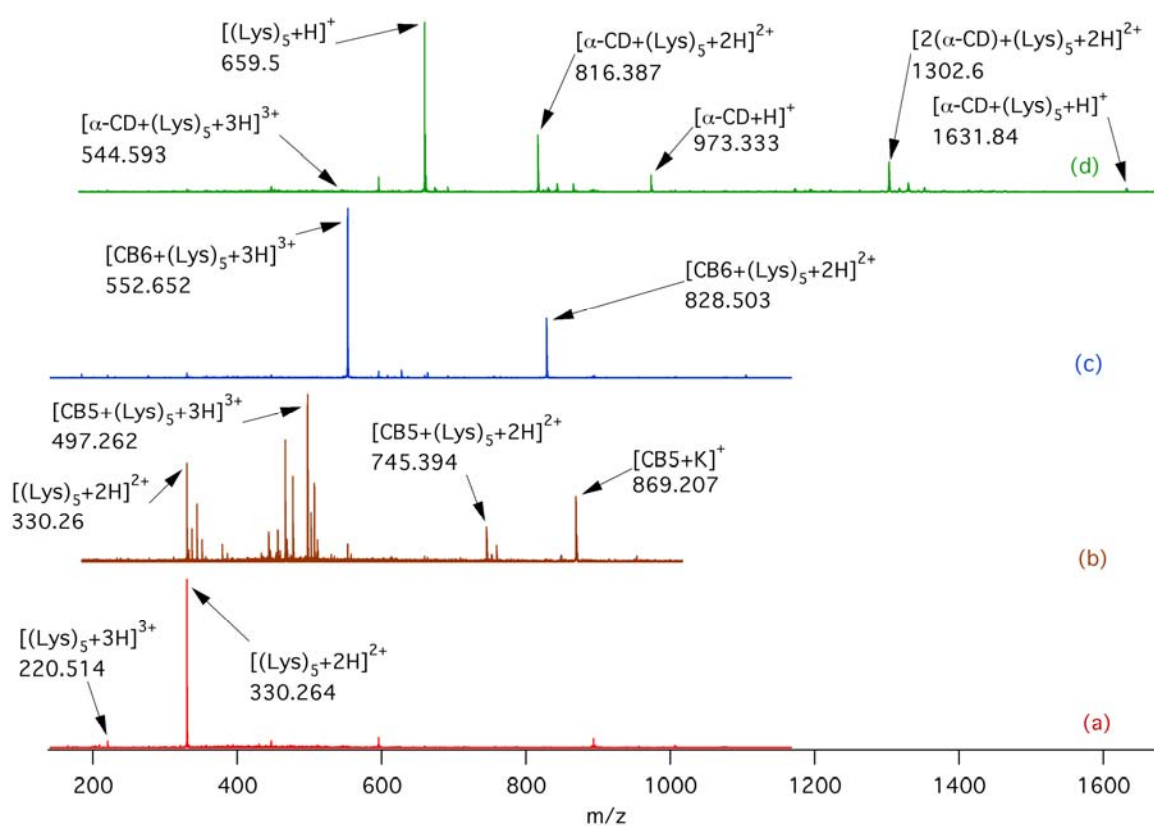


Figure 3.6: ESI spectra of a) pentalysine, b) pentalysine + CB5, c) pentalysine + CB6, and d) pentalysine + α -CD.

b) SORI of pentalysine and its complexes

Figure 3.7a shows SORI-CID spectra of the +2 charge states of pentalysine and its complexes with CB5 and CB6. Collisional activation of uncomplexed pentalysine

results in water losses and the complete series of b fragment ions.

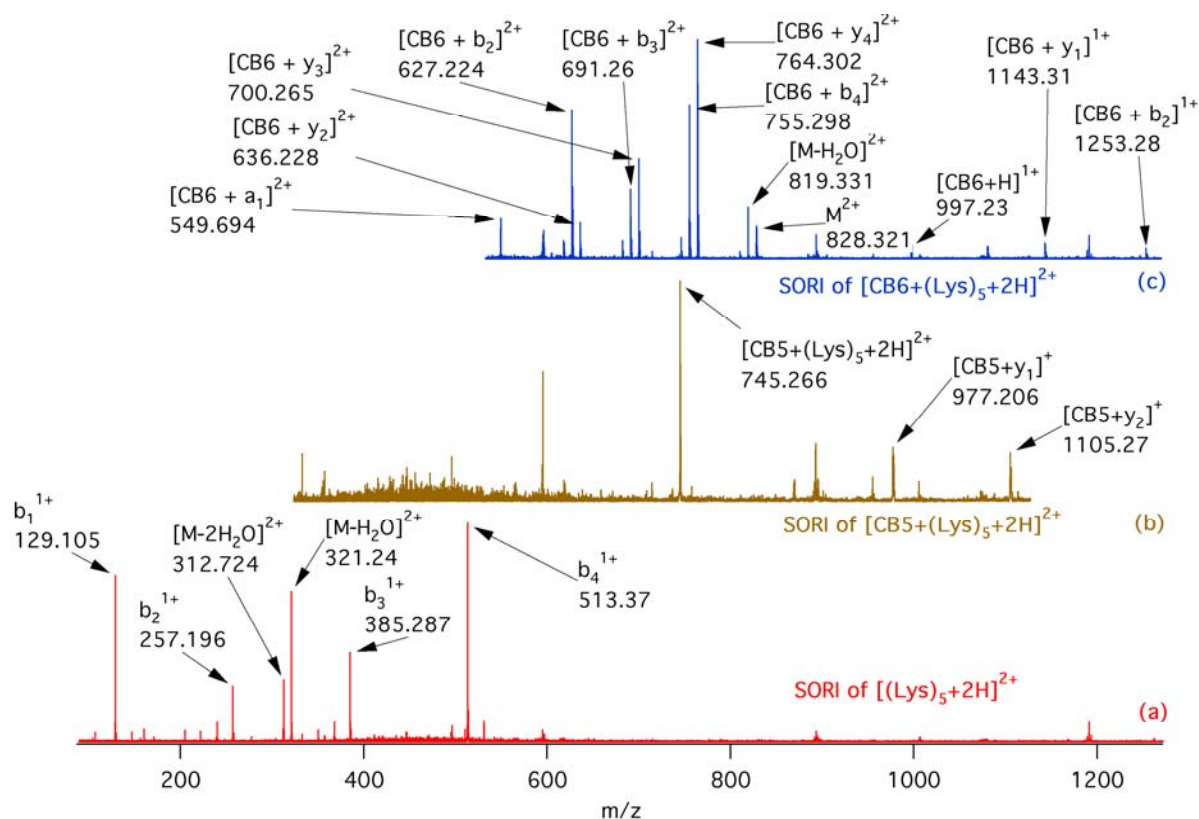


Figure 3.7: SORI-CID spectra of the +2 charge states of a) pentalysine; b) pentalysine + CB5; (c) pentalysine + CB6.

Complexation with CB5 significantly modifies the SORI spectrum (Figure 3.7 b). The b_n fragment ions are no longer evident, and the only definite fragments are singly charged y_1 and y_2 cleavage products with CB5 remaining attached. Interestingly, simple loss of CB5 from the peptide, which would yield m/z 330 (for $(Lys_5+2H)^{2+}$) or m/z 659.5 (for $(Lys_5+H)^{1+}$), is not observed.

In the CID spectrum of the +2 pentalysine-CB6 complex (Figure 3.7 c), all the observed fragment ions are bound to CB6, and most are doubly charged. The only

observed singly charged fragments are y_1 and b_2 , again both bound to CB6. The $(CB6+y_n)^{2+}$, $n = 2-4$ ions are quite prominent. Each is accompanied by peaks 18 and 36 amu lower in mass. The peaks at -18 amu could be $(CB6+b_n)^{2+}$, or they could be water losses from $(CB6+y_n)^{2+}$, which are isobaric with $(CB6+b_n)^{2+}$. Similarly, the peaks 36 amu below $(CB6+y_n)^{2+}$ may be double water losses from $(CB6+y_n)^{2+}$ or single water losses from $(CB6+b_n)^{2+}$. Losses of water from fragment ions have been reported previously.³⁵⁻³⁷ It is interesting that, despite the fact that the b_1 fragment is prominent in the CID spectrum of +2 pentalysine, the b_1 fragment was not observed in the CID spectrum of the CB6 complex. Instead, a $(CB6+a_1)^{1+}$ product is present.

CID of the +3 charge state, $(CB6+Lys_5+3H)^{3+}$, (not shown) gives similar results to those observed for the +2 charge state, except that the relative abundance of the $(CB6+y_n)^{2+}$ fragments decreases and the $(CB6+a_1)^{2+}$ fragment becomes the most abundant peak. No triply charged fragments were observed.

In contrast with the cucurbituril complexes, the α -CD complexes of pentalysine fragment via simple cleavages under SORI conditions. Thus, the principle products from SORI of $[\alpha\text{-CD}+(Lys)_5+2H]^{2+}$ are $[\alpha\text{-CD}+H]^{1+}$ and $[(Lys)_5+H]^{1+}$ (not shown).

Discussion

Threaded vs. non-threaded structures in the gas phase

We recently demonstrated that threaded and non-threaded structures involving CB6 and 1,4-diaminobutane can be distinguished mass spectrometrically via their

CID and reactivity behaviors.¹⁹ The threaded complex dissociated via covalent cleavages of the host and guest, whereas the non-threaded complex dissociated via separation of the two intact molecules. Exposure of the threaded complex to a neutral amine resulted in a slow addition of the amine to the complex, but the non-threaded complex was much more reactive, with the added amine rapidly replacing non-threaded 1,4-diaminobutane. Complexes of lysine with CB5, CB6, and α -CD can be characterized in the same way, and the characterizations are in addition supported by ion mobility experiments and computational studies.

Lysine binds externally to both CB5 and α -CD in the gas phase. The SORI-CID results (Figure 3.5) are clearest for the α -CD complex: $[\alpha\text{-CD+Lys+H}]^{1+}$ dissociates via simple cleavage of the noncovalent associations between the two molecules, yielding $[\text{Lys+H}]^{1+}$ and $[\alpha\text{-CD+H}]^{1+}$, consistent with external binding. The interaction between Lys and CB5 evidently is stronger, because simple noncovalent cleavage products are not observed. Rather, Lys dissociates from the complex with loss of water, which remains associated with protonated CB5 to form $[\text{CB5+H}_3\text{O}]^{1+}$.

Similarly, reactivity experiments suggest lysine binds externally to both CB5 and α -CD. For both complexes, neutral *n*-propylamine rapidly displaces lysine. Perhaps the strongest experimental evidence that the gas phase complexes of lysine with CB5 or α -CD involve external binding comes from ion mobility. For both complexes, the measured arrival time distributions and corresponding collision cross sections (Figure 3.4) are in close agreement with computed externally bound lysine structures, and are not consistent with threaded structures, which are significantly more compact. Finally,

the computational results show that the lowest-energy externally-bound structures are considerably lower in energy than the threaded structures, by 233 and 647 kJ mol⁻¹ for the CB5 and α -CD complexes, respectively.

All the available experimental and computational evidence supports a threaded structure for the complex of doubly charged lysine with CB6. When the complex is collisionally activated (Figure 3.5), lysine loses water and carbon monoxide, yielding a doubly charged fragment ion that remains associated with CB6. Thus, covalent cleavages are more favorable than simple disruption of all the ionic hydrogen bonds (as many as 6) in the complex. When the complex is exposed to *n*-propylamine, displacement of lysine does not occur; rather, the *n*-propylamine slowly adds to the complex. This is directly analogous to the previously observed reactivity of the threaded 1,4-diaminobutane complex with CB6, and in contrast to the rapid displacement observed when that complex is not threaded.¹⁹ The ion mobility results (Figure 3.4 b) show close agreement between experimental and computed collision cross sections for the threaded structure, whereas the cross section for the structure with lysine bound externally is about 10% greater than the experimental value. Computationally, the threaded structure lies 661 kJ mol⁻¹ lower in energy at the B3LYP/6-31G* level than the lowest energy externally bound structure.

Influence of complexation on zwitterion stability

It has long been known that amino acids form zwitterions in aqueous solution at neutral pH because the separated charges are stabilized via solvation, but it has

recently been shown that absent that stabilization they exist as non-zwitterions when isolated in the gas phase.^{14,15} Complexation with a large host molecule represents an intermediate state between isolation in the gas phase and full solvation. Are amino acids most stable as zwitterions when complexed? Can we control their charge distribution by controlling the complexation environment? Our studies of lysine complexation address these questions.

Three sites on the lysine molecule can be protonated: the N-terminal amino group, the side chain amino group, and the carboxylate group. Singly charged (+1) lysine could therefore be protonated at either of the basic sites along with the acid group, or it could be protonated at both basic sites with a deprotonated carboxylate (thereby forming a zwitterion with a net charge of +1). Relative energies of singly-protonated gas phase lysine in various environments are given in Table 3.2. At the B3LYP/6-31G* level of theory for protonated lysine isolated in the gas phase, placement of the proton on the amino side chain is the lowest energy form, followed by N-terminal protonation (21 kJ mol⁻¹ higher), with the zwitterionic salt bridge form being highest in energy (56 kJ mol⁻¹ above the side chain protonated form).

Table 3.2: B3LYP/6-31G* Relative Energies of Gas Phase Lysine +1 Tautomers and Their Complexes, kJ mol⁻¹.

Host	N-terminal	Side Chain	Salt Bridge
none	21	0	56
CB5 (external)	50	0	42
CB6 (external)	34	0	36
CB6 (internal)	0	12	not a minimum
α -CD (external)	3	3	0

Lebrilla and coworkers recently demonstrated that interactions between amino acids and the primary rim of β -cyclodextrin can stabilize zwitterion formation.¹⁸ The polar groups of the cyclodextrin present a local methanol-like environment to the amino acid, stabilizing the separation of charge in the salt bridge form. It is therefore reasonable to expect that complexes with other host molecules possessing polar substituents should have similar effects. The B3LYP/6-31G* computational results in Table 3.2 suggest this expectation has merit. Because of its close similarity to β -cyclodextrin, complexation with α -CD would be expected to lower the relative energy of the salt bridge form of protonated lysine. Figure 3.8 shows this is the case; all three tautomers of protonated lysine have very similar energies at this level of theory when bound to α -CD. Presumably, the smaller number of hydroxyl groups and decreased flexibility for α -CD make this complexation environment less methanol-like than that provided by β -cyclodextrin, so the degree of salt bridge

stabilization provided by α -CD is less than that provided by β -cyclodextrin.

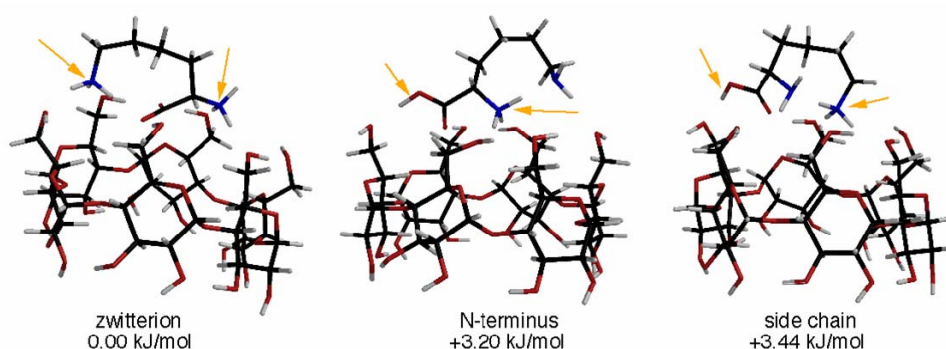


Figure 3.8: B3LYP/6-31G* calculations on three possible singly-charged lysine- α -CD complexes with the lowest energy for zwitterion formation.

Like α -CD, the cucurbiturils also present a region of hydrogen bond acceptors at their rims. Will the cucurbiturils also stabilize the lysine zwitterion? For the externally-bound lysine complexes, the computational results in Table 3.2 suggest the cucurbituril rims do lower the energy of the salt bridge form relative to the side chain protonated form of lysine. As the cucurbituril gets larger and the ligand becomes more flexible and solvent-like, the relative energy of the salt bridge form drops. The cucurbituril environment strongly destabilizes N-terminal protonation relative to side chain protonation, probably because side chain protonation is strongly stabilized by the polar cucurbituril rim.

The interior of the CB6 cavity is a very different environment, where the salt bridge structure is destabilized to the point it is not a minimum. The steric constraints imposed by the cavity force the carboxylic acid group close to the partial negative charges of the CB6 carbonyl groups, hindering formation of a negative carboxylate.

Protonation at either of the amino sites is favorable when singly-protonated lysine is bound inside CB6, but N-terminal protonation is 12 kJ mol^{-1} more favorable than side chain protonation.

In contrast to the α -CD complex, only the doubly charged complex of CB6 was observed via electrospray mass spectrometry. Given the functional groups of lysine, the lysine in this complex cannot be a zwitterion; the lysine must be protonated at both amino groups and at the carboxylate to have a +2 charge. This suggests that the interior of CB6 provides an electrostatic environment that favors protonation at both amino groups and disfavors negative charge on the carboxyl. Further insight comes from B3LYP/6-31G* geometry optimizations that began with the lysine threaded through the CB6, but with the lysine in a +1 charge state, salt bridged form. Despite beginning with a zwitterionic structure, the final structure does not converge to a salt bridge form, but rather undergoes intramolecular proton transfer in the course of the minimization. The initial and computed final structures are given in Figure 3.9. In the optimized structure, the proton originally located on the N-terminus has moved to the carboxyl, dramatically illustrating the destabilization of the zwitterion by CB6, and nicely explaining why only +2 complexes are observed in the ESI-MS spectrum. Thus, the complexation environment plays a large role in the energetics of lysine protonation, and can be used to control which sites are protonated. Of course, this is not particularly surprising, and these principles are widely expressed in protein chemistry.

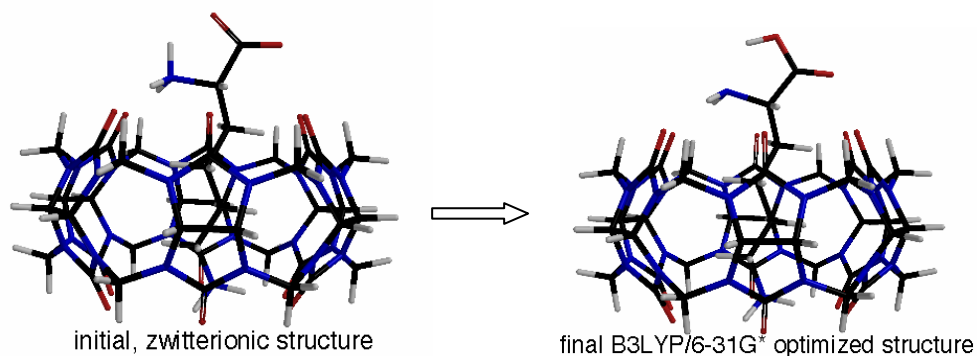


Figure 3.9: Initial zwitterion structure for the Lys@CB6H^+ complex (from Monte Carlo-MMFF conformational searching) goes to a nonzwitterion after B3LYP/6-31G* geometry optimization.

Influence of complexation on collision-induced dissociation

Formation of a supramolecular complex can have a number of effects on the collision-induced dissociation of an ion. First, complexation always increases the number of internal degrees of freedom available for energy dispersal in an activated ion, which should increase the threshold energy required for dissociation. Unfortunately, our experiments are not well suited for accurate measurement of dissociation thresholds, so we will not further discuss threshold shifts. Second, because complexation involves weak interactions between molecules, it introduces new low-energy dissociation pathways associated with cleavage of the non-covalent interactions that hold the complex together. These low-energy pathways may or may not be experimentally important, depending primarily on the relative entropies of activation for the various dissociation channels. For instance, if many weak bonds must be broken in a concerted fashion for a particular channel to be observed, it may

not be observed despite being energetically favorable. For this reason, it is possible to observe cleavages of covalent bonds even in the presence of weaker hydrogen bonds, for example. Finally, complexation may create an environment that stabilizes or destabilizes certain dissociation pathways. For instance, complexation with a polar host molecule may favor products that are polar or otherwise exhibit charge separation.

Comparison of the CID spectra of lysine ion and its complexes with α -CD, CB5, or CB6 (Figure 3.5) serves as a probe of how complexation can influence ion fragmentation in simple yet subtle ways. Collisionally-activated lysine ion dissociates by losing small, stable fragments: ammonia, water, and carbon monoxide. Complexation with α -CD shuts down these pathways, which involve cleavage of covalent bonds, in favor of a new low-energy pathway involving disruption of the non-covalent interactions that hold the complex together. Hence, CID of the $[\text{Lys}+\alpha\text{-CD}+\text{H}]^+$ complex yields protonated Lys and protonated α -CD, as expected for a weakly-associated complex with Lys bound on the exterior of α -CD. Similar behavior is observed for $[\text{Lys}+\text{CB5}+\text{H}]^+$: Lys is externally bound via relatively weak hydrogen bonding interactions, and collisional activation of the complex results in simple cleavage of the hydrogen bonds.

Perhaps the most interesting results are those for the doubly-charged Lys-CB6 complex. B3LYP/6-31G* geometry optimization for this complex results in a doubly-protonated lysine ion threaded through the hollow cavity of CB6, held in place by hydrogen bonding with the electronegative oxygens of the CB6 portals to form a

stable rotaxane. Collectively, the six hydrogen bonds between the lysine ion and CB6 are so strong that collisional activation breaks the covalent bonds within lysine more readily than the entropically-disfavored disruption of all the hydrogen bonds to free the guest from the host. Like lysine alone, the complex dissociates by losing water and carbon monoxide, but the resulting doubly-charged fragment ion remains captured inside CB6. Interestingly, the prominent ammonia loss pathway observed for singly-charged, isolated lysine is not observed for $[\text{Lys}+\text{CB6}+2\text{H}]^{2+}$. Again this is consistent with the computed structure; both amino groups of doubly-charged Lys are protonated and held in place by hydrogen bonds in the complex. Loss of ammonia would disrupt this energetically favorable arrangement.

Pentalysine complexation with CB6. We have already shown that when basic amino acids like lysine bind to CB6, both the observed electrospray charge state and CID pathway are modified. Similar trends are seen when complexes are formed with a larger partner, pentalysine.

Unlike isolated lysine, pentalysine is likely to exist as a zwitterion in the gas phase; molecular modeling suggests the side chain amine groups on the longer amide backbone can easily form a salt bridge with a C-terminal anion, stabilizing the zwitterion. Above, we have argued that the electronegative portal of CB6 can destabilize the lysine zwitterion, causing the net charge to shift up by one. The observed charge state shift for pentalysine on complexation with CB6 may be explained in a similar way (Figure 3.6).

Pentalysine has 5 side chain amino sites as well as the N-terminus; any of these

sites may be protonated. Where does CB6 attach to this longer chain? Computationally, the simplest way to address this question is to protonate all the possible sites and perform a conformational search in which the CB6 is free to move. The lowest energy structure found in such a calculation has CB6 threaded on the N-terminal lysine residue, such that the two CB6 portals form multiple hydrogen bonds with the protonated N-terminus and the protonated amino group of the N-terminal side chain. This suggests that this N-terminal site is the preferred binding site for CB6. However, the results of CID experiments imply that the N-terminal site is not the only one occupied (*vide infra*).

Individual amino acids usually lose small neutral molecules (like water) in CID experiments. However, for polypeptides, bonds along the peptide backbone are generally the most easily broken, with cleavage at the peptide bond yielding b and y fragments when the charge is retained on the N-terminal and C-terminal sides of the break, respectively. We have seen above that binding by CB6 causes changes in the CID spectrum of lysine. We therefore expect binding with CB6 will also cause changes in the CID spectrum of pentalysine, and the experimental results confirm this expectation.

For the +2 charge state of pentalysine (Fig. 3.7 a) the observed fragmentations include loss of water and various cleavages resulting in b fragments (b_1 - b_4). Interestingly, the complementary y fragments are not observed. If the C-terminus is deprotonated as it would be in a pentalysine zwitterion, it is possible that the y fragments have a net charge of zero, preventing mass spectrometric detection.

The CID spectrum of the +2 pentalysine-CB6 complex (Fig. 3.7 b) has several interesting differences from the CID spectrum of +2 pentalysine alone. First, all of the products are complexed with CB6, providing strong evidence that any of the five side chains can bind with CB6. Also, in CID of the +2 complex, both b and y pentalysine fragments are observed (all bound to CB6), and the y fragments are quite prominent. This provides additional support for the hypothesis that binding by CB6 destabilizes the C-terminal anion: if the C-terminus is protonated, net positive charge remains on the y fragment and it is detected. It is also interesting that almost all of the fragments are +2 charge states (except y_1 and b_2). Again, this is consistent with the idea that the two cation binding sites of CB6 stabilize two positive charges.

Finally, despite the fact that the b_1 fragment is prominent in the CID spectrum of +2 pentalysine, the b_1 fragment is not observed in the CID spectrum of the CB6 complex. Instead, an a_1 -CB6 product is present. In an attempt to understand these observations, we performed B3LYP/6-31G* calculations to compare the relative stabilities of the doubly-charged a_1 -CB6 and b_1 -CB6 complexes. The former minimized easily, but the complex that initially had the acylium b_1 -CB6 structure produced by simple cleavage of the peptide did not converge to a stable minimum. Rather, as the geometry optimization progressed, the b_1 -CB6 complex lost carbon monoxide, becoming an a_1 -CB6 complex, in beautiful agreement with experimental observations. This is consistent with suggestions in the literature³⁸ that the acylium form is not stable; rather, cyclization of the b_1 ion via nucleophilic attack of the side chain on the carbonyl does yield a stable b_1 ion, but this cannot happen if the side

chain is threaded through CB6. Binding with CB6 therefore destabilizes the b_1 fragment, and stabilizes the unexpected a_1 fragment instead.

CID of +3 pentalysine-CB6 (Fig. 3.7 c) gives similar results to those observed for the +2 charge state, except that the relative abundance of the y fragments decreases and the a_1 fragment becomes the most abundant peak. In the +3 charge state, the likelihood of protonating the N-terminus and the N-terminal side chain increases relative to the +2 charge state, simply because more protons are available in the +3 state. As was noted above, formation of a rotaxane on the N-terminus is the energetically preferred binding mode for CB6. If N-terminal protonation and complexation by CB6 is more likely in the +3 state, C-terminal protonation is less likely, decreasing the likelihood of observing the y fragments. Similarly, fragmentation of pentalysine-CB6, with CB6 on the N-terminal site, yields the doubly-charged a_1 -CB6 product ion, whose abundance is increased for the +3 charge state.

Conclusions

The basic side chain of lysine leads to a singly charged ion when electrosprayed into the gas phase. However, formation of supramolecular complexes through the addition of CB5, CB6, or α -CD significantly modifies the gas phase chemistry of the resulting ions. The side chain of lysine threads through the hollow cavity of CB6, which stabilizes positive charge on both ends of the molecule, resulting in a doubly-charged rotaxane complex. However, lysine molecules bind externally on CB5

or on the primary rim of α -CD, which acts to solvate the amino acid and stabilize the zwitterion form, just as is observed in aqueous solution. B3LYP/6-31G* calculations show that hydrogen bonding between lysine and α -CD can stabilize the zwitterion form, whereas binding with CB6 actually destabilizes the lysine zwitterion.

These structural differences result in distinct dissociation behaviors in CID experiments. Lysine easily dissociates from α -CD, because the lysine is externally attached to the host. In contrast, collisional activation of the CB6-lysine complex results in cleavage of covalent bonds within the lysine molecule rather than breaking the hydrogen bonds between the protonated amine group and the CB6 carbonyl groups. The collective strength of the hydrogen bonding causes the complex to dissociate by losing water and carbon monoxide.

Pentalysine forms a +2 charged ion in the gas phase that is probably a zwitterion. When it is electrosprayed with CB6, both the +2 and +3 complexes are observed in the mass spectrum, with +3 being the most abundant peak. CID experiments on +2 pentalysine yield b_1 - b_4 fragments but no y type fragments. One possible reason for missing the y type is because the y type fragments form zwitterions with a net charge of zero, and are thus undetected. Since CB6 can destabilize the zwitterion form of lysine, both b and y type fragments (bound to CB6) are observed in the CID spectra of both the +2 and +3 pentalysine-CB6 complexes. B3LYP/6-31G* calculations show that binding with CB6 destabilizes the b_1 fragment and stabilizes the a_1 fragment, in agreement with the experimental observation of the a_1 fragment bound to CB6 and the absence of the b_1 fragment in the spectra. Compared to the +2 pentalysine-CB6

complex, the +3 complex yields a higher abundance of a₁-CB6 fragments. This suggests that as the pentyllysine charge state increases the probability of CB6 binding to the N-terminal side chain increases.

Complexed ions can be regarded as an intermediate state between full solvation in solution and the isolated gas phase ion. Our research describes this intermediate state in terms of charge state and collisional dissociation modification of complexed amino acid or peptide ions, which leads to a deeper insights into the host-guest chemistry.

References

- (1) Cram, D. J.; Cram, J. M. *Science* **1974**, *183*, 803-809.
- (2) Schneider, H. J. *Angew. Chem. Int. Ed. Engl.* **1991**, *30*, 1417-1436.
- (3) Bender, M. L.; Komiyama, M. *Cyclodextrin Chemistry*; Springer-Verlag: Berlin, 1978.
- (4) *Cyclodextrins*; Szejtli, J.; Osa, T., Ed.; Elsevier: Oxford, 1996; Vol. 3.
- (5) Mock, W. L. In *Comprehensive Supramolecular Chemistry*; F. Vögtle, Ed.; Elsevier: New York, 1996; Vol. 2; pp. 477-493.
- (6) Lagona, J.; Chakrabarti, S.; Isaacs L. *Angew. Chem. Int. Ed.* **2005**, *44*, 4844-4870.
- (7) Kim, J.; Jung, I.-S.; Kim, S.-Y.; Lee, E.; Kang, J.-K.; Sakamoto, S.; Yamaguchi, K.; Kim, K. *J. Am. Chem. Soc.* **2000**, *122*, 540-541.
- (8) Vincenti, M. *J. Mass Spectrom.* **1995**, *30*, 925-939.
- (9) Brodbelt, J. S.; Dearden, D. V. In *Physical Methods in Supramolecular Chemistry*; J. E. D. Davies and J. A. Ripmeester, Ed.; Pergamon: Oxford, 1996; Vol. 8; pp. 567-591.
- (10) Dearden, D. V. In *Physical Supramolecular Chemistry*; L. Echegoyen and A. E. Kaifer, Ed.; Kluwer: Dordrecht, the Netherlands, 1996; pp. 229-247.
- (11) Dearden, D. V.; Zhang, H.; Chu, I.-H.; Wong, P.; Chen, Q. *Pure Appl. Chem.* **1993**, *65*, 423-428.
- (12) Vincenti, M.; Pelizzetti, E.; Dalcanale, E.; Soncini, P. *Pure Appl. Chem.* **1993**, *65*, 1507-1512.

- (13) Julian, R. R.; Beauchamp, J. L. *Int. J. Mass Spectrom.* **2001**, *210/211*, 613-623.
- (14) Sherrie, C.; Rogers, M. T.; Marzluff, E. M.; Beauchamp, J. L.. *J. Am. Chem. Soc.* **1995**, *117*, 8159-8170.
- (15) Xu, M.; Inoue, N.; Eyring, E. M.; Petrucci S. *J. Phys. Chem.* **2003**, *119*, 10696-10701.
- (16)Lebrilla, C. B. *Acc. Chem. Res.* **2001**, *34*, 653-661.
- (17)Ramirez, J.; Ahn, S. H.; Grigorean, G.; Lebrilla, C. B. *J. Am. Chem. Soc.* **2000**, *122*, 6884-6890.
- (18)Ahn, S. C., X.; Lebrilla, C. B.; Gronert, S.. *ournal of the American Society for Mass Spectrometry* **2005**, *16*, 166-175.
- (19)Zhang, H.; Paulsen, E. S.; Walker, K. A.; Krakowiak, K. E.; Dearden, D. V. *J. Am. Chem. Soc.* **2003**, *125*, 9284-9285.
- (20)Senko, M. W.; Canterbury, J. D.; Guan, S.; Marshall, A. G. *Rapid Commun. Mass Spectrom.* **1996**, *10*, 1839-1844.
- (21)Wigger, M.; Nawrocki, J. P.; Watson, C. H.; Eyler, J. R.; Benner, S. A. *Rapid Commun. Mass Spectrom.* **1997**, *11*, 1749-1752.
- (22)Chen, L.; Wang, T.-C. L.; Ricca, T. L.; Marshall, A. G. *Anal. Chem.* **1987**, *59*, 449-454.
- (23)Gauthier, J. W.; Trautman, T. R.; Jacobson, D. B. *Anal. Chim. Acta* **1991**, *246*, 211-225.
- (24)Jiao, C. Q.; Ranatunga, D. R. A.; Vaughn, W. E.; Freiser, B. S. *J. Am. Soc.*

Mass Spectrom. **1996**, 7, 118-122.

(25)Wyttenbach, T., Kemper, P. R. and Bowers, M. T. *International Journal of Mass Spectrometry* **2001**, 212, 13-23.

(26)Bowers, M. T. vonHelden, G.; vanKoppen, P. A. M. *Science* **1993**, 260, 1446.

(27)Clemmer, D. E. Jarrold, M. F. *J. Mass Spectrom.* **1997**, 32, 577.

(28)Mason, E. A. MacDaniel, E. W. *Transport Properties of Ions in Gases*; Wiley: New York, 1988.

(29)Case, D. A.; Caldwell, T. E.; Cheatham III, J.; Wang, W. S.; Ross, C. L.; Simmerling, T. A.; Darden, K. M.; Merz, R. V.; Stanton, A. L.; Cheng, J. J.; Vincent, M.; Crowley, V.; Tsui, H.; Gohlke, R. J.; Radmer, Y.; Duan, J.; Pitner, I.; Massova, G. L.; Seibel, U. C.; Singh, P. K.; Weiner, P. A. "AMBER 7," Ver. (2002); University of California; San Francisco.

(30)Wyttenbach, T.; Batka, J. J.; Carlat, D.; Bowers M. T. *J. Am. Soc. Mass Spectrom.* **1997**, 8, 275.

(31)Halgren, T. A. *J. Comput. Chem.* **1996**, 17, 490-519.

(32)Apra, E. W., T. L.; Straatsma, T. P.; Bylaska, E. J.; de Jong, W.; Hirata, S.; Valiev, M.; Hackler, M. T.; Pollack, L.; Kowalski, K.; Harrison, R. J.; Dupuis, M.; Smith, D. M. A.; Nieplocha, J.; Tipparaju, V.; Krishnan, M.; Auer, A. A.; Brown, E.; Cisneros, G.; Fann, G. I.; Fruchtl, H.; Garza, J.; Hirao, K.; Kendall, R.; Nichols, J. A.; Tsemekhman, K.; Wolinski, K.; Anchell, J.; Bernholdt, D.; Borowski, P.; Clark, T.; Clerc, D.; Dachsel, H.; Deegan, M.; Dyall, K.; Elwood, D.; Glendening, E.; Gutowski, M.; Hess, A.; Jaffe, J.; Johnson, B.; Ju, J.; Kobayashi, R.; Kutteh, R.; Lin, Z.;

Littlefield, R.; Long, X.; Meng, B.; Nakajima, T.; Niu, S.; Rosing, M.; Sandrone, G.; Stave, M.; Taylor, H.; Thomas, G.; van Lenthe, J.; Wong, A.; Zhang, Z.; "NWChem, A Computational Chemistry Package for Parallel Computers," Ver. 4.7 (2005); Pacific Northwest National Laboratory; Richland, Washington 99352-0999, USA.

(33) Oh, K. S.; Yoon, J.; Kim, K. S. *J. Phys. Chem. B* **2001**, *105*, 9726-9731.

(34) Humphrey, W., Dalke, A. and Schulten, K., *J. Molec. Graphics* **1996**, *14*, 33-38.

(35) Jockusch, R. A.; Schnier, P. D.; Price, W. D.; Strittmatter, E. F.; Demirev, P. A.; Williams, E. R. *Anal. Chem.* **1997**, *69*, 1119-1126.

(36) Mao, D.; Douglas, D. J. *J. Am. Soc. Mass Spectrom.* **2003**, *14*, 85-94.

(37) Wattenberg, A.; Organ, A. J.; Schneider, K.; Tyldesley, R.; Bordoli, R.; Bateman, R. H. *J. Am. Soc. Mass Spectrom.* **2002**, *13*, 772-783.

(38) Ackermann, B. L.; Barbuch, R. J.; Coutant, J. E.; Krstenansky, J. L.; Owen, T. *J. Rapid Commun Mass Spectrom* **1992**, *6*, 257-264.

Chapter 4

Controlling Lid Removal from a Molecular Box: Ion Molecule Reactions of Supramolecular Mixed-Metal Cucurbituril Complexes via Electrospray Ionization Fourier Transform Ion Cyclotron Resonance Mass Spectrometry

Introduction

The field of molecular nanodevices¹ built from single molecules or supramolecular assemblies is one of the most cutting-edge research topics today. Typical techniques used to characterize molecular nanodevices include NMR, X-ray, and imaging techniques such as STM or AFM. Most recently electrospray mass spectrometry (ESI-MS) has been used to investigate supramolecular systems in the gas phase.²⁻⁶ Compared to typical techniques, ESI-MS avoids disadvantages such as large sample consumption and matrix effects. ESI-MS is also well known as a fast and ultra-sensitive technique.

Cucurbiturils are pumpkin-shaped cyclic polymers of glycoluril with hollow interior cavities. As shown in Figure 4.1, carbonyl oxygen atoms line the portals and form ideal binding sites for positive ions, while the interior cavities can contain neutral molecules of proper size. Cucurbiturils composed of n glycoluril units are named cucurbit[n]urils, CB n hereafter for brevity. The R group can be H-, CH₃- or

Ph- to form cucurbituril derivatives. For example, when the R group is CH₃- and five of these glycoluril units are combined, decamethylcucurbit[5]uril (mc5) is formed.

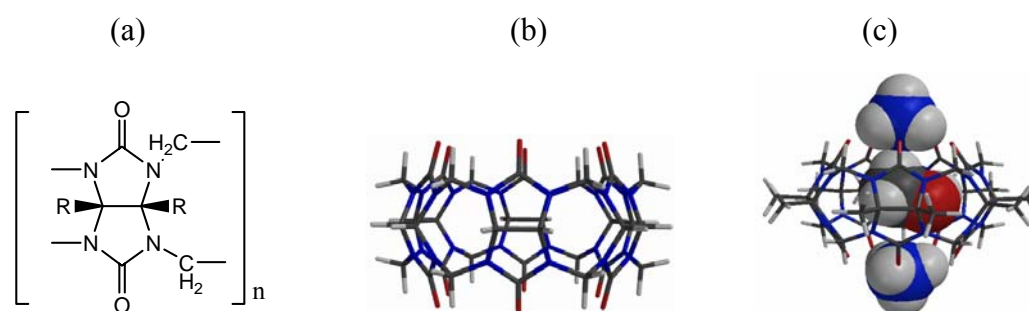


Figure 4.1: (a) Structure of cucurbituril. (b) Molecular model of cucurbit[6]uril (c) Decamethylcucurbit[5]uril bound to two NH₄⁺ ions to form a molecular box trapping one molecule of methanol inside.

With rigid, symmetric structures available in a range of sizes, cucurbiturils are ideal prototypical host molecules in host-guest chemistry. Much of the pioneering work about the most common cucurbituril, CB6, has been reviewed by Mock and co-workers.⁷ More recently Kim et al.^{8,9} have synthesized and characterized smaller (CB5) and bigger (CB7,8) cucurbiturils, making cucurbiturils more flexible host molecules.

Dearden et al.¹⁰ reported decamethylcucurbit[5]uril (mc5) binds ammonium ions at both ends and selectively captures small molecules such as N₂ and methanol inside, as shown in Figure 4.1 (c), using ESI Fourier transform mass spectrometry (ESI-FT-ICR-MS). They also used 18-crown-6 as an ionophore to react with the complex and remove the ion “lids,” and compared the rates of ammonium ion removal with different guest molecules captured inside.

CB5 can form a “molecular box” just like mc5 does, except it is more flexible compared to mc5 and it can therefore trap larger molecules inside, such as ethanol, which can not be trapped inside mc5. The “lids” of the “molecular box” can be alkali metal ions (Li^+ , Na^+ , K^+ , Cs^+), NH_4^+ , or other more highly charged metal ions (Ca^{2+} , Sr^{2+} , Ba^{2+} , Pb^{2+}).

Sustained-off resonance irradiation-collision induced dissociation (SORI-CID)¹¹ is a type of low energy activation technique that has been used in our lab to investigate the structure of supramolecular complexes.¹² The greatest advantage of the SORI-CID technique is that it can deposit internal energy into the complexes gradually and the average collision energy can be calculated fairly accurately. The energy-resolved SORI-CID technique provides a unique way to qualitatively and semi-quantitatively characterize the collisional dissociation behavior of supramolecular complexes.

Typically, two different methods are used to remove the “lids” (metal ions) from “molecular boxes”. First, collision induced dissociation (CID) can be used to “knock off” the lids; second, lids can be chemically removed via reaction with ionophores such as 18-crown-6.

Futrell et al.¹³ have investigated energy transfer between parent ions and neutral molecules during SORI-CID experiments in an FT-ICR trapping cell. The maximum kinetic energy transfer in the center of mass reference frame for single collisions during the SORI-CID process is given by the following equation.

$$E_{\max} = (\alpha^2 q^2 V^2 / 32 \pi^2 m d^2 \Delta v^2) \cdot M / (M + m) \quad (4-1)$$

In this equation, α is the geometry factor for the trapping cell, d is the cell diameter, m and q are the mass and charge of the ion, V is the SORI amplitude in volts, $\Delta\nu$ is the difference between the cyclotron frequency of the ion and the RF excitation frequency, and M is the mass of the neutral molecule. Under multiple collision conditions, the collision frequency is another important parameter that is proportional to the calculated maximum energy conversion (from center of mass kinetic energy to internal energy available to cause dissociation). For a collision cross section independent of velocity, the collision frequency is proportional to the ion velocity. If we assume the ions all have the same kinetic energy when injected into the trapping cell, the collision frequency is inversely proportional to the square of the ion mass. If we keep the frequency offset, ion charge, neutral collision partner, and geometry parameter constant, the energy absorbed by the ions will only depend on the SORI excitation amplitude and the ion mass, which can be expressed as:

$$E_{\max} \propto (V^3/m^2) \cdot M/(M+m). \quad (4-2)$$

Generally the CID energy threshold is the minimum energy required to dissociate the ion lids. If we assume no reverse activation barrier, the threshold energy is equal to the binding energy between the lid ion and the remainder of the complex.

In this chapter I will address whether we can control ion removal from the molecular box and how the guest molecules inside the “molecular box” influence the lid removal behavior. Experimental investigation as well as high level computational methods will lead to fundamental insights about molecular nanodevice manipulation.

Experimental

Instrument. All experiments were carried out using a Bruker model APEX 47e FT-ICR mass spectrometer controlled by a MIDAS data system¹⁴ and equipped with a microelectrospray source modified from an Analytica design, with a heated metal capillary drying tube based on the design of Eyer.¹⁵

Materials. CB5 samples were synthesized in Dr. Kim's lab at the Pohang University of Science and Technology (Pohang, Republic of Korea).⁸ Samples of mc5 were obtained from IBC Advanced Technologies (American Fork, UT).¹⁶ CB5 or mc5 were dissolved in 88% formic acid (Fisher Scientific, New Jersey), diluted to about 1 mM in 50:50 methanol/water, and mixed with about 2 mM alkali metal ions. The samples were electrosprayed at a typical flow rate of 10 μ L/hr.

SORI-CID experiments. Stored waveform inverse Fourier transform¹⁷ techniques were used to isolate target peaks. Sustained off-resonance irradiation collision-induced dissociation (SORI-CID)¹⁸ experiments were performed by irradiating 1 kHz below the resonant frequency of the ion of interest. The collision gas (air) was introduced using a Freiser-type pulsed leak valve.¹⁹ SORI events involved pulsing the background pressure in the trapping cell up to 10^{-5} Torr and applying the off-resonant RF for 5 seconds. The amplitude of the SORI RF pulse was varied programmatically through a range of values from less than the threshold for dissociation to several times the threshold value. Ten scans were averaged for each SORI amplitude. Data analysis was performed with a modified version of the MIDAS Analysis software that was capable of extracting peak amplitudes from a set of spectra

that differ in one or more experimental parameters (in this case, SORI amplitude).

Reactivity experiments. Neutral 18-crown-6 or 15-crown-5 was leaked into the trapping cell to achieve a constant pressure ($\sim 10^{-7}$ mbar) for reaction with the CB5-metal molecular box. The reaction time was varied programmatically. Data analysis was performed with a modified version of the MIDAS Analysis software that was capable of extracting peak amplitudes from a set of spectra that differ in one or more experimental parameters (in this case, reaction time).

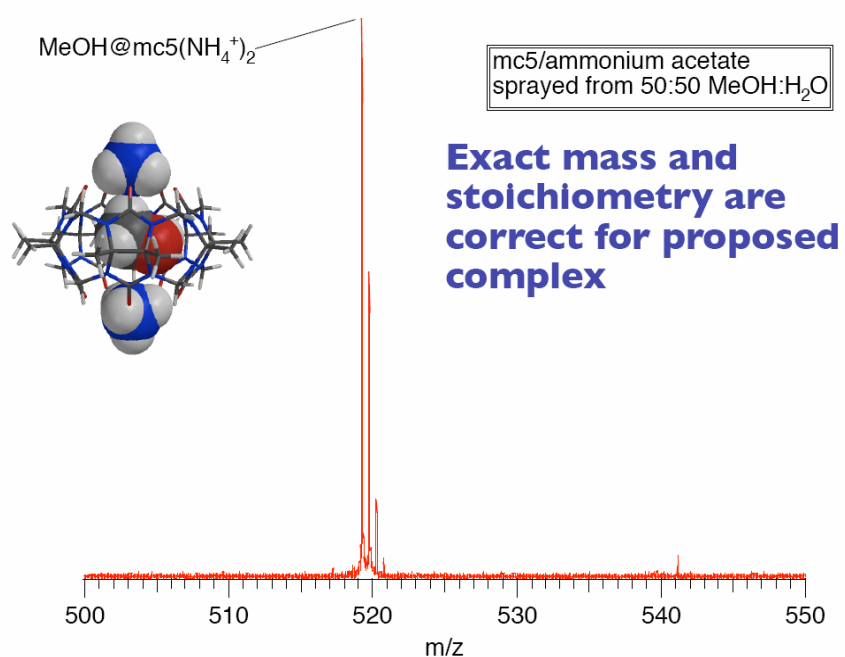
Computational methods. Our overall strategy is to use fast, relatively less accurate methods (molecular mechanics conformational searching) to screen for low-energy complex structures, which are then examined with increasingly accurate, increasingly costly techniques (primarily B3LYP/6-31G* and related methods). In general, our calculations used the following protocols. Structures were sketched using the Maestro/Macromodel modeling package (Macromodel version 7.1; Schrödinger, Inc.; Portland, OR). Conformational searches were performed using the MMFF94s²⁰ force field with no nonbonded cutoffs and with conjugate gradient minimization, and using the MCMM search method with automatic setup and 50,000 starting structures.

The lowest-energy structures found in the conformational searches were used as the starting point for B3LYP/6-31G* DFT geometry optimizations. These calculations were performed using NWChem (version 4.7; Pacific Northwest National Laboratory; Richland, WA)²¹ and used NWChem default convergence criteria.

Results

Formation of molecular box by electrospray. Our group has demonstrated¹⁰ that mc5 is highly size-selective about the inclusion of guest molecules. As Figure 4.2(a) shows, electrospray of mc5 and ammonium acetate from 50:50 MeOH:H₂O solvent results in the formation of a doubly-charged molecular box, MeOH@mc5(NH₄⁺)₂. Here methanol has a suitable size for the mc5 cavity. However, when mc5 and ammonium acetate are electrosprayed from 50:50 EtOH:H₂O solvent, no ethanol inclusion complex forms because ethanol, with a larger size than methanol, can not fit inside the mc5 cavity, as the spectrum of Figure 4.2 (b) shows. Rather, mc5-ammonium/potassium molecular boxes form with N₂ or O₂ included inside the cavity (potassium ion is from sample contamination-probably left over from the synthesis; N₂ and O₂ are from air).

(a)



(b)

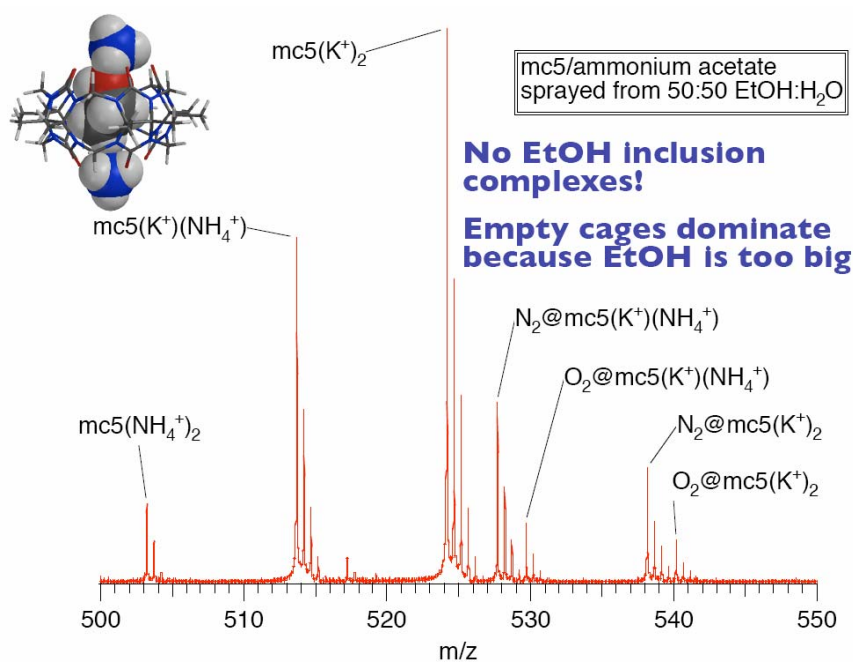


Figure 4.2: Electrospray mass spectrum of mc5 / ammonium acetate. (a) Methanol inclusion complex sprayed from 50:50 MeOH:H₂O. (b) No EtOH inclusion complex when sprayed from 50:50 EtOH:H₂O.

CB5 can form “molecular boxes” just like mc5 does, except CB5 is more flexible compared to mc5 and can trap larger molecules such as ethanol inside. CB5 and equimolar alkali metal ions were electrosprayed along with methanol, ethanol and water solvent, and CB5-metal complex ion peaks were observed in the mass spectra corresponding to CB5 with one or two different metal ions attached. The CB5 complexes with two metal ions attached can form “molecular boxes” either that are empty, have one methanol inside, or have one ethanol inside, as shown in Figure 4.3.

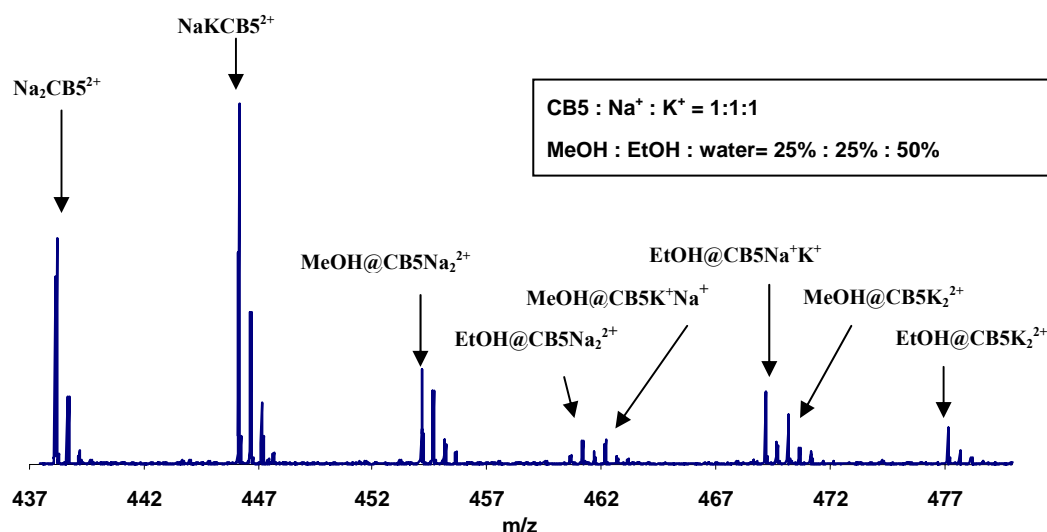


Figure 4.3: Electrospray of CB5 in the presence of K^+ and Na^+ complexes along with methanol, ethanol and water mixed solvent produces various molecular box products.

Collisional removal. Doubly charged CB5-metal complex ions were isolated using SWIFT and 1 kHz off-resonance SORI was applied to the complexes with SORI amplitudes varied programmatically. When the SORI amplitude was great enough, one K^+ ion was dissociated from the $[CB5+2K]^{2+}$ complex. Figure 4.4 shows the

SORI experiment results for $[\text{CB5}+2\text{K}]^{2+}$ complexes on three different days. From the dissociation curve it is evident that as the SORI amplitude increases the relative abundance of the parent ion $[\text{CB5}+2\text{K}]^{2+}$ decreases and the relative abundance of product ion $[\text{CB5}+\text{K}]^+$ goes up. If the thresholds are extracted by linear fitting of the rising portion of the product curve and extrapolation to the x-intercept of the fitted line, Figure 4.4 shows good reproducibility for these SORI thresholds on different days.

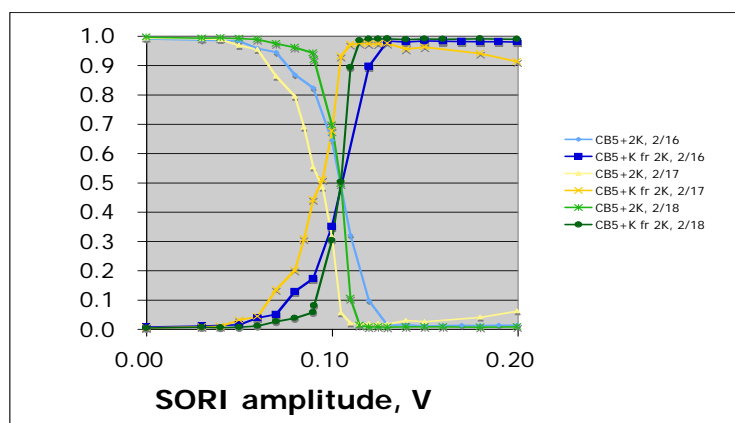


Figure 4.4: SORI experiments dissociating the $[\text{CB5}+2\text{K}]^{2+}$ complex on different days show high reproducibility of dissociation threshold.

SORI experiments were performed on $[\text{CB5}+2\text{K}]^{2+}$ and $[\text{CB5}+2\text{Na}]^{2+}$ complexes on the same day. As Figure 4.5 shows, the threshold for Na^+ loss is higher than that for K^+ loss. This is consistent with the expected order of alkali cation binding affinities for other gas phase ionophores, such as the crown ethers, for which the binding energies decrease monotonically with increasing cation size.²² Not surprisingly, when SORI was performed on the $[\text{CB5}+\text{Na}+\text{K}]^{2+}$ complex, exclusive loss of K^+ was observed. As expected, SORI results in cleavage of the weakest

interactions in the complex, the electrostatic attachment of K^+ . Furthermore, the threshold was about the same as that of the $[CB5+2K]^{2+}$ complex.

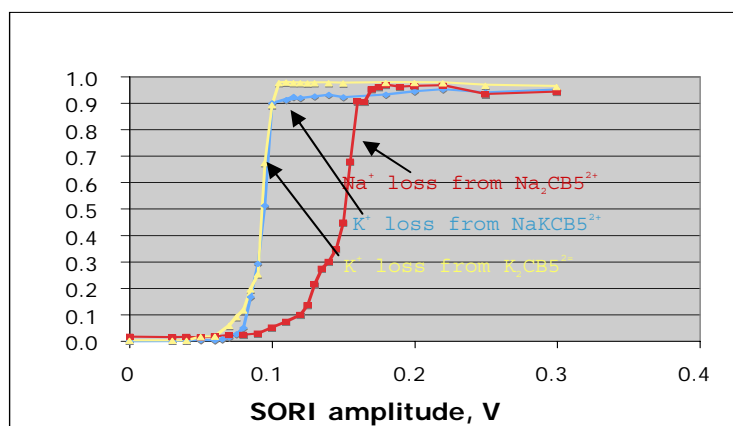


Figure 4.5: SORI results for $[CB5+2K]^{2+}$, $[CB5+2Na]^{2+}$ and $[CB5+Na+K]^{2+}$ complexes. The Na^+ appearance threshold is higher than that of K^+ .

Figure 4.6 shows an overlay of product ion curves for $[CB5+2Li]^{2+}$, $[CB5+2Na]^{2+}$, and $[CB5+2K]^{2+}$. Each involves loss of a metal ion. The thresholds decrease with increasing metal ion size, again in accord with expectation.¹⁹

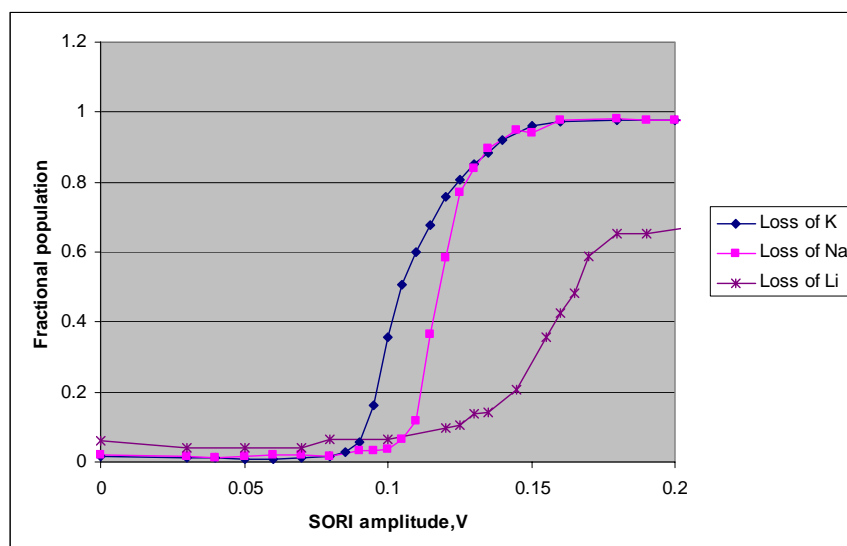


Figure 4.6: Product ion appearance curves for $[CB5+2Li]^{2+}$, $[CB5+2Na]^{2+}$, and $[CB5+2K]^{2+}$.

The results of experiments comparing $[\text{CB5}+2\text{K}]^{2+}$ and $[\text{mc5}+2\text{K}]^{2+}$ are shown in Figure 4.7. K^+ loss occurs at a higher threshold for the methylated cucurbituril mc5 than for simple CB5.

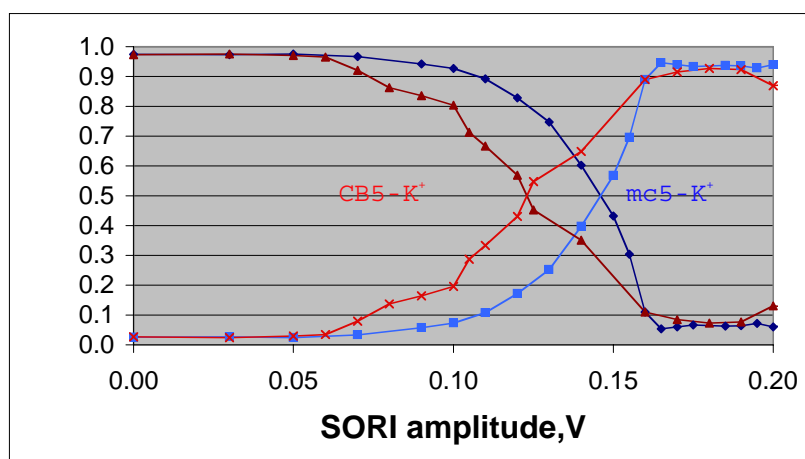


Figure 4.7: SORI experiments comparing $[\text{CB5}+2\text{K}]^{2+}$ and $[\text{mc5}+2\text{K}]^{2+}$.

Computational results. Table 4.1 shows the binding energies of CB5 with the alkali metal ions computed at the B3LYP/6-31G*//HF/6-31G* level of theory. The results indicate that the smaller the metal ion, the stronger it binds with CB5, in agreement with the experimental results of Figure 4.6. As expected, $D(\text{M}^+-\text{CB5M}^+)$ is always significantly less than $D(\text{M}^+-\text{CB5})$, because of Coulombic repulsion in the former that is absent in the latter. The difference in these two binding energies is indicated in the Repulsion column of Table 4.1; this repulsion also decreases monotonically with increasing metal size as the metal-metal distance increases.

Table 4.1: Computed Binding Energies for Complexes of CB5 with Alkali Metal Ions, B3LYP/6-31G*//HF/6-31G*, kJ mol⁻¹.

M	D(M ⁺ -CB5M ⁺)	D(M ⁺ -CB5)	Repulsion	Distance (Å)	M-M	Coulomb
						Energy
Li	291	449	158	6.68		208
Na	238	384	145	6.89		202
K	179	315	136	8.00		174
Rb	131	183	51	8.64		161
Cs	106	143	37	9.40		148

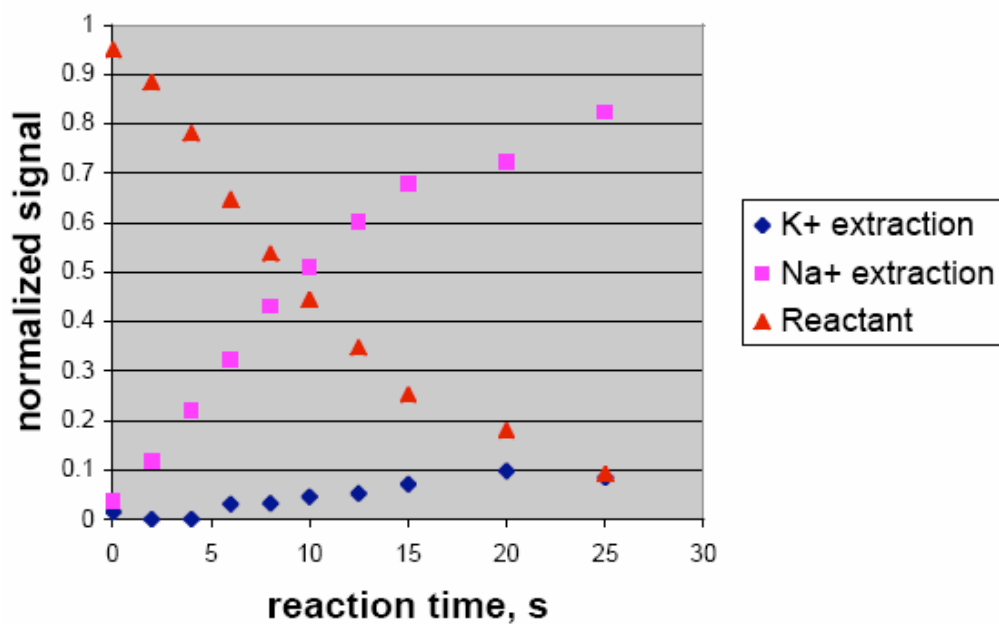
Further computational results at the HF/6-31G* level of theory show D(K⁺-CB5K⁺), 183 kJ mol⁻¹, is significantly less than D(K⁺-mc5K⁺), 213 kJ mol⁻¹.

Chemical removal of metals by ionophores. In mixed-metal complexes of CB5 ([CB5+X+Y]²⁺, where X and Y are alkali metal ions) the affinities of the complex for two different metals can be simultaneously compared. We electrosprayed such mixed metal complexes without and with trapped species (Guest@[CB5+X+Y]²⁺, Guest = nothing, methanol, or ethanol) and examined their reactions with the ionophores 18-crown-6 and 15-crown-5. The ion of interest was isolated using SWIFT, defining the start of a kinetic measurement, and then was allowed to react with ionophore at a partial pressure typically about 1 x 10⁻⁷ mbar.

Figure 4.8 (a) is a kinetic plot showing the reaction of 18-crown-6 with [CB5+Na+K]²⁺. Fitting the experimental data assuming pseudo-first-order kinetics

shows removal of Na^+ is 19 ± 4 times faster than removal of K^+ . For other mixed metal complexes, in each case the smaller metal is removed by 18-crown-6 at a higher rate than the larger metal. 15-Crown-5 is even more selective. As shown in Figure 4.8 (b), removal of Na^+ is complete in about 40 s, but no K^+ removal is observed during the same time. Interestingly, the use of an ionophore to remove the metal ion has selectivity *opposite* to that observed when collisional dissociation is employed.

a)



(b)

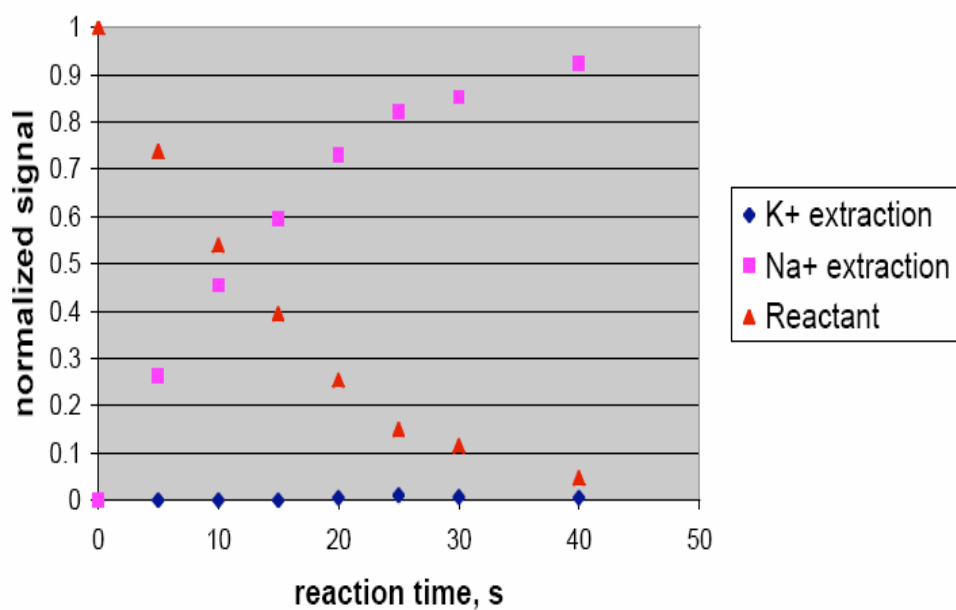


Figure 4.8: Kinetic plots showing the reaction of 18-crown-6 (a) and 15-crown-5 (b)

with $[CB5+Na+K]^{2+}$.

Table 4.2 shows the influence on the removal rates (by 18-crown-6) of filling the CB5 cavity with a guest. For methanol inclusion, the sodium removal rate decreases, and at the same time the potassium removal rate increases. Inclusion of ethanol increases the removal rates for both Na^+ and K^+ , because ethanol is large enough to sterically interfere with the binding of both lid cations. The net effect of either methanol or ethanol guests is decreased selectivity in the Na^+ and K^+ removal rates.

Table 4.2: Relative Metal Cation Removal Rates for Guest@[CB5+Na+K]²⁺ Complexes Reacting with 18-Crown-6 (normalized to the rate of Na^+ removal from [CB5+Na+K]²⁺).

Guest	Na^+	K^+	Na/K
None	1.00 ± 0.07	0.05 ± 0.01	19 ± 4
MeOH	0.68 ± 0.07	0.25 ± 0.04	2.7 ± 0.5
EtOH	1.22 ± 0.07	0.34 ± 0.02	3.6 ± 0.3

Discussion

Collisional removal vs. chemical removal

Table 4.1 shows that smaller alkali metal ions have higher binding energies for CB5 than do larger ones. This is consistent with the SORI-CID experimental results for mixed-metal complexes, which indicate that larger metal ions are more easily removed collisionally. However, when metal ions are removed via reaction with an

ionophore, the opposite result is observed; removal of the smaller, more charge dense metal is more rapid (Figure 4.7).

What explains this difference in reactivity? Although Na^+ has a higher CB5 binding energy, which disfavors its removal via collisional activation, it also binds better with the crown ether than K^+ . Computing the overall energy change in the Na^+ and K^+ removal channels of the reaction of 18-crown-6 with $[\text{CB5+Na+K}]^{2+}$, both channels are found to be energetically favorable (-146 and -141 kJ mol^{-1} for Na^+ and K^+ removal, respectively). However, Na^+ removal is more favorable than K^+ removal by about 5 kJ mol^{-1} . In gas phase reactions such as these, net energetic differences are often directly reflective of differences in activation energies. The entropies of activation in the two channels are likely to be quite similar, hence the energetic differences between the two channels explain the differences in reaction rates. 15-crown-5, which has a smaller binding cavity than 18-crown-6, shows even higher selectivity for lid removal.

Influence of included guests on lid removal

When methanol is included in the $[\text{CB5+Na+K}]^{2+}$ molecular box, 18-crown-6 removes sodium more slowly and removes potassium more rapidly than for the empty box (Table 4.2). Figure 4.9 shows computed structures of $[\text{CB5+Na+K}]^{2+}$ molecular boxes without and with alcohol guests included in the ligand cavity. It is interesting to note that the oxygen atom of the alcohol is oriented toward the sodium ion lid because

of its higher charge density; for the methanol guest, the lowest energy structure with the oxygen oriented toward the K^+ lid is 14 kJ mol^{-1} higher in energy. The guests also induce structural changes in the box complex. Compared to the empty box (Figure 4.9 a), the additional interaction of the sodium ion with the methanol oxygen pulls the sodium closer to the equatorial plane of CB5 by about 0.2 \AA , and simultaneously the methyl group of the methanol pushes the potassium ion out by about 0.1 \AA (Figure 4.9 b), making it more exposed to approaching ionophores. It is therefore reasonable that 18-crown-6 removes the potassium about 5 times faster and sodium about 30% slower than when the box is empty (Table 4.2).

Ethanol, with a larger size than methanol, can also be captured inside the CB5 cavity (Figure 4.9c). Although the oxygen atom of ethanol still points toward the sodium ion, the steric bulk of ethanol prevents it from pulling the sodium ion into the cavity. Rather, the only option is to push the sodium ion further out of the cavity. Similarly, the ethyl group pushes potassium outward. This likely explains the experimental result that both sodium and potassium removal by 18-crown-6 becomes faster upon inclusion of ethanol (Table 4.2). Overall, inclusion of either methanol or ethanol results in decreased selectivity in the cation removal reaction.

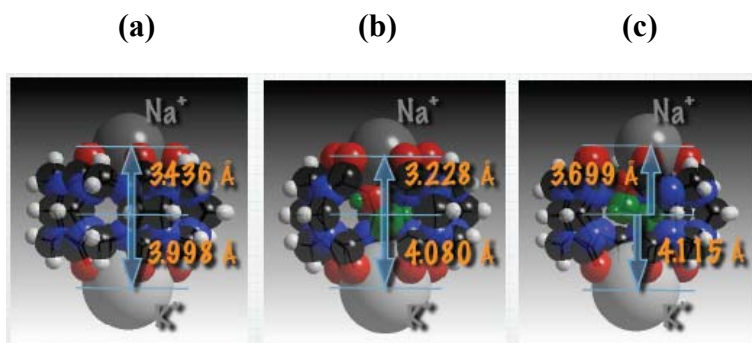


Figure 4.9: Lowest energy structures of $[\text{CB5}+\text{Na}+\text{K}]^{2+}$ molecular box (a) empty (b) with methanol captured inside (c) with ethanol captured inside. The oxygen atom of the alcohol points to the sodium ion because of its higher charge density.

Lid repulsion effects

Coulombic repulsion between the two ionic lids is another important factor that influences lid removal from the molecular box. The computed binding energies (Table 4.1) indicate that binding the second metal is much weaker than the first; Coulombic repulsion decreases as the metals get larger and the charges are farther apart.

Figure 4.10 illustrates that the structure of the complex can also be influenced by repulsion, if only weakly. Here, the distance from the K^+ ion to the CB5 equatorial plane is measured in computed structures as the second metal ion is varied. Surprisingly, this distance is the same whether the second metal is Na^+ or K^+ ; significant effects are only seen when the second metal is Cs^+ , whose bulk places the second charge sufficiently far away that the K^+ ion relaxes toward the ligand center by about 0.01 Å.

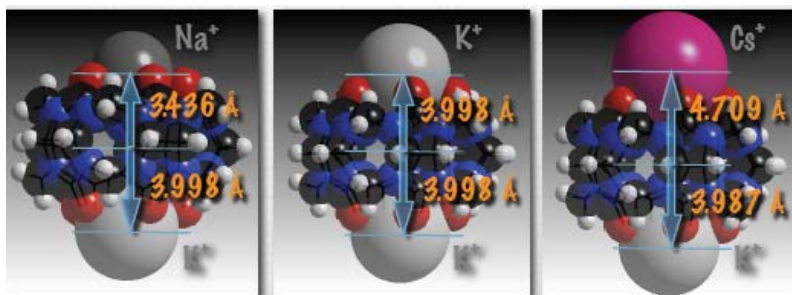


Figure 4.10: Larger size of ion lid on one end of CB5 results in longer distance between the two ion lids, and smaller repulsion strength between the ion lids.

The effect of the methanol guest on Na^+ and K^+ binding strengths is shown in Table 4.3. Methanol inclusion weakens the binding to both metals, which at first glance seems inconsistent with the effects on structure noted above. If the methanol oxygen provides additional binding interactions and pulls the Na^+ cation into the ligand cavity, how can the binding energy be less than when the cavity is empty? The answer to this question may lie in simple Coulombic repulsion effects. For the empty box, the Na^+ and K^+ lie 7.43 Å apart; when methanol is included, the separation decreases to 7.31 Å. However, the difference in electrostatic potential due to this difference in separations is only about 3 kJ mol^{-1} , less than 1/3 the difference computed at the HF/6-31G* level of theory.

Table 4.3: Metal Binding Energies and Changes upon Inclusion of a Guest in the CB5 Cavity (kJ mol^{-1} , B3LYP/6-31G*//HF/6-31G*).

	Empty	Methanol	Δ
$D(\text{Na}^+ \text{-Guest}@[\text{CB5}+\text{K}]^+)$	242	231	-11
$D(\text{K}^+ \text{-Guest}@[\text{CB5}+\text{Na}]^+)$	173	150	-23

Conclusions

This study characterizes the binding and dissociation behavior of alkali metal ions bound to CB5 host molecules. Both energy-resolved SORI-CID and chemical reactivity methods were used experimentally.

The computed metal binding energies increase with decreasing metal size. These computational results are qualitatively consistent with the threshold energies determined from SORI dissociation thresholds.

However, the reactivity experiment shows an opposite result to the collisional dissociation trends observed using SORI-CID: the smaller metal ion is more readily removed by an ionophore such as 18-crown-6. That is because the smaller ion with a higher charge density also has a higher binding affinity with the ionophore compared to larger metal ions. The overall reaction between CB5-metal complexes and the ionophore favors the smaller metal ions. Further, adding a guest molecule into the CB5 cavity has an influence on metal ion removal rates. For a methanol guest, the electronegative oxygen atom of methanol selectively points toward the higher charge-density smaller metal ion, and pulls the metal ion into the ligand cavity, making it less accessible and therefore decreasing the removal rate for the smaller metal ion by the ionophore. At the same time the methyl group of methanol pushes the larger ion at the other end of CB5 outward, making it more accessible, and increases the removal rate of the larger ion by the ionophore. The overall effect of the methanol guest is to decrease the rate removal selectivity between small and large metal ions. The size effect of the ethanol guest molecule is more evident; ethanol increases the

removal rate for both large and small metal ions, because it is large enough to push both cations outward.

In this research we have gained new insights into the mechanism for removal of metal ions from CB5 complexes. We also demonstrate that metal removal can be modulated by varying the contents of the CB5 cavity. We believe these kinds of insights can also be applied to additional supramolecular systems.

Acknowledgements

We thank Dr. Kim for kindly providing CB5 samples and thank the Ira and Marylou Fulton Supercomputing Center at Brigham Young University for computer time.

References

- (1) Newton, D. E. *Recent Advances and Issues in Molecular Nanotechnology*; Greenwood Press: Westport, CT, 2002.
- (2) Schalley, C. A. *Int. J. Mass Spectrom.* **2000**, *194*, 11-39.
- (3) Smith, R. D.; Loo, J. A.; Loo, R. R. O.; Busman, M.; Udseth, H. R. *Mass Spectrom. Rev.* **1991**, *10*, 359-451.
- (4) Mann, M.; Wilm, M. *Trends Biochem. Sci.* **1995**, *20*, 219-224.
- (5) Dearden, D. V. In *The Encyclopedia of Mass Spectrometry*; Armentrout, P. B., Ed.; Elsevier: San Diego, 2003; Vol. 1 (Theory and Ion Chemistry), pp 763-770.
- (6) Brodbelt, J. S.; Dearden, D. V. In *Physical Methods in Supramolecular Chemistry*; Davies, J. E. D., Ripmeester, J. A., Eds.; Pergamon: Oxford, 1996; Vol. 8, pp 567-591.
- (7) Mock, W. L. In *Comprehensive Supramolecular Chemistry*; Vogtle, F., Ed.; Elsevier: New York, 1996; Vol. 2, pp 477-493.
- (8) Kim, J.; Jung, I.-S.; Kim, S.-Y.; Lee, E.; Kang, J.-K.; Sakamoto, S.; Yamaguchi, K.; Kim, K. *J. Am. Chem. Soc.* **2000**, *122*, 540-541.
- (9) Lee, J. W.; Samal, S.; Selvapalam, N.; Kim, H.-J.; Kim, K. *Acc. Chem. Res.* **2003**, *36*, 621-630.
- (10) Kellersberger, K. A.; Anderson, J. D.; Ward, S. M.; Krakowiak, K. E.; Dearden, D. V. *J. Am. Chem. Soc.* **2001**, *123*, 11316-11317.
- (11) Marshall, A. G.; Schweikhard, L. *Int. J. Mass Spectrom. Ion Proc.* **1992**, *118/119*, 37-70.

- (12)Zhang, H.; Paulsen, E. S.; Walker, K. A.; Krakowiak, K. E.; Dearden, D. V. *J. Am. Chem. Soc.* **2003**, *125*, 9284-9285.
- (13)Laskin, J.; Byrd, M.; Futrell, J. *Int. J. Mass Spectrom.* **2000**, *195/196*, 285-302.
- (14)Senko, M. W.; Canterbury, J. D.; Guan, S.; Marshall, A. G. *Rapid Commun. Mass Spectrom.* **1996**, *10*, 1839-1844.
- (15)Wigger, M.; Nawrocki, J. P.; Watson, C. H.; Eyler, J. R.; Benner, S. A. *Rapid Commun. Mass Spectrom.* **1997**, *11*, 1749-1752.
- (16)Flinn, A.; Hough, G. C.; Stoddart, J. F.; Williams, D. J. *Angew. Chem. Int. Ed. Engl.* **1992**, *31*, 1475-1477.
- (17)Chen, L.; Wang, T.-C. L.; Ricca, T. L.; Marshall, A. G. *Anal. Chem.* **1987**, *59*, 449-454.
- (18)Gauthier, J. W.; Trautman, T. R.; Jacobson, D. B. *Anal. Chim. Acta* **1991**, *246*, 211-225.
- (19)Jiao, C. Q.; Ranatunga, D. R. A.; Vaughn, W. E.; Freiser, B. S. *J. Am. Soc. Mass Spectrom.* **1996**, *7*, 118-122.
- (20)Halgren, T. A. *J. Comput. Chem.* **1996**, *17*, 490-519.
- (21)Apra, E. W., T. L.; Straatsma, T. P.; Bylaska, E. J.; de Jong, W.; Hirata, S.; Valiev, M.; Hackler, M. T.; Pollack, L.; Kowalski, K.; Harrison, R. J.; Dupuis, M.; Smith, D. M. A.; Nieplocha, J.; Tipparaju, V.; Krishnan, M.; Auer, A. A.; Brown, E.; Cisneros, G.; Fann, G. I.; Fruchtl, H.; Garza, J.; Hirao, K.; Kendall, R.; Nichols, J. A.; Tsemekhman, K.; Wolinski, K.; Anchell, J.; Bernholdt, D.; Borowski, P.; Clark, T.;

Clerc, D.; Daxsel, H.; Deegan, M.; Dyll, K.; Elwood, D.; Glendening, E.; Gutowski, M.; Hess, A.; Jaffe, J.; Johnson, B.; Ju, J.; Kobayashi, R.; Kutteh, R.; Lin, Z.; Littlefield, R.; Long, X.; Meng, B.; Nakajima, T.; Niu, S.; Rosing, M.; Sandrone, G.; Stave, M.; Taylor, H.; Thomas, G.; van Lenthe, J.; Wong, A.; Zhang, Z.; 4.7 ed.; Pacific Northwest National Laboratory: Richland, Washington 99352-0999, USA, 2005.

(22)More, M. B.; Ray, D.; Armentrout, P. B. *J. Am. Chem. Soc.* **1999**, *121*, 417-423.

Chapter 5

Cucurbit[6]uril Pseudorotaxanes: Distinctive Gas-Phase Dissociation and Reactivity

Introduction

One of the prototypical supramolecular structures, rotaxane,¹ involves a wheel-and-axle architecture with a linear molecule (the “axle”) threaded through another cyclic species (the “wheel”). Bulky groups at the ends of the axle prevent the wheel molecule from slipping off; pseudorotaxanes have a similar architecture but lack the bulky stopping groups. Mass spectrometry is increasingly being used to characterize such supramolecular structures,² but most studies do not go beyond establishment of the stoichiometry of the complex. Can pseudorotaxanes formed in solution survive the electrospray ionization process intact, and if so, will they exhibit characteristics that set them apart from conventional complexes that lack the pseudorotaxane architecture?

Cucurbit[6]uril³ (Figure 5.1) has long been known to form pseudorotaxanes with diammonium cations⁴ and other species^{5,6} in condensed media. Recently, we have shown that electrospray ionization of a related molecule with a smaller central cavity, decamethylcucurbit[5]uril, results in the observation of cage complexes in the gas phase.⁷ Here we report electrospray ionization mass spectrometric experiments that

demonstrate cucurbit[6]uril pseudorotaxanes survive into the gas phase and exhibit dissociation and reactivity distinct from that of nonrotaxanes.

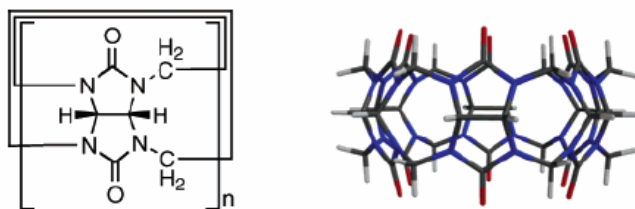


Figure 5.1: Structure of cucurbit[n]uril (left); cucurbit[6]uril model (gray = carbon, red = oxygen, blue = nitrogen, white = hydrogen).

Experimental

All experiments were performed using a Fourier transform ion cyclotron resonance mass spectrometer^{8,9} (model APEX 47e, Bruker Daltonics; Billerica, MA) and a microelectrospray ionization source modified from an Analytica (Analytica of Branford; Branford, MA) design.¹⁰ The instrument was controlled using a MIDAS data system¹¹ (National High Magnetic Field Ion Cyclotron Resonance Facility; Tallahassee, FL). Cucurbit[n]urils (hereafter abbreviated “CB n ,” where n is the number of monomer units) were synthesized as has been described.¹² Samples were prepared for electrospray by first dissolving the CB n , at a concentration of 7.5 mM, in 88% formic acid. A 100 μL aliquot of this solution was mixed with 50 μL of aqueous amine, 7.5 mM, and the mixture was diluted to 1 mL. Electrospray (tip voltage, 1300 V; flow rate, 10 $\mu\text{L h}^{-1}$) resulted in strong signals for positive ions consistent with

complexes of ammonium ions with CBn. Sustained off-resonance irradiation-collision induced dissociation (SORI-CID)¹³ was performed by using a stored waveform inverse Fourier transform (SWIFT)¹⁴ pulse to isolate the ions of interest, followed by a 6.5 ms pulse of air (at atmospheric backing pressure) and irradiation with a low amplitude, 3 s duration constant-frequency rf pulse 750 Hz below resonance with the ion to be excited. For reactivity studies, neutral amines were introduced into the trapping region of the instrument via controlled variable leak valves (Varian), typically to pressures around 1×10^{-7} mbar (as indicated by an uncorrected cold cathode gauge (Balzers)). Electrosprayed ions were injected into the trap and allowed to react with the neutral amines; reactant and product ions were monitored as a function of time.

Results and Discussion

We present evidence that CB6 and doubly protonated 1,4-butanediamine (DAB) cations form pseudorotaxanes that survive the electrospray process and exhibit distinctive behavior in the gas phase. This conclusion is based on the stoichiometries of observed doubly protonated CBn complexes with DAB ions, on the collision-induced dissociation behavior of the complexes, and on the reactivities of the complexes with neutral amines. In each case we compare the behavior of the proposed pseudorotaxane with that of a complex that cannot adopt the pseudorotaxane architecture.

Electrospray of DAB with CBn. Electrospray of an acidic mixture of CBn ($n = 5-6$) with DAB results in the mass spectrum shown in Figure 5.2. Only one complex is observed for CB5, a doubly charged ion corresponding to two singly protonated DAB ions attached to CB5 (a 2:1 complex). Almost all of the CB6 complexes, on the other hand, correspond to *one* doubly protonated DAB cation attached to the cucurbituril (1:1 complex), with only about 1% of the signal arising from a 2:1 complex analogous to that observed for CB5. On the basis of the observed stoichiometry, we propose that the CB6 complex with doubly protonated DAB is a pseudorotaxane.

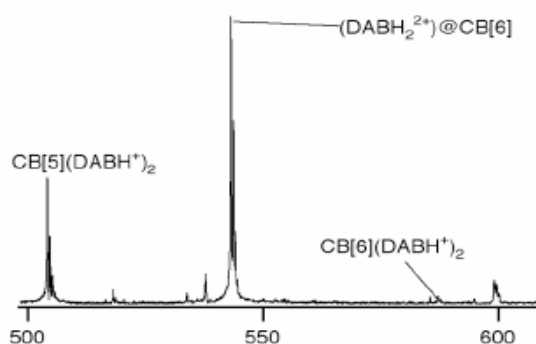
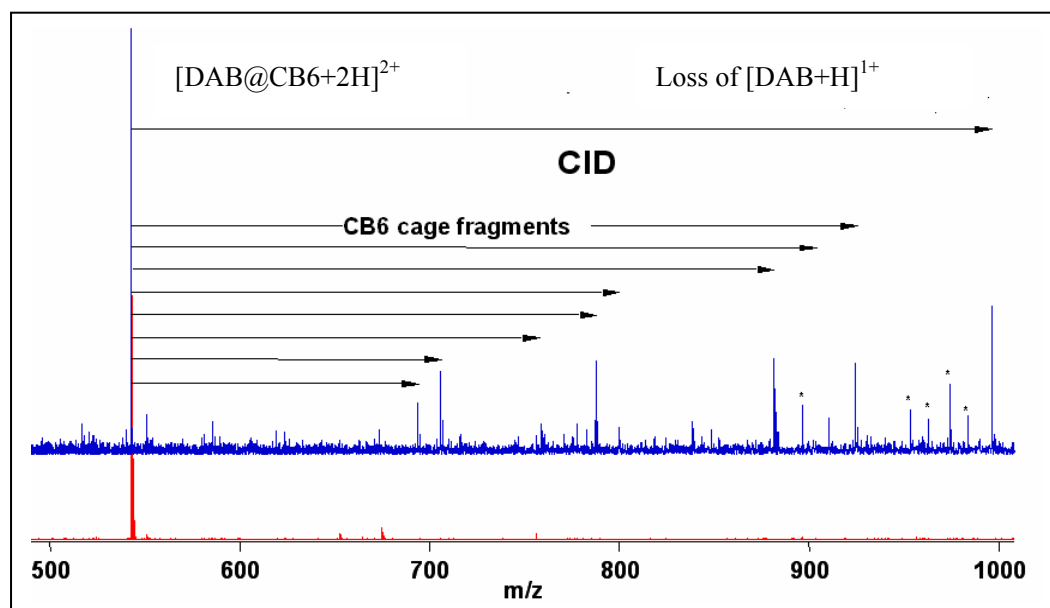


Figure 5.2: Electrospray Fourier transform mass spectrum of an acidic mixture of 1,4-diaminobutane with cucurbit[n]uril (“CBn”), $n = 5-6$.

SORI-CID experiment. To test this conjecture, we performed SORI-CID on the proposed $(\text{DAB} + 2\text{H})@\text{CB}6^{2+}$ ion, m/z 543.2. A typical SORI-CID spectrum is shown in Figure 5.3a. Fragment ions were observed only at the highest SORI pulse amplitudes attempted, accompanied by severe attenuation of all the ion signal, suggesting that ejection of the parent ion from the trap is competitive with SORI-CID.

The largest fragment peak, at m/z 997.3, corresponds to loss of singly protonated DAB from the complex, resulting in protonated CB6. Other peaks, of similar intensity, are consistent with loss of protonated DAB coupled with fragmentation of the CB6 cage (m/z 694.2, 706.2, 759.2, 788.2, 800.2, 882.3, 911.3, and 925.3). The SORI-CID results therefore suggest the proposed $(\text{DAB} + 2\text{H})@\text{CB}^{2+}$ ion is strongly bound; loss of DAB and breakup of the CB6 cage occur at similar energies.

(a)



(b)

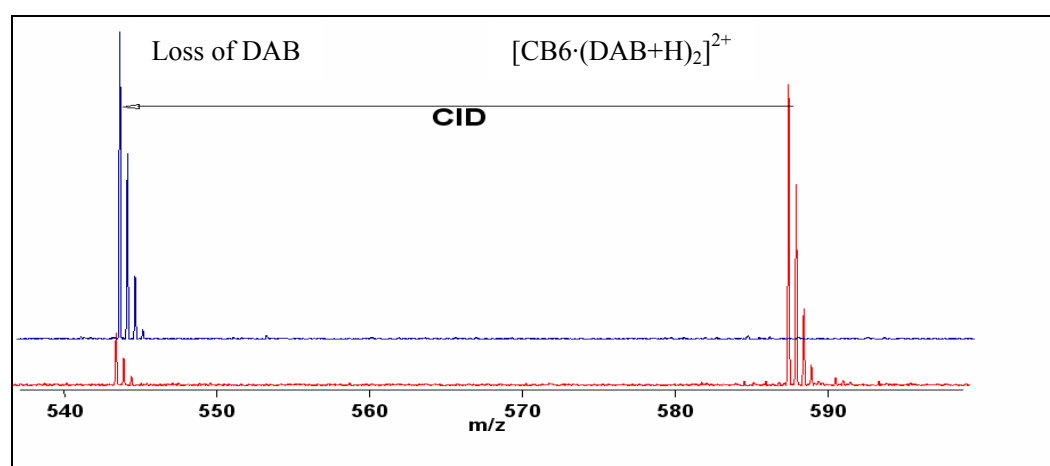


Figure 5.3: (a) SORI-CID of proposed $(\text{DAB+2H})\text{@CB6}^{2+}$ pseudorotaxane. The SORI excitation pulse is disabled in the lower (red) trace. The upper (blue) trace, with SORI enabled, exhibits extensive fragmentation of the CB6 cage. Asterisks indicate noise peaks. (b) SORI-CID of the nonrotaxane $\text{CB6}\cdot(\text{DAB+H})_2^{2+}$. Some loss of neutral DAB is observed even with the SORI pulse disabled, due to dissociation while isolating the parent ion (lower, red trace). SORI-CID results in facile loss of neutral DAB.

We examined SORI-CID of two other species as controls. When sprayed with an excess of DAB, the 2:1 DAB:CB6 complex is observed at nominal m/z 587.2. Using the same amplitude, duration, and frequency offset as was employed for the 1:1 complex, the SORI-CID spectrum shown in Figure 5.3b was obtained. Dissociation of the 2:1 complex via loss of neutral DAB, producing a doubly charged product ion with the same nominal m/z as the 1:1 complex, is facile and quantitative. It is difficult to isolate the 2:1 complex because dissociation to produce the 1:1 complex occurs during the isolation.

We also prepared complexes of ethylenediamine with CB6. Electrospray of acidic mixtures of these two components results exclusively in doubly protonated 2:1 complexes with nominal m/z of 559.2, consistent with a $\text{CB6}\cdot[\text{H}_2\text{N}(\text{CH}_2)_2\text{NH}_2 + \text{H}]_2^{2+}$ complex. Molecular models suggest ethylenediamine is too short to simultaneously bind both rims of CB6. Again, complete isolation of the parent complex ion is difficult because dissociation of protonated ethylenediamine occurs during the isolation event. SORI-CID of the 2:1 protonated ethylenediammonium:CB6 complex results in facile loss of protonated ethylenediammonium as well as loss of an additional neutral molecule of ethylenediamine. In summary, the 2:1 protonated diamine:CB6 complexes are easily dissociated via loss of the diamine (with or without the charge), whereas the 1:1 doubly protonated DAB:CB6 complex fragments primarily via breakup of the CB6 cage, consistent with a pseudorotaxane structure for the 1:1 complex.

Reactivity experiment. The reactivity of the proposed pseudorotaxane in the gas

phase is also distinctive and consistent with a pseudorotaxane structure. Reaction of the proposed $(\text{DAB} + 2\text{H})@\text{CB6}^{2+}$ ion with neutral *tert*-butylamine in the gas-phase results in slow *addition* of the *tert*butylamine to the complex, with kinetics that clearly do not show the expected simple pseudo-first-order behavior. Reasonable fits to the experimental reactant and product intensities as a function of time are obtained by assuming a model that involves slow conversion of the complex from an unreactive form to a reactive form, followed by addition of the amine. The addition reaction proceeds to equilibrium. Using this model, the rate of *tert*butylamine addition is $1.3 \pm 0.2 \times 10^{-11} \text{ cm}^3 \text{ molecule}^{-1} \text{ s}^{-1}$.

This reactivity contrasts with that exhibited by $\text{CB6} \cdot (\text{NH}_3 + \text{H})_2^{2+}$ with *tert*-butylamine in the gas phase. The *tert*-butylamine reacts with this nonrotaxane ion by *displacing* neutral ammonia from the complex, in two sequential steps. Excellent fits to the experimental data are obtained, assuming simple pseudo-first-order kinetics, yielding rate constants of $2.2 \pm 0.1 \times 10^{-10}$ and $1.4 \pm 0.1 \times 10^{-10} \text{ cm}^3 \text{ molecule}^{-1} \text{ s}^{-1}$ for the first and second displacements, respectively.

These results are consistent with $(\text{DAB} + 2\text{H})@\text{CB6}^{2+}$ having a pseudorotaxane structure in the gas phase; the pseudorotaxane ion cannot react via amine displacement because the ammonium ion is attached to the cucurbituril at both ends. Externally bound ammonium, on the other hand, is easily displaced by another amine.

Conclusions

All available evidence indicates $(\text{DAB} + 2\text{H})@\text{CB6}^{2+}$ is a pseudorotaxane in the gas phase. Molecular mechanics modeling suggests an appropriate size relationship between the two molecules for pseudorotaxane formation. The 1:1 stoichiometry of the observed complexes is consistent with this interpretation, and the SORI-CID experiments strongly support a pseudorotaxane structure. Finally, the complex exhibits reactivity consistent with a pseudorotaxane structure. These results suggest that SORI-CID and reactivity tests can be used to identify such structures for gas-phase ions.

References

- (1) Sauvage, J.-P.; Dietrich-Buchecker, C., *Eds. Molecular Catenanes, Rotaxanes, and Knots*; Wiley-VCH: Weinheim, Germany, 1999.
- (2) Schalley, C. A. *Int. J. Mass Spectrom.* **2000**, *194*, 11-39.
- (3) Mock, W. L. In *Comprehensive Supramolecular Chemistry*; Vogtle, F., Ed.; Elsevier: New York, 1996; Vol. 2, pp 477-493.
- (4) Mock, W. L.; Shih, N.-Y. *J. Org. Chem.* **1986**, *51*, 4440-4446.
- (5) Kim, K. *Chem. Soc. Rev.* **2002**, *31*, 96-107.
- (6) Buschmann, H.-J.; Wego, A.; Schollmeyer, E.; Dopp, D. *Supramolecular Chem.* **2000**, *11*, 225-231.
- (7) Kellersberger, K. A.; Anderson, J. D.; Ward, S. M.; Krakowiak, K. E.; Dearden, D. V. *J. Am. Chem. Soc.* **2001**, *123*, 11316-11317.
- (8) Dearden, D. V.; Dejsupa, C.; Liang, Y.; Bradshaw, J. S.; Izatt, R. M. *J. Am. Chem. Soc.* **1997**, *119*, 353-359.
- (9) Pope, R. M.; Shen, N.; Nicoll, J.; Tarnawiecki, B.; Dejsupa, C.; Dearden, D. V. *Int. J. Mass Spectrom. Ion Proc.* **1997**, *162*, 107-119.
- (10) Wigger, M.; Nawrocki, J. P.; Watson, C. H.; Eyler, J. R.; Benner, S. A. *Rapid Commun. Mass Spectrom.* **1997**, *11*, 1749-1752.
- (11) Senko, M. W.; Canterbury, J. D.; Guan, S.; Marshall, A. G. *Rapid Commun. Mass Spectrom.* **1996**, *10*, 1839-1844.
- (12) Day, A. I.; Arnold, A. P.; Blanch, Rodney J.: World Intellectual Property

Organization, 2000.

(13)Gauthier, J. W.; Trautman, T. R.; Jacobson, D. B. *Anal. Chim. Acta* **1991**, *246*, 211-225.

(14)Chen, L.; Wang, T.-C. L.; Ricca, T. L.; Marshall, A. G. *Anal. Chem.* **1987**, *59*, 449-454.

Chapter 6

Binding Affinities of Alkyldiammonium Ions of Various Chain Lengths for Cucurbit[6]uril in the Gas Phase Using Electrospray Ionization FT-ICR Mass Spectrometry

Introduction

Cucurbiturils¹ are pumpkin-shaped cyclic polymers of glycoluril with hollow interior cavities. As shown in Figure 6.1a, b, carbonyl oxygen atoms line the portals of the cucurbituril and form ideal binding sites for positive ions, while the interior cavities can contain neutral molecules of proper size. Cucurbiturils composed of n glycoluril units are named cucurbit[n]urils, CB n hereafter for brevity.

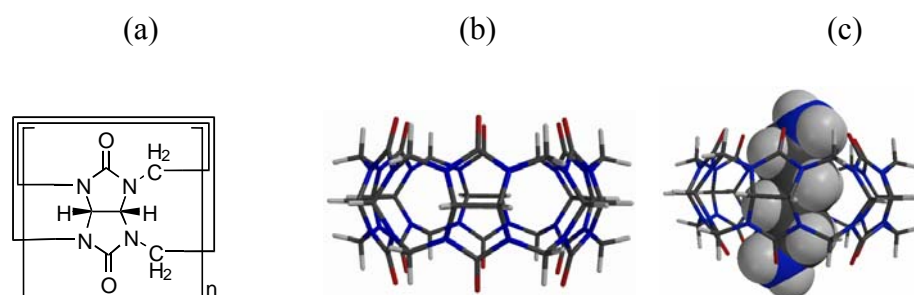


Figure 6.1: (a) Chemical structure of cucurbit[n]uril. (b) Molecular model of cucurbit[6]uril. (c) Molecular model of cucurbit[6]uril-diaminobutane complex.

CB6 is known to form complexes with α,ω -alkyldiammonium cations in solution.¹ In condensed media, these complexes have rotaxane structures, where the diammonium chain is threaded through the cucurbituril (Figure 6.1, c).¹

Electrospray mass spectrometry has been widely used to investigate host-guest interactions in the gas phase.²⁻⁶ Characterization of cucurbituril complexes in the gas phase will help to improve fundamental understanding in host-guest chemistry. Free from solvent effects, gas phase studies provide unique information that is directly comparable to the results of computational studies. Comparison of the behavior of host-guest interactions between the gas phase and solution conditions can also qualitatively and quantitatively clarify solvent effects. Our group has characterized distinct dissociation and reactivity behavior for the complex of CB6 and 1,4-diaminobutane ion in the gas phase using electrospray ionization Fourier transform ion cyclotron resonance mass spectrometry (ESI-FTICR-MS).⁷

Affinity data for α,ω -alkyldiammonium ions ($\text{H}_3\text{N}^+(\text{CH}_2)_n\text{NH}_3^+$, $n=3-10$) complexed with CB6 have been reported in formic acid solvent.¹ However, the binding constants likely are influenced by the solvent, making direct comparison with computed binding energies difficult. Binding strengths characterized in the gas phase are more comparable to the computed results.

Sustained-off resonance irradiation-collision induced dissociation (SORI-CID)⁸ is a type of low energy activation technique that has been widely used in FT-ICR MS to investigate the structure of supramolecular complexes. The greatest advantage of the SORI-CID technique is that it can deposit internal energy into the complexes

gradually, and the energy absorbed by the complexes can be calculated fairly accurately. Thus the energy-resolved SORI-CID technique provides a unique way to qualitatively and semi-quantitatively characterize the collisional dissociation behavior of supramolecular complexes.

Futrell et al.⁹ have investigated energy transfer between parent ions and neutral molecules during SORI-CID experiments in an FT-ICR trapping cell. Their work has been discussed in Chapter 4. Generally the CID threshold is the minimum energy required to cause dissociation of the guest ions. If we assume no reverse activation barrier, the threshold energy is equal to the binding energy between host and guest.

In this chapter, energy-resolved SORI-CID experiments on α,ω -alkyldiammonium complexes (n=3-10) of CB6 are performed in the gas phase to investigate the relationship between binding strength and diammonium chain length. High-level computational studies were performed to compare with the experimental results.

Experimental

Instrument. All experiments were carried out using a Bruker model APEX 47e FT-ICR mass spectrometer controlled by a MIDAS data system¹⁰ and equipped with a microelectrospray source modified from an Analytica design, with a heated metal capillary drying tube based on the design of Eyler.¹¹

Materials. CB6 and n-alkyldiamine (n = 3 – 10) were purchased from Sigma

Chemical Co. (St. Louis MO) and used without further purification. CB6 was dissolved in 88% formic acid (Fisher Scientific, New Jersey), diluted to about 1mM in 50:50 methanol/water, and mixed with about 2 mM n-alkyldiamine. The samples were electrosprayed at a typical flow rate of 10 μ L/hr.

SORI-CID experiments. Stored waveform inverse Fourier transform¹² techniques were used to isolate target peaks. Sustained off-resonance irradiation collision-induced dissociation (SORI-CID)¹³ experiments were performed by irradiating 1 kHz below the resonant frequency of the ion of interest. Collision gas (air) was introduced using a Freiser-type pulsed leak valve.¹⁴ SORI events involved pulsing the background pressure in the trapping cell up to 10^{-5} mbar and applying the off-resonance irradiation for 5 seconds. The amplitude of the SORI RF pulse was varied programmatically through a range of values from less than the threshold for dissociation to several times the threshold value. Ten scans were averaged for each SORI amplitude. Data analysis was performed with a modified version of the MIDAS Analysis software that was capable of extracting peak amplitudes from a set of spectra that differ in one or more experimental parameters (in this case, SORI amplitude). Thresholds were extracted by linear fitting to the rising portion of the ion fragmentation breakdown curve and extrapolation to the x-intercept of the fitted line.

Computational methods. Our overall strategy is to use fast, relatively less accurate methods (molecular mechanics conformational searching) to screen for low-energy complex structures, which are then examined with increasingly accurate, increasingly costly techniques (primarily HF/6-31G* and related methods). In general,

our calculations used the following protocols. Structures were sketched using the Maestro/Macromodel modeling package (Macromodel version 7.1; Schrödinger, Inc.; Portland, OR). Conformational searches were performed using the MMFF94s¹⁵ force field with no nonbonded cutoffs and with conjugate gradient minimization, and using the MCMM search method with automatic setup and 50,000 starting structures.

The lowest-energy structures found in the conformational searches were used as the starting point for HF/6-31G* geometry optimizations.

Results and Discussion

Binding affinity in solution compared with the gas phase. Binding constants in formic acid solution for α,ω -alkyldiammonium ions ($\text{H}_3\text{N}^+(\text{CH}_2)_n\text{NH}_3^+$, $n=3-10$, C_n hereafter for brevity) complexed with CB6 have been reported by Mock and co-workers (Figure 6.2 a).¹ Apparently C5 and C6 have the highest binding affinity with CB6, which indicates linear alkyldiammonium ions with five or six carbon atoms separating the terminal ammonium groups are optimum for CB6 portal binding in solution. Figure 6.2b shows a plot of computed binding energy versus alkyldiammonium carbon number. The plot shows a pattern similar to that observed in solution, except that the largest binding energy occurs for C5. Figure 6.2c is a plot of SORI-CID threshold values versus alkyldiammonium chain length. These SORI-CID threshold values indicate C4 and C5 have the highest binding affinity in the gas phase, and C6 has a surprisingly low threshold value. The exceptionally low threshold value of C6 might be the result of opening a new dissociation channel at this chain length. If

the $n = 6$ data are disregarded, the linear correlation between computed binding energies and SORI-CID thresholds is quite good ($R^2 = 0.95$) (Figure 6.2 d). The highest binding energy and highest dissociation threshold occur for the $n = 5$ diammonium complex. This compares with a maximum in aqueous formic acid solution complex formation constants at $n = 6$, probably reflecting superior solvation of the terminal ammonium groups for the longer chain, which is absent in the gas phase.

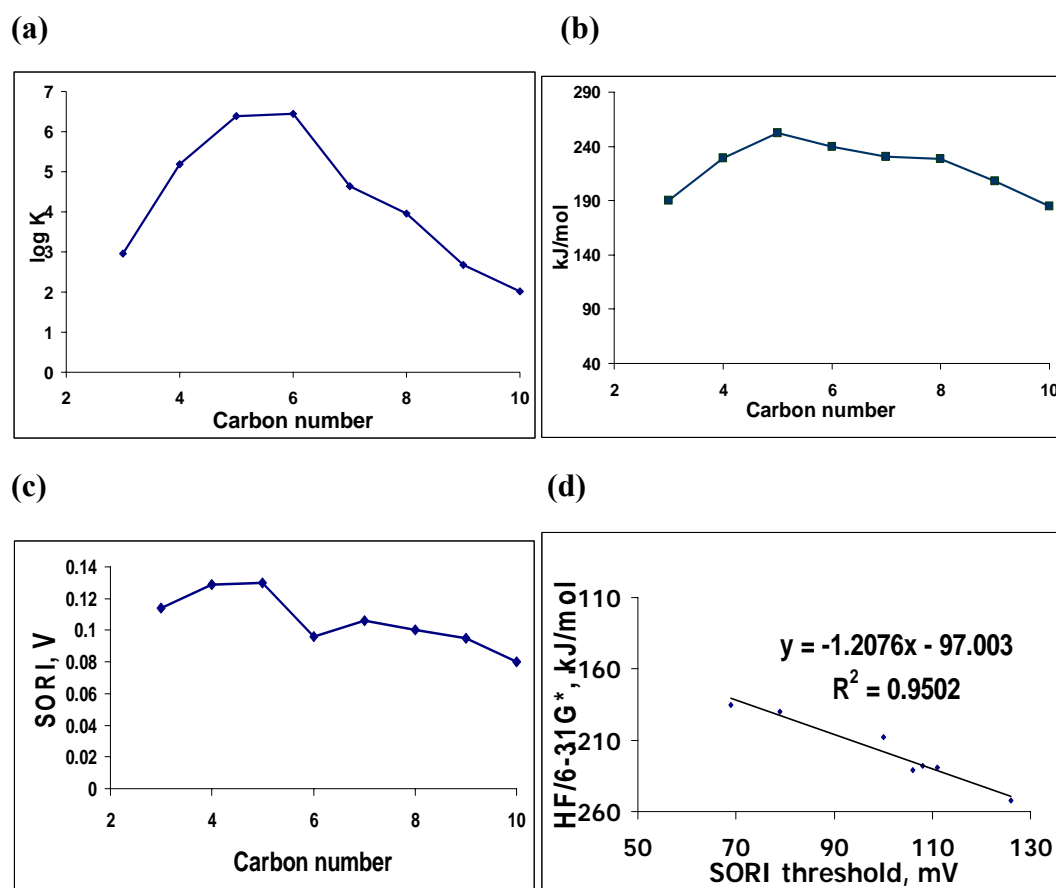


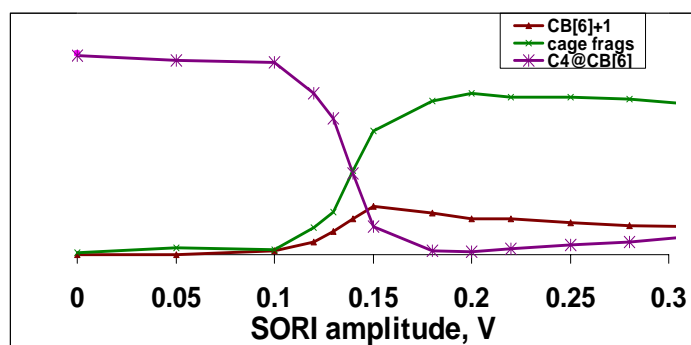
Figure 6.2: Binding affinity of α,ω -alkyldiammonium ions ($\text{H}_3\text{N}^+(\text{CH}_2)_n\text{NH}_3^+$, $n=3-10$) complexed with CB6. (a) Binding constants versus carbon number in H_2O -85% HCOOH (1:1, v/v) solution.¹ (b) Computed binding energy versus carbon number. (c) Experimental SORI-CID threshold value versus carbon number. (d)

Linear correlation between HF/6-31G* computed binding energy and SORI-CID threshold values, with C6 being disregarded.

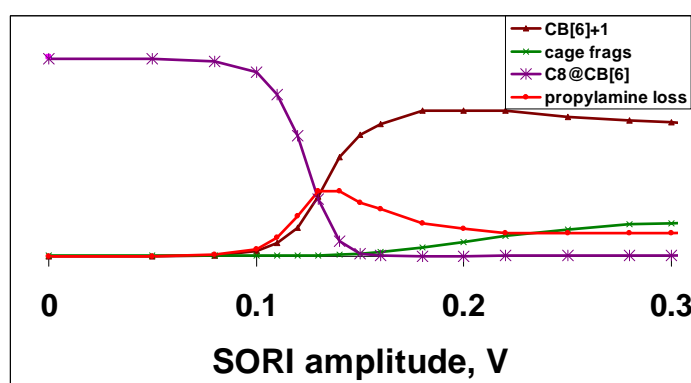
Characteristic dissociation channels during SORI-CID. The dissociation channels differ according to carbon number. For $n=3-7$, fragmentation of the CB6 cage is the dominant dissociation channel (Figure 6.3 a), whereas for $n = 8-10$ fragmentation occurs via breakage of the diamine chain. Interestingly, the $n = 8$ and $n = 10$ diammonium complexes dissociate primarily through loss of neutral propylamine (Figure 6.3 b), whereas the $n = 9$ complex undergoes losses of ethylamine and butylamine that are almost equal in amplitude to propylamine loss (Figure 6.3 c); the reasons for this even-odd alternation are not clear.

Apparently fragmentation of the CB6 cage ($n = 3-7$) occurs at higher threshold values compared to breakage of diamine chain ($n = 8-10$), with the exception of C6. Why does varying the chain length lead to changes in dissociation channel? Alkyldiammonium ions with carbon number less than 7 can thread through the CB6 cage with the whole chain length being encapsulated within the CB6 cage, and these are the complexes that dissociate via cage fragmentation rather than diamine chain length breakage. However, C8-C10 alkyldiammonium ions, with chain lengths longer than the CB6 cavity height (9.1 Å), thread through the CB6 cavity with part of the carbon chain exposed on the surface of the complex. These are the complexes that undergo diamine chain breakage.

(a)



(b)



(c)

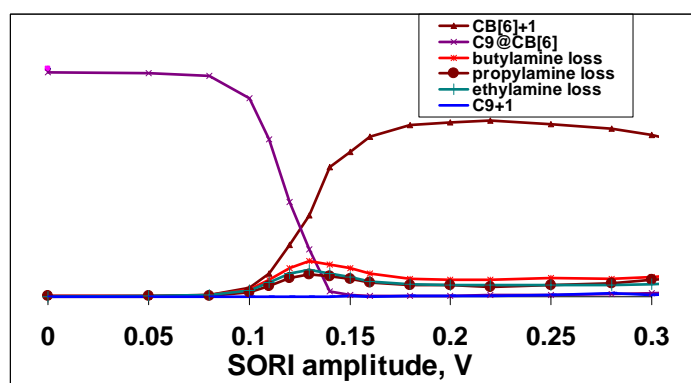


Figure 6.3: Selected dissociation curves of α,ω -alkyldiammonium ions complexed with CB6 as a function of SORI pulse amplitude. (a) C4, diaminobutane; (b) C8, diaminoctane; (c) C9, diamnononane.

Conclusions

Energy-resolved SORI-CID was performed to investigate the effect of carbon chain length on binding affinity for α,ω -alkyldiammonium ions ($\text{H}_3\text{N}^+(\text{CH}_2)_n\text{NH}_3^+$, $n=3-10$) complexed with CB6 in the gas phase using electrospray ionization FT-ICR mass spectrometry. The results were compared to the binding constants in solution and to computed binding energies. C6 has the highest binding affinity in solution, whereas C5 shows the highest value in both SORI-CID thresholds and in high-level computational energy in the gas phase. This difference likely indicates the influence of solvation. The C6 complex has an unexpectedly low SORI-CID threshold, which might be the result of its unique dissociation behavior. During SORI-CID, C3-C7 complexes dissociate via cage fragmentation, whereas C8-C10 dissociate via diamine chain breakage.

References

(1) Mock, W. L. In *Comprehensive Supramolecular Chemistry*; Vogtle, F., Ed.; Elsevier: New York, 1996; Vol. 2, pp 477-493.

(2) Vincenti, M. *J. Mass Spectrom.* **1995**, *30*, 925-939.

(3) Brodbelt, J. S.; Dearden, D. V. In *Physical Methods in Supramolecular Chemistry*; Davies, J. E. D., Ripmeester, J. A., Eds.; Pergamon: Oxford, 1996; Vol. 8, pp 567-591.

(4) Dearden, D. V. In *Physical Supramolecular Chemistry*; Echegoyen, L., Kaifer, A. E., Eds.; Kluwer: Dordrecht, the Netherlands, 1996, pp 229-247.

(5) Dearden, D. V.; Zhang, H.; Chu, I.-H.; Wong, P.; Chen, Q. *Pure Appl. Chem.* **1993**, *65*, 423-428.

(6) Vincenti, M.; Pelizzetti, E.; Dalcanale, E.; Soncini, P. *Pure Appl. Chem.* **1993**, *65*, 1507-1512.

(7) Zhang, H.; Paulsen, E. S.; Walker, K. A.; Krakowiak, K. E.; Dearden, D. V. *J. Am. Chem. Soc.* **2003**, *125*, 9284-9285.

(8) Marshall, A. G.; Schweikhard, L. *Int. J. Mass Spectrom. Ion Proc.* **1992**, *118/119*, 37-70.

(9) Laskin, J.; Byrd, M.; Futrell, J. *Int. J. Mass Spectrom.* **2000**, *195/196*, 285-302.

(10) Senko, M. W.; Canterbury, J. D.; Guan, S.; Marshall, A. G. *Rapid Commun. Mass Spectrom.* **1996**, *10*, 1839-1844.

(11) Wigger, M.; Nawrocki, J. P.; Watson, C. H.; Eyler, J. R.; Benner, S. A. *Rapid*

Commun. Mass Spectrom. **1997**, *11*, 1749-1752.

(12)Chen, L.; Wang, T.-C. L.; Ricca, T. L.; Marshall, A. G. *Anal. Chem.* **1987**, *59*, 449-454.

(13)Gauthier, J. W.; Trautman, T. R.; Jacobson, D. B. *Anal. Chim. Acta* **1991**, *246*, 211-225.

(14)Jiao, C. Q.; Ranatunga, D. R. A.; Vaughn, W. E.; Freiser, B. S. *J. Am. Soc. Mass Spectrom.* **1996**, *7*, 118-122.

(15)Halgren, T. A. *J. Comput. Chem.* **1996**, *17*, 490-519.

(16)Apra, E. W., T. L.; Straatsma, T. P.; Bylaska, E. J.; de Jong, W.; Hirata, S.; Valiev, M.; Hackler, M. T.; Pollack, L.; Kowalski, K.; Harrison, R. J.; Dupuis, M.; Smith, D. M. A.; Nieplocha, J.; Tipparaju, V.; Krishnan, M.; Auer, A. A.; Brown, E.; Cisneros, G.; Fann, G. I.; Fruchtl, H.; Garza, J.; Hirao, K.; Kendall, R.; Nichols, J. A.; Tsemekhman, K.; Wolinski, K.; Anchell, J.; Bernholdt, D.; Borowski, P.; Clark, T.; Clerc, D.; Dachsel, H.; Deegan, M.; Dyall, K.; Elwood, D.; Glendening, E.; Gutowski, M.; Hess, A.; Jaffe, J.; Johnson, B.; Ju, J.; Kobayashi, R.; Kutteh, R.; Lin, Z.; Littlefield, R.; Long, X.; Meng, B.; Nakajima, T.; Niu, S.; Rosing, M.; Sandrone, G.; Stave, M.; Taylor, H.; Thomas, G.; van Lenthe, J.; Wong, A.; Zhang, Z.; 4.7 ed.; Pacific Northwest National Laboratory: Richland, Washington 99352-0999, USA., 2005.

Chapter 7

Summary and Perspective

Fourier transform ion cyclotron resonance mass spectrometry (FT-ICR-MS) was used to investigate gas-phase supramolecular complexes based on cyclic polymers, cucurbiturils (CBn). Electrospray ionization was used to introduce fragile host-guest complex ions into the gas phase and made gas phase characterization possible. The gas phase studies in this dissertation lead to fundamental insights into supramolecular chemistry.

Versatile tandem mass spectrometry techniques such as collision-induced dissociation (CID) and ion-molecule reaction experiments become powerful tools to probe the structures of the complexes. For example, the “wheel-and-axle” architecture complex formed by CB6 and 1,4-diaminobutane was characterized in chapter 5. Thus “mass” is not the only information mass spectrometry yields. With the help of high level computational methods, quantitative results can be achieved for gas phase studies. For example, energy-resolved SORI-CID was used to find the optimum alkyldiammonium chain length for CB6 binding in chapter 6, and the experimental results were compared with computational studies.

Host-guest interactions are very common within biological molecules, such as enzyme-substrate interactions. Studies of the interactions between CBn and peptides in this dissertation provide a simple but subtle model to mimic interactions within

biological molecules. For example, lysine selectively threads through the CB6 cavity to form a stable complex, whereas lysine only binds externally to the α -CD rims to form a loosely attached complex. The high binding selectivity resulting from factors such as size and hydrophobic effects is also related to modification of charge state and CID behavior upon complex formation. Other experiments show CBn binds effectively not only to peptides, but also to small proteins. With more amino acid residues present, larger molecule weights, and higher charge states, characterization work for CBn-protein interactions is more complex than for single amino acids or small polypeptides. Further studies of these larger systems will probably lead to CBn applications in biological or medical fields.

I also carried out fundamental studies of molecular device manipulation. The CB5 molecular container provides an interesting model for ion chemistry and molecular recognition. For example, a metal ion “lid” can be removed by either CID or by reaction with an ionophore. Interestingly, the ionophore selectively removes the more strongly bound metal. Further, calculations indicate the relationship between lid removal rate and binding affinity. In addition to fundamental insights, formation of the molecular container also suggests important potential applications in drug delivery or gas filtration.

The CBn family was synthesized 100 years ago and the structure was first elucidated during the 1980s. This dissertation contributes to knowledge of host-guest interactions of CB5 and CB6 in the gas phase, and some of the interactions, such as those between peptides and CB6, are brand new; they have not been observed before

either in the gas phase or in solution. Larger-cavity CB_n such as CB7 and CB8 have not been extensively investigated in this dissertation. With larger cavities and more flexible geometries, CB7 and CB8 will be important hosts for future supramolecular system projects.

Gas phase studies of supramolecular systems have gained recent interest because they eliminate matrix complexity. With the development of new mass spectrometry techniques, such as FT-ICR-MS, I believe gas phase studies of supramolecules will enter a new era in this century.